An International ICT R&D Journal Sponsored by ZTE Corporation

ISSN 1673-5188
CN 34-1294/ TN
CODEN ZCTOAK

ZTE COMMUNICATIONS

中兴通讯技术(英文版)

tech.zte.com.cn

February 2018, Vol. 16 No. 1

SPECIAL TOPIC:
Wireless Data and Energy Integrated Communication Networks

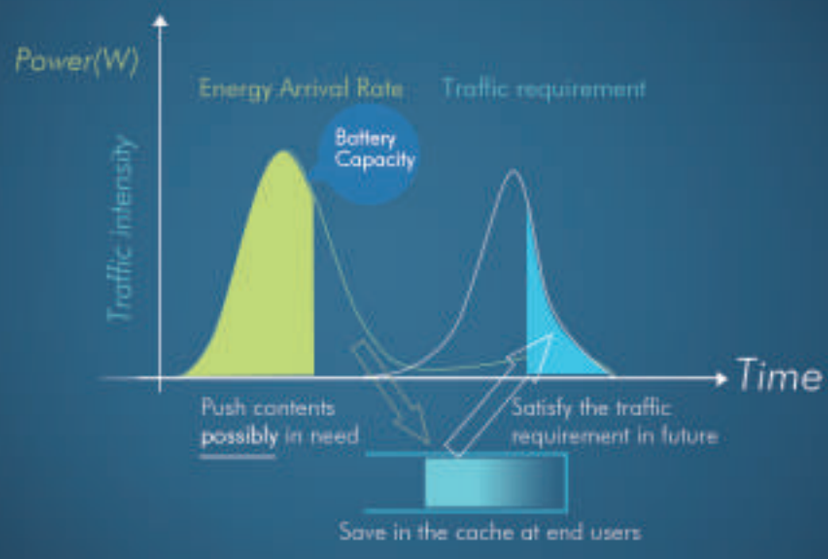

ZTE中兴 ZTE COMMUNICATIONS 中兴通讯技术(英文版)

VOLUME 16 NUMBER 1 FEBRUARY 2018

ZTE Communications Editorial Board

CONTENTS

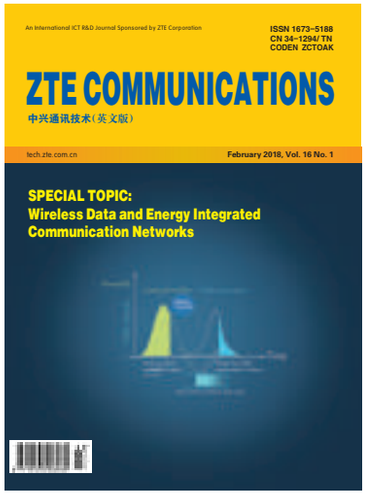

Special Topic: Wireless Data and Energy Integrated Communication Networks

CONTENTS

ZTE COMMUNICATIONS
Vol. 16 No. 1 (Issue 61)
Quarterly
First English Issue Published in 2003

Supervised by:
Anhui Science and Technology Department

Sponsored by:
Anhui Science and Technology Information Research Institute;
Magazine House of ZTE Communications

Published and Circulated (Home and Abroad) by:
Magazine House of ZTE Communications

Staff Members:
Editor-in-Chief: CHEN Jie
Executive Associate Editor-in-Chief: HUANG Xinming
Editor-in-Charge: ZHU Li
Editors: XU Ye and LU Dan
Producer: YU Gang
Circulation Executive: WANG Pingping
Assistant: WANG Kun

Editorial Correspondence:
Add: 12F Kaixuan Building,
329 Jinzhai Road,
Hefei 230061, China
Tel: +86-551-65533356
Fax: +86-551-65850139
Email: magazine@zte.com.cn

Printed by:
Hefei Tiancai Color Printing Company

Publication Date:
February 25, 2018

Publication Licenses:
ISSN 1673-5188
CN 34-1294/ TN

Annual Subscription:
RMB 80

DOI: 10.3969/j.issn.1673-5188.2018.01.001
http://kns.cnki.net/kcms/detail/34.1294.TN.20180201.1735.004.html, published online February 1, 2018

Editorial

Wireless Data and Energy Integrated Communication Networks

▶ Guest Editors

YANG Kun received his Ph.D. from the Department of Electronic & Electrical Engineering of University College London (UCL), UK, and M.Sc. and B.Sc. from the Computer Science Department of Jilin University, China. He is currently a chair professor in the School of Computer Science & Electronic Engineering, University of Essex, UK, leading the Network Convergence Laboratory (NCL). He is also an affiliated full professor at University of Electronic Science and Technology of China. Before joining in University of Essex at 2003, he worked at UCL on several European Union (EU) research projects for several years. His main research interests include wireless networks, future Internet technology and network virtualization, mobile cloud computing and networking. He manages research projects funded by various sources such as UK EPSRC, EU FP7/H2020 and industries. He has published 100+ journal papers in addition to 80+ conference papers. He is a senior member of IEEE and a fellow of IET. He serves on the editorial boards of both IEEE and non-IEEE journals (Wiley and Springer) and have guest-edited several special issues in the above research areas. He has also served as (co-)chair (general or TPC) in many IEEE conferences.

HU Jie received his B.Eng. and M.Sc. degrees from Beijing University of Posts and Telecommunications, China in 2008 and 2011, respectively, and received the Ph.D. degree from the Faculty of Physical Sciences and Engineering, University of Southampton, UK in 2015. Since March 2016, he has been working with the School of Communication and Information Engineering, University of Electronic Science and Technology of China, as an associate professor. His research is being funded by National Natural Science Foundation of China (NSFC). He is also in great partnership with industry, such as ZTE and Huawei. He has a broad range of interests in wireless communication and networking, such as cognitive radio and cognitive networks, mobile social networks, data and energy integrated networks as well as communication and computation convergence.

In the vision of the incoming 5G era, billions of people as well as trillions of machines are expected to be connected by the next generation mobile network. However, functions of massive communication devices have been substantially limited by insufficient power supply. As an efficient solution, dedicated RF signals are capable of carrying well-controlled energy towards the rechargeable devices in order to achieve on-demand energy transfer. Although RF signals are capable of simultaneously carrying both data and energy, diverse requirements of data and energy transfers pose huge challenges in their effective integration. For example, the energy receiver and the data receiver have diverse sensitivity to the received power. The received power as low as −80 dBm is sufficient for recovering contaminated packets, thanks to the-state-of-the-art channel encoding/decoding techniques. However, only when the received power is higher than −20 dBm, the energy reception circuit can be effectively activated for converting a fraction of the energy carried by RF signals to the direct current (DC).

As a result, the integration of wireless data and energy transfer is worth deep exploration. For the implementation of RF-based energy transfer, we have to make the energy receiver adapt to a wider range of the received power, while increasing RF-DC conversion efficiency. The advanced transceiver for integrated data and energy transfer/reception is also required in the physical layer. The coexistence of multiple energy and data transmitters/receivers calls for deep exploration on interference management schemes, medium access control (MAC) algorithms as well as data/energy routing protocols, which systematically yield data and energy integrated communication networks (DEINs).

This special issue aims for educating about, promoting and accelerating technical evolution towards the promising and exciting research area of DEINs.

The most fundamental for the DEIN implementation is hardware design for the energy reception. Therefore, in this special issue, LI Zhenbing et al. design an ultra-low power high-efficiency wireless energy harvester operating in the UHF band. Furthermore, in order to extend the lifetime of the future IoT, an RF energy harvesting tag operating in the UHF band is designed by LI Gang et al. for powering the batteryless IoT devices in the next generation of cellular networks.

The DEIN basic function is to jointly coordinate energy and information flows. GONG Jie et al. thus propose a new paradigm for energy harvesting aided communications. They exploit the correlations of energy and information in cellular networks for guaranteeing abundant energy flows to the areas having intense communication demands.

Relying on the RF signals for conveying both the energy and information imposes great challenges for the system design. LIU Binghong et al. provide a thorough survey on the latest advances of the simultaneous wireless information and power transfer in cellular networks. By further considering security issues in the DEIN, Alexander Okandeji et al. design an optimal beamforming scheme for maximising the secrecy throughput in a full-duplex aided MISO system.

The aforementioned five excellent works have solved a range of key challenges of the integrated data and energy transfer, which includes the hardware implementation issue, the transceiver design in the physical layer, and the resource allocation in the MAC layer. We hope that these pioneering works may stimulate the interests of both the academia and industry in the promising research of DEIN.

DOI: 10.3969/j.issn.1673-5188.2018.01.002
http://kns.cnki.net/kcms/detail/34.1294.TN.20180321.1610.004.html, published online March 21, 2018

Ultra-Low Power High-Efficiency UHF-Band Wireless Energy Harvesting Circuit Design and Experiment

LI Zhenbing, LI Jian, ZHOU Jie, ZHAO Fading, and WEN Guangjun
(Centre for RFIC and System, School of Communication and Information Engineering, University of Electronic Science and Technology of China, Chengdu 611731, China)

Abstract

In this paper, an ultra-low power high-efficiency ultra-high frequency (UHF)-band wireless energy harvesting circuit based on the diode SMS7360 is designed and experimentally demonstrated, being operated in all released Global System for Mobile Communications (GSM) bands in China (GSM900 band: 0.87–0.96 GHz and GSM1800 band: 1.71–1.86 GHz). This UHF-band wireless energy harvesting circuit can harvest energy at 0.87–0.96 GHz and 1.71–1.86 GHz bands simultaneously in outdoor or indoor environment. The test results show that a radio-frequency (RF)-to-direct-current (DC) conversion efficiency in the range of 20%–63.2% is obtained for an available input power of −22 dBm to 1 dBm in GSM900 band and that in the range of 13.8%–55.5% is achieved for an available input power of −22 dBm to 3 dBm in GSM1800 band. The harvested RF energy is converted into DC energy and be stored in a 6.8 mF super capacitor through the energy management circuit. This super capacitor's capacity is more than 20 mJ, which can meet the demand of high-speed broadband wireless communication transceivers. This ultra-low power high-efficiency UHF-band wireless energy harvesting circuit could be used to achieve the low power wireless sensor network node (tag).

Keywords

GSM900; GSM1800; rectifier; RF energy harvesting; wireless sensor network

1 Introduction

As one of the world's top ten technologies, network sensor technology has been widely researched. The wireless sensor network (WSN) nodes were powered by the non-rechargeable battery which would severely limit the development of wireless sensor network techniques. Energy harvesting WSN (EH-WSN) utilizes energy harvesting technology to collect the available energy in the environment to power the whole system, which can effectively reduce the energy limitation of the sensor nodes.

Unlike most of the energy sources, the raido frequency (RF) energy sources are continuously available in the atmosphere environment. However, the power density of space RF sources is very low [1]. For example, when the distance from a China Mobile Communications Corporation (CMCC) GSM base station to the receiver is 60 meters, the wireless power intensity is 5.25 μW/cm^2; when the distance from a China Unicom GSM base station to the receiver is 70 meters, the wireless power intensity is 5.94 μW/cm^2 [2]. Moreover, if the antenna aperture is 50 cm^2, such wireless power that can meet the rectifying circuits is about -22 dBm.

Previous works on RF harvesting circuits focused on a single operating frequency [3], [5], [6]. When multiple RF energy sources are available, the amount of harvested energy can be increased if the system is designed to work in multiple frequency bands [4] as proposed in this paper. From theory analysis supported by simulation results and measurements, an ultra-low power (-22 dBm) high-efficiency UHF-band wireless energy harvesting circuit has been designed to work at the GSM900 and GSM1800 bands. The GSM900 entire band is from 870 MHz to 960 MHz including uplink (UL) and downlink (DL) modes. The DCS1800 is from 1710 MHz to 1880 MHz (including UL and DL modes). Finally, the harvested energy is stored in the super capacitor through the energy management circuit BQ25570.

This paper is organized as follows. Section 2 presents the state-of-the-art research progress and the rectifier impact on

This work was supported in part by Guangdong Provincial Science and Technology Planning Program (Industrial High-Tech Field) of China under Grant No.2016A010101036, and in part by Sichuan Provincial Science and Technology Planning Program (Technology Supporting Plan) of China under Grant Nos.2016GZ0061, 2016GZ0116 and 2017GZ0336, in part by the Fundamental Research Funds for the Central Universities under Grant No. ZYGX2016Z011, in part by the National Natural Science Foundation of China under Grant Nos .61371047, 61601093 and 61701082, and in part by Science and Technology on Electronic Information Control Laboratory.

the multiband RF harvester architecture. Section 3 explains the designed rectifier in the dual-band RF harvester and presents the dual-band RF harvester simulations. Section 4 shows the dual-band RF harvester experiments and measurements. Section 5 concludes this work.

2 State-of-the-Art: Rectifier Impact on Multiband RF Harvester Architecture

The goal of a wireless energy harvesting circuit (RF energy harvester) is to convert the RF energy received from ambient RF sources (GSM900/GSM1800 in this paper) into direct current (DC) power. A typical wireless energy harvesting circuit consists of a receiving antenna followed by an RF band-pass filter, a rectifier, a low-pass filter, and a load. Many of the previous studies are single band RF harvesting circuits [3], [5], [6] while some other studies use multi-band RF harvesting circuits [4]. However, when the operating frequency is changed from the optimal resonance frequency, a single-band harvesting circuit is not suitable to supply the sensor, since mismatching between the source and the rectifying circuits will degrade the rectification efficiency. In fact, the predominant frequencies may be different in different locations. Therefore, a multi-band energy harvesting circuit is more desirable. Some works have reported on multi-band structures [4], [7]–[13]. This type of energy harvester benefits from the accumulation of RF radiation for several frequencies and a higher amount of energy can be harvested [9].

2.1 Dual-Band RF Harvester Topology Choice

In order to harvest energy from GSM900 and GSM1800 RF bands, several RF harvester topologies should be investigated. The main difference among these topologies is the design of RF band-pass filter. The role of the RF band-pass filter is to match the antenna impedance and the conjugate impedance of the rectifier circuit. In the previous studies, there are two common topologies, as shown in **Fig. 1a** and **Fig. 1b**.

In the first topology, the RF bandpass filter covers a large bandwidth; however, its shortcoming is significant. As we all know, the rectifier circuit input impedance with the antenna impedance varies as a function of the frequency and the incident power. The impedance mismatch will undoubtedly affect the RF-to-DC conversion efficiency. As shown in Fig. 1a, the RF-to-DC conversion efficiency is 8% at 1550 MHz RF band, when the incident power is 20 dBm [11]. However, this efficiency is 15% in [8] with the same incident power and same topology, but at 300 MHz RF band. Because our harvester is designed for GSM900 and GSM1800 bands, we cannot use this topology.

For the second one, its RF band-pass filter is a multi-band band-pass filter (Fig. 1b), and many designs [6], [11], [13], [14] have used this architecture. The complexity of RF band-pass filter will affect the RF-to-DC conversion efficiency and make the circuit design more difficult. The filter components are im-

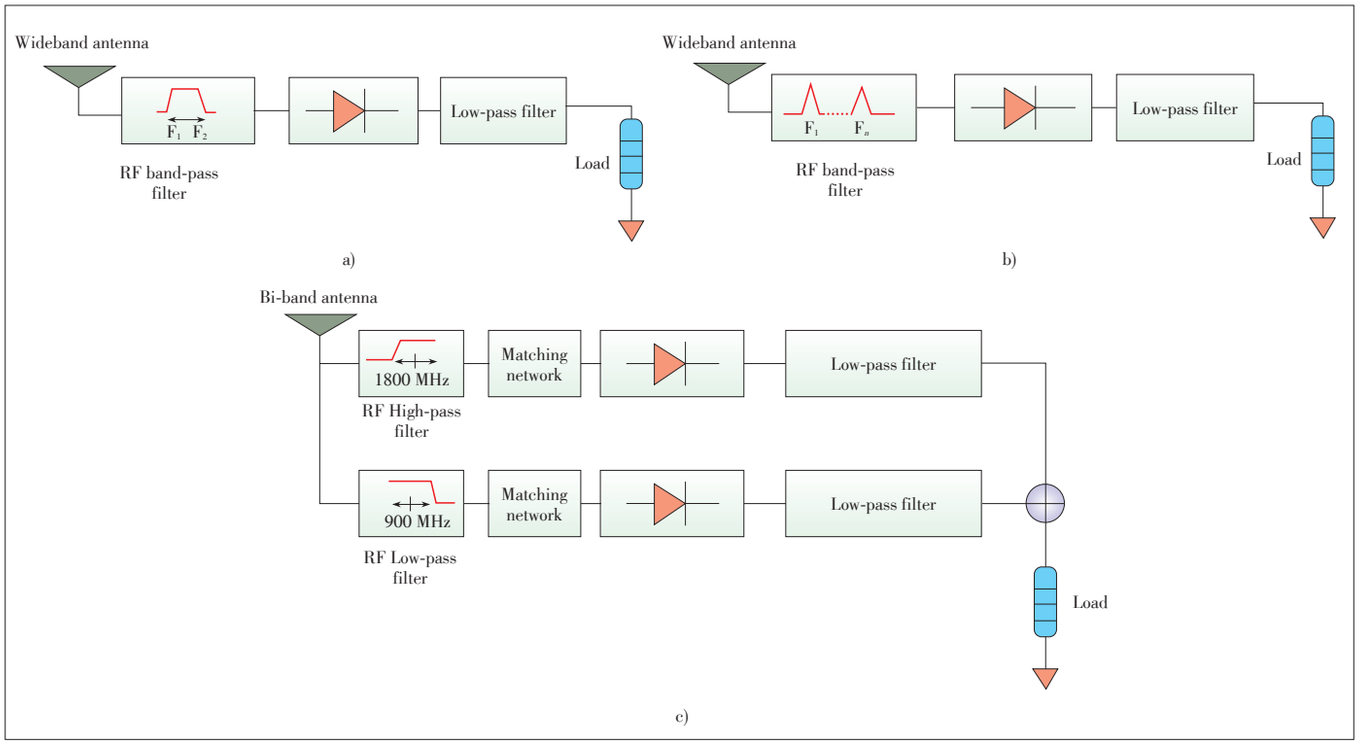

▲Figure 1. Multi-band RF harvesters a) with only one designed broadband RF band-pass filter, b) for a multi-band band-pass circuit, and c) in the proposed architecture in this paper.

portant for obtaining the correct adaptations between the antenna and the rectifier.

RF energy around multiple frequencies can be harvested by stacking several rectifier circuits. In this case, a structure for four bands with RF-to-DC efficiency up to 84% is proposed in [4]. Based on the similar idea, Fig. 1c illustrates the architecture proposed in this paper, which is for GSM900 and GSM1800 bands. The diplexer (a RF high-pass filter or a RF low-pass filter), the matching network, the rectifier, and the low-pass filter compose an RF branch (Fig. 1c). In this paper, we will not focus on the design of the dual-band antenna. The input of a diplexer is connected to a single access dual-band antenna, in order to match two parallel rectifiers at the dedicated frequencies. This structure is more compact. There is a matching network circuit between the diplexer and rectifier in each branch to allow the maximum energy to reach input of the rectifier to improve the RF-to-DC conversion efficiency. Finally, the rectifier branch DC output is connected to the load (one independent load for each or a shared one). Any RF signals must be blocked by a low-pass filter which is connected at the end of rectifier, so this structure only allows the DC component to pass through.

2.2 Voltage Doubler Rectifier Topology Choice

There are several rectifier topologies which depend on the incident power and frequency (**Fig. 2**). Fig. 2a shows the series topology. This topology is suitable for the situations of low input power [12]–[14]. Fig. 2c is the Greinacher topology [7]. This topology has a higher output DC voltage levels. However, it has twice as many diodes as a voltage doubler (Fig. 2b) and four times more than a series rectifier. In the case of outdoor applications, the number of rectifier's diodes must be limited as the RF density power is low, thus the Greinacher rectifier is not a good candidate. The voltage doubler topology is chosen to maintain high RF-to-DC conversion efficiency at low RF input power while maximizing the output DC voltage of rectifier. The voltage doubler topology has a higher output voltage than the series topology and helps implement cold/hot start of the subsequent DC-DC boost devices, so that it gets the sensitivity of minimum input RF power and the voltage doubler's diode number is just two. Based on these discussions, the voltage doubler topology is selected.

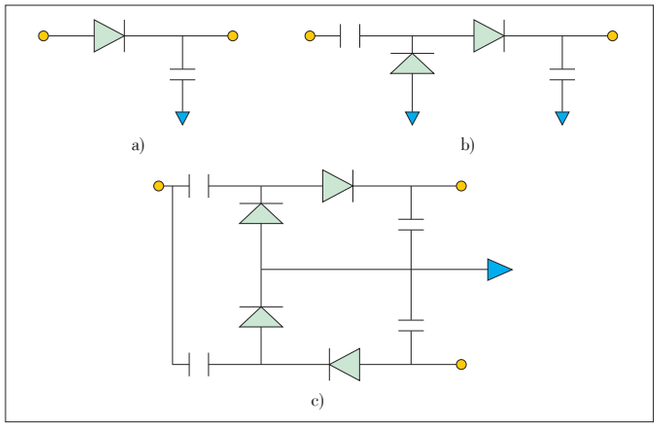

▲Figure 2. Three topologies of rectifier: a) series, b) voltage doubler, and c) Greinacher.

3 Dual-Band RF Harvester Design and Simulations

The ultra-low power high-efficiency UHF-band wireless energy harvesting circuit (**Fig. 3**) consists of five major parts: diplexer, matching networks, rectifiers, BQ25570 and its peripheral circuit diagram, and super capacitor.

3.1 Diplexer Design

The diplexer consists of a high-pass filter and a low-pass filter and is located between the antenna and the matching network. The ambient RF energy is divided into two parts, respectively located in the GSM900MHz and GSM1800MHz bands after RF energy through the diplexer. Since this novel design will not reduce the incident energy of each branch, it can improve the RF-to-DC conversion efficiency and output voltage.

This diplexer circuit is to divide the GSM900/GSM1800 signal energy collected by antenna into two branches: the 870–960 MHz output connected to the GSM900 rectifier circuit and the 1710–1860 MHz output connected to the GSM1800 RF-DC rectifier circuit. The input and output impedance of the diplexer is matched to 50 Ω.

3.2 Diplexer Simulation Setup in ADS

The diplexer was simulated using the Advanced Design System (ADS) software from Agilent Technologies.

The return loss of the diplexer circuit's RF input port is larger than 18 dB in the 100–3000 MHz band, larger than 22 dB in the GSM900 band, and larger than 18 dB in the GSM1800 band. Furthermore, the return loss of the RF output port (GSM900 band) is larger than 20 dB, while the insertion loss of the input port and the RF output port (GSM900 band) is less than 0.3 dB. The return loss of the RF output port (GSM1800 band) is larger than 17 dB, while the insertion loss of the input port and the RF output port (GSM1800 band) is less than 0.3 dB. Finally, the minimum isolation between RF GSM900 output port and GSM1800 output port is greater than 8 dB (1100–1500 MHz).

3.3 Matching Network Design

We next focus on the design of the matching network. Thanks to the maximum power transfer theory, the highest power can be transferred to the load if the source and load complex impedances are complex conjugates. This is achieved by means of an impedance matching network placed between the diplexer and the rectifier. Whenever a source or a load has a reactive component, the adaptation depends on the frequency

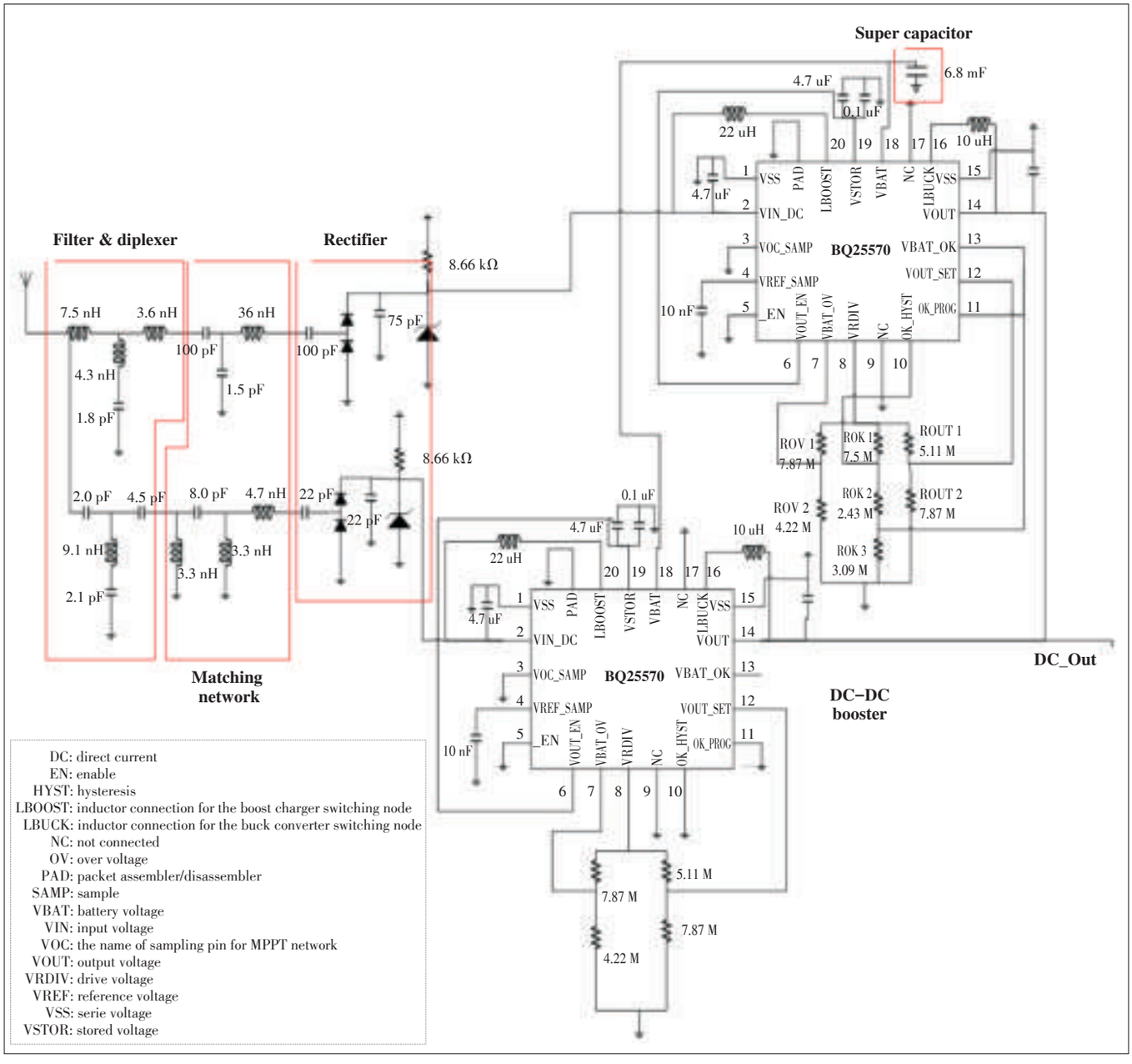

▲Figure 3. Wireless energy harvesting circuit schematic diagram.

for which it is designed. The most frequently used matching networks are the L-type, the Π-type and the T-type networks [14]. With the aid of ADS, we get the T-type matching network for GSM900 and the Π-type matching network for GSM1800, and the specific parameters are shown in Fig. 3.

3.4 Matching Network Simulation Setup in ADS

These matching networks were simulated by ADS and the simulation results are shown in **Fig. 4**.

Based on the simulation results, the return loss (S11) of the GSM1800 matching network and that of the GSM900 matching network are larger than 13 dB in the GSM900/GSM1800 band.

3.5 Dual-Band RF Harvester Design

In order to obtain higher rectification efficiency from low power incident RF sources, we choose one-stage voltage doubler rectifier circuits. The overall design of the dual-band RF harvester is shown in Fig. 3. At the end of the rectifier in the figure, a Zener diode is connected parallel to limit the voltage for protecting the follow-up circuit. Finally, the end of the circuit is an 8.66 kΩ load. We must point out that the resistance is only required under the test environment and it is not includ-

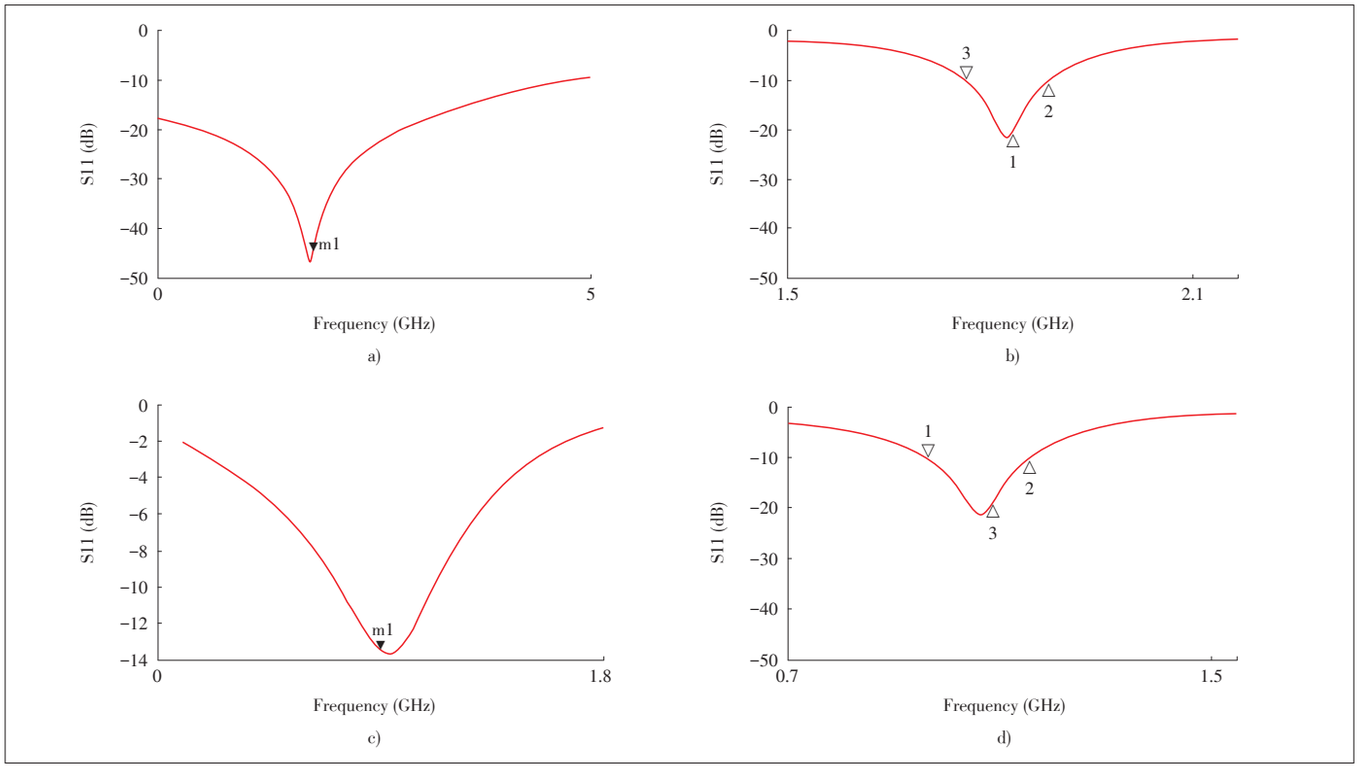

▲Figure 4. a) The simulation results of GSM1800 matching network; b) the test results of GSM1800 matching network; c) the simulation results of GSM900 matching network; d) the test results of GSM900 matching network.

ed in the actual tag.

3.6 Dual-Band RF Harvester Simulation Setup in ADS

The dual-band RF harvester was simulated by the ADS. In the cases of different incident power levels with the same frequency and different frequencies with the same incident power, the RF-to-DC conversion efficiency was simulated (**Fig. 5**).

Based on the simulation results, when the RF incident power is greater than - 14 dBm, the DC output voltage of GSM900MHz rectifier circuit in the 850–950 MHz bandwidth is greater than 0.365 V, and the efficiency is higher than 39%. This voltage meets energy management circuit BQ25570's cold start condition. The DC output voltage of GSM1800MHz rectifier circuit in the 1800–1860 MHz bandwidth is greater than 0.370 V, and the efficiency is higher than 40%. This voltage also meets energy management circuit BQ25570's cold start condition.

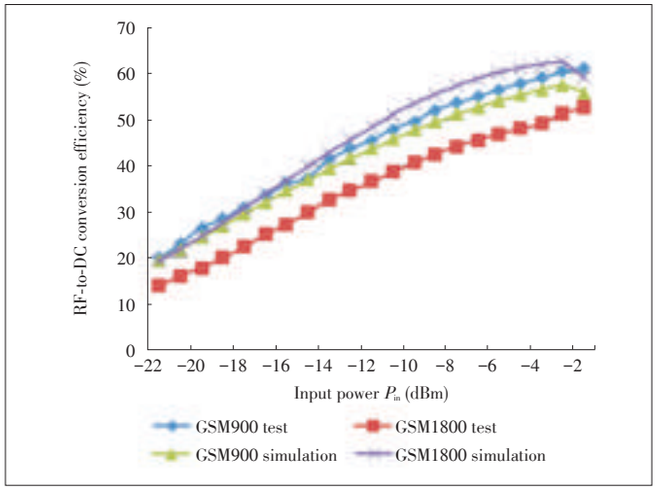

▲Figure 5. The RF-to-DC conversion efficiency of the GSM900/GSM1800 branch varies with the input power.

3.7 DC-DC Boost and Energy Management Circuit

The DC-DC boost and energy management circuit use two BQ25570s as core components, and the input ports are connected to the output of GSM900 rectifier circuit and the output of GSM1800 rectifier circuit, respectively. The output is the power supply for other chips. These two BQ25570s' pin VBATs are connected in parallel to a 6.8 mF super capacitor.

To prevent rechargeable batteries from being exposed to excessive charging voltages and to prevent overcharging a capacitive storage element, the over-voltage (*VBAT_OV*) threshold level can be set based on (1) using two external resistors (R_{OV1}, R_{OV2}), where *VBIAS*=1.21 V.

$$VBAT\_OV = \frac{3}{2}VBIAS\left(1+\frac{R_{ov2}}{R_{ov1}}\right). \quad (1)$$

Battery voltage within operating range (VBAT_OK Output)

can be set based on (2) and (3) through external three resistors (R_{OK1}, R_{OK2}, R_{OK3}).

$$VBAT\_OK\_PROG = VBIAS\left(1 + \frac{R_{OK2}}{R_{OK1}}\right), \quad (2)$$

$$VBAT\_OK\_HYST = VBIAS\left(1 + \frac{R_{OK1} + R_{OK2}}{R_{OK1}}\right). \quad (3)$$

The OUT regulation voltage (V_{OUT}) is then given by (4):

$$V_{OUT} = VBIAS\left(\frac{R_{OUT2} + R_{OUT1}}{R_{OUT1}}\right). \quad (4)$$

The V_{OUT} output pin can be used directly as the supply voltage for other chips without the aid of low dropout regulator (LDO).

4 Dual-Band RF Harvester Experiments and Measurements

To validate the approach described in the previous section, the following experiments were performed.

4.1 Diplexer Measurements

The diplexer was tested using the vector network analyzer. The diplexer has three ports, one input port and two output ports. We used a vector network analyzer and a 50 Ω load to experiment.

The return loss of the diplexer circuit's RF input port is larger than 7 dB in the 600–24,000 MHz band, larger than 34 dB in the GSM900 band, and larger than 16 dB in the GSM1800 band. Furthermore, the return loss of the RF output port (GSM900 band) is larger than 5 dB, while the insertion loss of the input port and the RF output port (GSM900 band) is less than 0.7 dB. The return loss of the RF output port (GSM1800 band) is larger than 20 dB, while the insertion loss of the input port and the RF output port (GSM1800 band) is less than 0.8 dB. Finally, the minimum isolation between RF GSM900 output port and GSM1800 output port is greater than 16 dB (1100–1500 MHz). The comparisons between simulations and test results indicate that these test results can validate the simulation values.

4.2 Matching Network Measurements

The matching network was tested using the same vector network analyzer. The front end of the matching network was connected to the vector network analyzer, and the back end of the matching network was connected to the rectifier circuit and the load. Therefore, S11 represents the degree of matching. Fig. 4 shows the test results.

Based on the test results, S11 of the GSM1800 matching network and that of the GSM900 matching network are larger than 13 dB in the GSM900/GSM1800 band.

4.3 Dual-Band RF-DC Rectifier Circuit Measurements

Then, we tested the ultra-low power high-efficiency UHF-band wireless energy harvesting circuit's RF-to-DC conversion efficiency. The test contained three parts: a) The GSM900 branch test, b) the GSM1800 branch test, and c) the GSM900+GSM1800 combined test.

First of all, we tested the RF-to-DC conversion efficiency of the GSM900 branch. The test system is built as shown in **Fig. 6b**. We connected the signal source directly to the input port of the GSM900's matching circuit, and then used the multimeter to observe the voltage on the load which was connected at the end of the GSM900 branch to calculate the RF-to-DC conversion efficiency.

In the GSM900 branch rectifier circuit, it could be seen that the RF-to-DC conversion efficiency reached 40.5% when the input power was −14 dBm, and the voltage across the load was 375 mV. This voltage meets BQ25570's cold start condition. In the case that the input power was 1 dBm, the RF-to-DC conversion efficiency reached 63.2%, while in the case that the low input power was −22 dBm, the RF-to-DC conversion efficiency reached 20%. Fig. 5 shows that the RF-to-DC conversion efficiency of the GSM900 branch varies with different input power.

The RF-to-DC conversion efficiency of the GSM900 branch varies with the frequency of the GSM900 band. When the frequency is 880 MHz, the RF-to-DC conversion efficiency of GSM900 is the highest which reaches to 41%.

Then, we tested the RF-to-DC conversion efficiency of the GSM1800 branch. The test system is built as shown in **Fig. 6a**. We connected the signal source directly to the input port of the GSM1800's matching circuit, and then used the multimeter to observe the voltage on the load which was connected at the end of the GSM1800 branch to calculate the RF-to-DC conversion efficiency.

Based on the test results, on the GSM1800 branch rectifier circuit, when the input power was -14 dBm, the RF-to-DC conversion efficiency reached 32.6%, and the voltage across the load was 335.7 mV. This voltage meets BQ25570's cold start condition. When the input power was 3 dBm, the RF-to-DC conversion efficiency reached 55.5%, and when the input power is -22 dBm, the RF-to-DC conversion efficiency reached 13.8%. Fig. 5 shows the RF-to-DC conversion efficiency of the GSM1800 branch varies with different input power.

The RF-to-DC conversion efficiency of the GSM1800 branch varies also with the frequency of the GSM1800 band, in the case that the input power is -14 dBm. When the frequency is 1770 MHz, the RF-to-DC conversion efficiency of GSM1800is the highest that reaches to 33.3%.

Finally, we tested the RF-to-DC conversion efficiency of the combined GSM900 and GSM1800 branches. The test system is

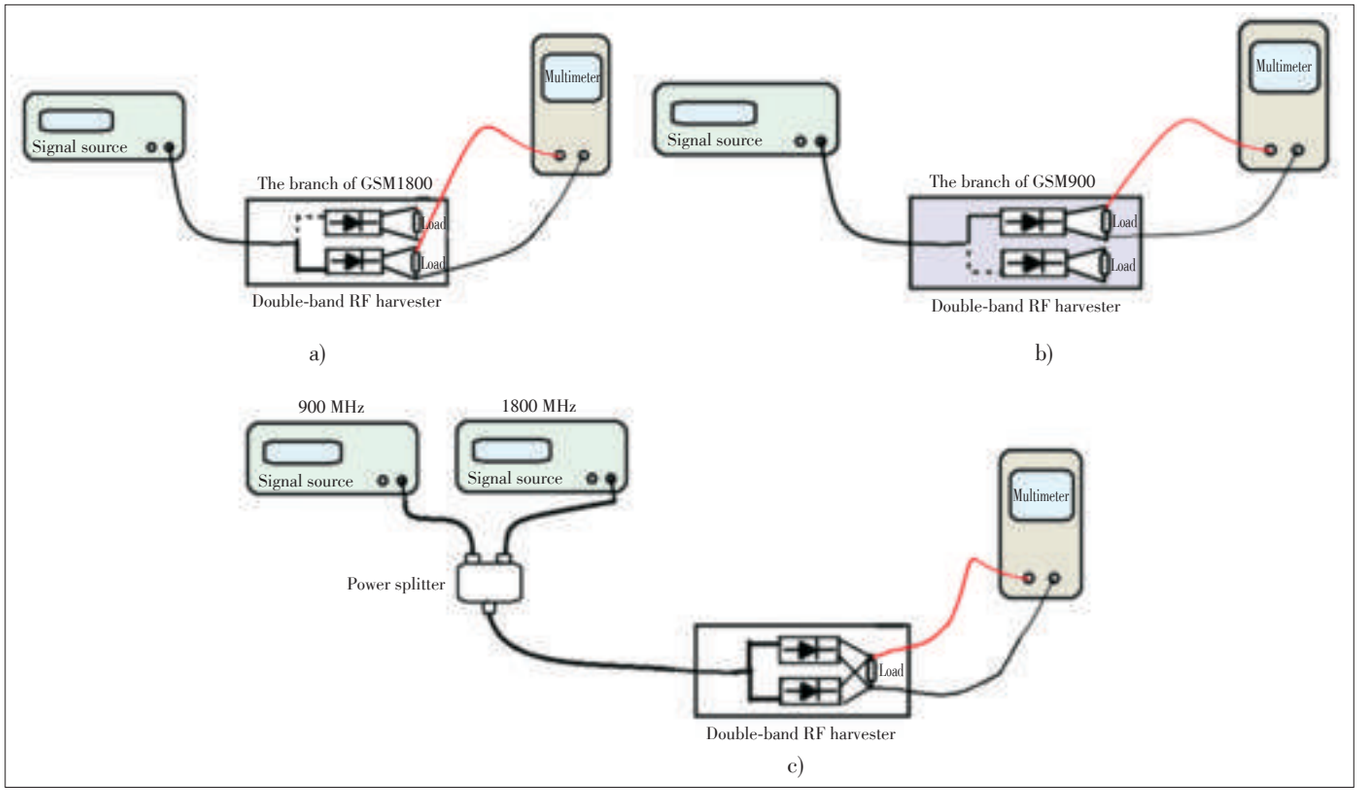

▲Figure 6. a) The test system of GSM1800, b) the test system of GSM900, and c) the test system of GSM900+GSM1800.

built as shown in Fig. 6c. We connected two signal sources and a power splitter to the input port of the diplexer, and then used the multimeter to observe the voltage on load.

Based on test results, in the case that both two input powers are -14 dBm (Double -14 dBm input powers equal to -11 dBm), the RF-to-DC conversion efficiency reaches 29.5%, due to the insertion loss of the diplexer. The voltage across the load is 451 mV, and this voltage meets BQ25570's cold start condition. In the case that the input power is 0 dBm, the RF-to-DC conversion efficiency reaches 42.7%, and in the case that the input power is -22 dBm, the RF-to-DC conversion efficiency reaches 11.7%.

Fig. 7 shows the RF-to-DC conversion efficiency of the combined GSM1800 and GSM900 branches varies with the changes of the input power.

The test results of RF-to-DC conversion efficiency of GSM900/GSM1800 which varies with the input power are basically the same as the simulation results with small difference. In the branch of GSM900 and that of GSM1800, the average difference between test results and simulation results is only 1.7% and 11.4% respectively. The test results of RF-to-DC conversion efficiency GSM900/GSM1800 which varies with frequency are also basically the same as the simulation results with small difference. In the branch of GSM900 and that of GSM1800, the average difference between test results and simulation results is only 5.46% and 11.46% respectively. The average difference of the branch of GSM1800 is large, but it is still in the acceptable range.

4.4 Analysis of Cold and Hot Start of BQ25570 Chip

The DC-DC boost and energy management circuits used two BQ25570 as core components, and the input were connected to the output of GSM900 rectifier circuit and the output of GSM1800 rectifier circuit respectively.

The BQ25570 device is specifically designed to efficiently extract microwatts (μW) to milliwatts (mW) of power generated

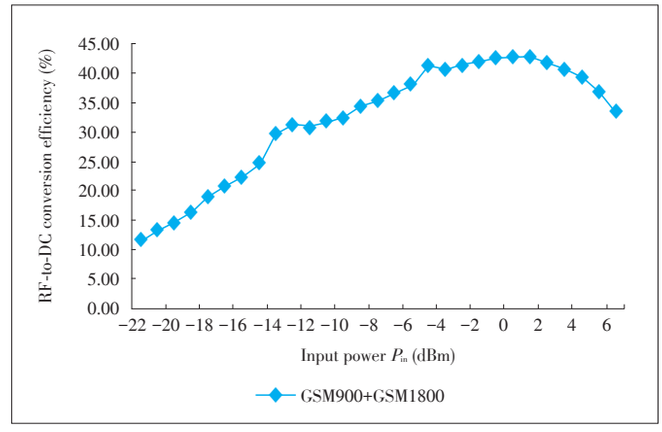

▲Figure 7. The RF-to-DC conversion efficiency of GSM900+GSM1800 varies with the input power.

from a variety of high output impedance DC sources. The boost charger can effectively extract power from low voltage output harvesters, such as our dual-band RF-DC rectifier circuit. The outputting voltages of harvesters go down to VIN(DC) (100 mV minimum), so it can be hot start. When starting from the voltage of the super capacitor < 100 mV, the cold start circuit needs at least VIN(CS), 330 mV typical to charge.

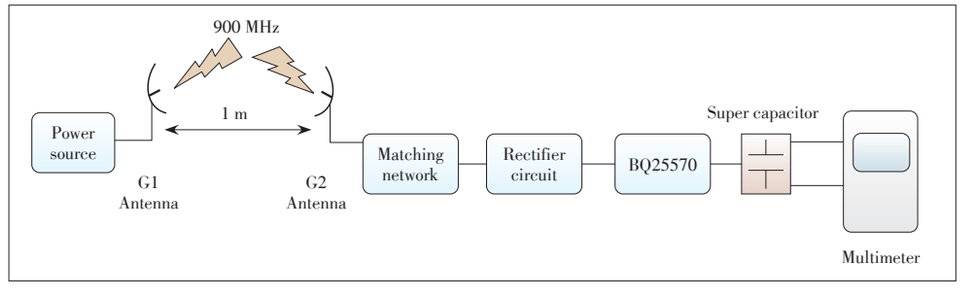

▲Figure 8. The prototype photograph of the test system.

The BQ25570 chip's DC input impedance is 8.66 kΩ which was simulated at the end of the rectifier circuit. Based on the test results of the rectifier circuit, in the case that the input power is greater than or equal to -14 dBm, the output of the GSM900/GSM1800 rectifier circuit can provide a voltage greater than 330 mV (GSM900: 375mV and GSM1800: 335mV) to cold and hot start BQ25570 chip.

4.5 Wireless Energy Charging Experiments

In order to verify the wireless charging performance of double-band RF harvester, we organized this wireless energy charging experiment. We used the method of wireless charging to charge the super capacitor on the dual-band RF harvester. The experimental system is built as shown in **Fig. 8**.

We used the R2000 reader as the power source, and connected the coaxial cable to the R2000 reader and transmitter antenna. The transmit power of R2000 reader was 30 dBm, and the gain of the transmitter antenna was 12 dBic. The receiving antenna which gain was 8 dBic was one meter away from transmitter antenna. As the reader was sending GSM900 band signal, we used the GSM900 branch rectifier circuit to charge the super capacitor. Due to the insertion loss, the diplexer was abandoned. Finally, we used the multimeter to observe the voltage in the super capacitor.

According to the Friss formula (electromagnetic wave propagation), we can calculate the power intensity at the front end of the rectifier circuit as follows.

$$Pe = P_1 + G_1 + G_2 + G_3 + 10\lg(\frac{\lambda}{4\pi r_1})^2, \quad (5)$$

where Pe is the power intensity at the front end of the rectifier circuit, P_1 is the transmit power of R2000 reader, G_1 is gain of the transmitter antenna, G_2 is gain of the receiving antenna, G_3 is the loss of pipelines (-2 dB), r_1 is distance between two antennas, and f is 900 MHz, which is used to calculate the wavelength λ. According to this formula, the Pe is 16.47 dBm.

The experimental system is built as shown in **Figs. 9** and **10**.

Based on the test results, the super capacitor was filled to the set voltage value 4.2 V in 24 seconds. This wireless energy charging experiment proves that our UHF-band wireless energy harvesting circuit can harvest wirelessly GSM900 energy and charge for supercapacitor.

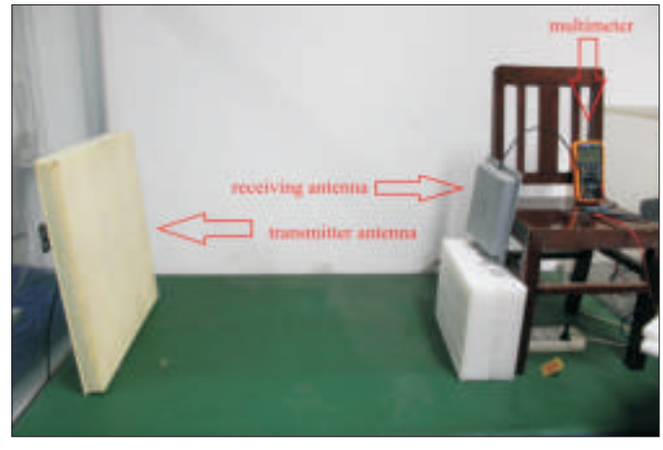

▲Figure 9. The prototype photograph of the test system.

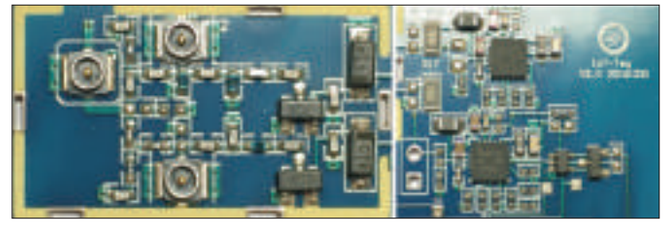

▲Figure 10. The prototype photograph of the dual-band RF harvester.

5 Conclusions

An ultra-low power high-efficiency UHF-band wireless energy harvesting circuit was designed for harvesting RF energy in the GSM900 and GSM1800 bands. This harvester features an RF-to-DC conversion efficiency in the range of 20%–63.2% for an available input power of –22 dBm to 1 dBm in the GSM900 band, and that in the range of 13.8%–55.5% for an available input power of –22 dBm to 3 dBm in the GSM1800 band. This harvester can charge the super capacitor through the energy management circuit BQ25570 in case of the input power greater than or equal to -14 dBm. Through the wireless energy charging experiments, we confirmed that this harvester could use just 24 seconds to fill the super capacitor. This ultra-low power high-efficiency UHF-band wireless energy harvest-

ing circuit has wide application prospect. For example, it can power small sensor systems, such as the wireless sensor network (WSN) nodes.

References

[1] H. J. Visser, A. C. F. Reniers, and J. A. C. Theeuwes, "Ambient RF energy scavenging: GSM and WLAN power density measurements," in *38th European Microwave Conference*, Amsterdam, Netherlands, Oct. 2008, pp. 721–724. doi: 10.1109/EUMC.2008.4751554.

[2] Y. Zhang, G. Zhang, W. Tian, et al., "Survey on urban environmental electromagnetic radiation level in a city," *Journal of Environmental Health*, vol. 22, no. 2, pp. 93–96, Mar. 2005. doi: 10.16241/j.cnki.1001-5914.2005.02.006.

[3] M. M. Tentzeris and Y. Kawahara, "Novel energy harvesting technologies for ICT applications," in *International Symposium on Applications and the Internet*, Turku, Finland, Aug. 2008, pp. 373–376. doi: 10.1109/SAINT.2008.113.

[4] V. Kuhn, C. Lahuec, F. Seguin, and C. Person, "A multi-band stacked RF energy harvester with RF-to-DC efficiency up to 84%," *IEEE Transactions on Microwave Theory and Techniques*, vol. 63, no. 5, pp. 1768–1778, May 2015. doi: 10.1109/TMTT.2015.2416233.

[5] W. Huang, B. Zhang, X. Chen, K.-M. Huang, and C.-J. Liu, "Study on an S-band rectenna array for wireless microwave power transmission," *Progress in Electromagnetics Research*, vol. 135, no.1, pp. 747–758, 2013. doi: 10.2528/PIER12120314.

[6] C. Mikeka, H. Arai, A. Georgiadis, and A. Collado, "DTV band micropower RF energy-harvesting circuit architecture and performance analysis," in *IEEE International Conference on RFID-Technologies and Applications*, Sitges, Spain, Sept. 2011, pp. 561–567. doi: 10.1109/RFID-TA.2011.6068601.

[7] D. Pavone, A. Buonanno, M. D'Urso, and F. G. Della Corte, "Design considerations for radio frequency energy harvesting devices," *Progress in Electromagnetics Research*, vol. 45, no. 45, pp. 19–35, 2012. doi: 10.2528/PIERB12062901.

[8] A. Nimo, D. Grgic, and L. M. Reindl, "Impedance optimization of wireless electromagnetic energy harvester for maximum output efficiency at W input power," in *Proc. Active and Passive Smart Structures and Integrated Systems*, San Diego, USA, 2012, vol. 8341, pp. 83410W1–14. doi: 10.1117/12.914778.

[9] V. Kuhn, F. Seguin, C. Lahuec, and C. Person, "A multi-tone RF energy harvester in body sensor area network context," in *Antennas and Propagation Conference*, Loughborough, UK, Nov. 2013, pp. 238–241. doi: 10.1109/LAPC.2013.6711891.

[10] H. Sun, Y.-X. Guo, M. He, and Z. Zhong, "A dual-band rectenna using broadband yagiantenna array for ambient RF power harvesting," *IEEE Antennas and Wireless Propagation Letters*, vol. 12, pp. 918–921, Jul. 2013. doi: 10.1109/LAWP.2013.2272873.

[11] A. Collado and A. Georgiadis, "Conformal hybrid solar and electromagnetic (EM) energy harvesting rectenna," *IEEE Transactions on Circuits and Systems I: Regular Papers*, vol. 60, no. 8, pp. 2225–2234, Aug. 2013. doi: 10.1109/TCSI.2013.2239154.

[12] M. Pinuela, P. D. Mitcheson, and S. Lucyszyn, "Ambient RF energy harvesting in urban and semi-urban environments," *IEEE Transactions on Microwave Theory and Techniques*, vol. 61, no. 7, pp. 2751–2726, May 2013. doi: 10.1109/TMTT.2013.2262687.

[13] Y. H. Suh and K. Chang, "A high-efficiency dual-frequency rectenna for 2.45- and 5.8-GHz wireless power transmission," *IEEE Transactions on Microwave Theory and Techniques*, vol. 50, no. 7, pp. 1784–1789, Aug. 2002. doi: 10.1109/TMTT.2002.800430.

[14] M. Thompson and J. K. Fidler, "Determination of the impedance matching domain of impedance matching networks," *IEEE Transactions on Circuits and Systems I: Regular Papers*, vol. 51, no. 10, pp. 2098–2106, Oct. 2004. doi: 10.1109/TCSI.2004.835682.

Manuscript received: 2017-11-09

Biographies

LI Zhenbing (thomaslizhenbing@163.com) received the B.S. and M.S. degrees in electronic for communicating system (ESCo) from the Occidental Britany University (UBO) of France in 2014 and 2016 respectively. He is currently an assistant researcher with the RFID laboratory in University of Electronic Science and Technology of China (UESTC), China. His research interests include RF, microwave and millimeter wave integrated circuits and system. His is also interested in the Internet of Things devices and system, RFID system and networks, antennas and its application in microwave engineering area. His representative publication is "W-band SIW Power Combiner/Divider Based on the Antipodal Fin-line SIW-RW Transition and Longitudinal-slot Coupling Techniques," in *Electromagnetics Research C* (vol. 72, pp. 43–54, 2017).

LI Jian (uestclijian@163.com) received the B.S., M.S. and Ph.D. degrees in communication engineering from UESTC, China in 2007, 2010, and 2015 respectively. He is currently an assistant professor with UESTC and is a visiting scholar with the University of Illinois at Urbana-Champaign, USA. His research interests include RF, microwave, and millimeter wave integrated circuits and system. He is also interested in electromagnetic metamaterial and its applications in substrate integrated waveguide.

ZHOU Jie (jie.zhou1994@hotmail.com) received the B.S. degree in electronic information engineering from Jilin University, China in 2016. She is currently working towards an M.S. degree at School of Communication & Information Engineering, UESTC, China. Her research interests include integrated RF energy harvesting systems, low-power wireless sensor network, and RFID.

ZHAO Fading (zhaofading@163.com) received his master's degree from School of Electronic Information Engineering, Southwest Petroleum University, China in 2012. He is currently working towards a Ph.D. degree at school of Communication & Information Engineering, UESTC, China. His research interests include integrated RF energy harvesting systems, low-power wireless sensor network, RFIC, and analog/mixed signal circuit design.

WEN Guangjun (wgj@uestc.edu.cn) received his M.S. and Ph.D. degrees in Chongqing University, China in 1995 and UESTC, China in 1998, respectively. He is currently a professor in UESTC. His research and industrial experience covers abroad spectrum of electromagnetics, including RF, microwave and millimeter wave integrated circuits and system design for wireless communications, navigation, identification, and mobile TV applications, RF-IC/MMIC/MMMIC device modeling, System on Chip (SoC) and System in Package (SiC) design, RF/microwave/millimeter wave power source design, the Internet of things devices and system, RFID system and networks, antennas, as well as model of electromagnetic metamaterial and its application in microwave engineering area.

DOI: 10.3969/j.issn.1673-5188.2018.01.003
http://kns.cnki.net/kcms/detail/34.1294.TN.201800319.1042.002.html, published online March 19, 2018

Design of Wireless Energy-Harvested UHF WSN Tag for Cellular IoT

LI Gang, XU Rui, LI Zhenbing, ZHOU Jie, LI Jian, and WEN Guangjun
(Centre for RFIC and System, School of Information and Communication Engineering, University of Electronic Science and Technology of China, Chengdu 611731, China)

Abstract

In this paper, a wireless energy-harvested ultra-high frequency (UHF) wireless sensor network (WSN) tag is designed and implemented for cellular IoT applications. The WSN tag is made up of a wireless energy harvesting circuit, a temperature sensing circuit, and a radio frequency identification (RFID) tag. The developed WSN tag is compatible with the ISO/IEC18000-6C protocol. The WSN tag can receive the GSM RF energy operating in China GSM900 and GSM1800 bands in the surrounding environment and the solar energy, then converts the RF energy to direct current (DC) by schottky diode-based rectifying circuit, and finally stores the DC energy in a supercapacitor through a DC-DC booster circuit. The DC-DC booster circuit drives the front-end circuit, TI MSP430 microcontroller, temperature sensing circuit, and other active circuits in the tag. The MSP430 works in low-power mode when it is powered up, and it can also reduce power consumption more by reducing main clock (MCLK) frequency according to different forward link rates. The implemented WSN tag demonstrated that the RF-to-DC conversion efficiency is higher than 39% when the receiving 900 MHz RF signal power is from -14 dBm to 0 dBm and could make the tag work normally. The signal receiving sensitivity of the WSN tag is up to -32 dBm at the rate of 40 kbit/s from the Reader to the WSN tag. The WSN tag supports Miller coding and extended Miller coding. This wireless energy harvested UHF WSN tag, compared with conventional UHF passive tags and battery-powered active UHF RFID Tags, has many advantages, such as far communication distance, long service life, and sensing functionality. It will have wide applications in the Internet of Things (IoT).

Keywords

DC-DC booster circuit; MSP430; RF energy harvest; WSN tag

1 Introduction

Radio frequency identification (RFID) is a well-known non-contact automatic identification technology widely used in identification, supply chain, logistics, retail, manufacturing, garment industry, medical industry, identity and anti-counterfeiting and many other related applications [1]. RFID tags can be classified as passive tags, active tags and semi-active tags. The passive tags gain the power from reader emitting out RF signal in the near distance, so it has no DC power supply [2]. Active tags have their own DC energy source and can transmit actively signal; therefore they have better performance than passive tags. Semi-active tags extract the power from their battery, and have a large operating distance.

In traditional wireless sensor network, almost all the wireless sensing nodes (it is also called as wireless sensing tags) operate in active mode or semi-active mode, they get the energy come from the rechargeable battery or other power supply. However, the rechargeable battery has the disadvantages of frequent maintenance and the limited number of charge cycles. For the advantage of battery-free operation, low-cost passive sensing tags have got much attention. A convenient solution is to provide energy for the sensing tags by harvesting ambient RF energy sources [3]. The RF energy from the environment can greatly extend the life of wireless sensor networks (WSN) [4]. The ambient RF energy is a type of new energy everywhere. Sustainability makes ambient RF energy more reliable than other types of new energy, such as solar energy and wind energy.

This work was supported in part by Guangdong Provincial Science and Technology Planning Program (Industrial High-Tech Field) of China under project contracts No. 2016A010101036, and in part by Sichuan Provincial Science and Technology Planning Program (Technology Supporting Plan) of China under project contracts No. 2016GZ0061 and No. 2016GZ0116 and No. 2017GZ0336, in part by the fundamental research funds for the Central Universities under project contract No. ZYGX2016Z011, and in part by the National Natural Science Foundation of China under project contracts No. 61371047, No. 61601093 and No. 61701082.

Many studies have been reported on energy harvesting systems operating on a single band or dual bands. The proposed techniques involve a quad-band energy harvester [5], a dual-band integrated wireless energy harvesting system [6], a rectenna operating in the GSM band [7], and a RF power harvesting system operating in GSM900 and Wi-Fi 2.45 GHz bands [8]. These techniques may be adopted to develop new battery-free wireless sensing tags and WSN. Herein, in this paper, a wireless energy-harvested ultra-high frequency (UHF) WSN tag is proposed. The WSN tag is designed to be implemented by the use of commercial discrete components, on PCB board, instead of conventional RFID ICs. The advantages of PCB design over IC design are fast design iteration time, low development cost and quickly changing the design according to the designer's intentions [9].

This paper is organized as follows. Section 2 describes the WSN tag system architecture. Section 3 details the WSN tag implementation, including the design method of tag circuits and the protocol programing procedure. Section 4 tests the WSN tag. Finally, Section 5 concludes this WSN tag design.

2 WSN Tag System Architecture

Fig. 1 shows the system structure of the proposed wireless energy-harvested UHF WSN tag. Here, the system architecture including the rectifying circuit, power manager, modulator, demodulator, sensor and baseband signal processor is described in detail below.

The rectifying circuit harvests RF energy from GSM900 and GSM1800 bands in China and is divided into two rectifier branches utilizing a diplexer, which has high pass and low pass filter functions. The RF-to-DC conversion efficiency is in the range of 20%–63.2% while the input power is in the range of −22 dBm to 1 dBm in GSM900 band, and in the range of 13.8%–55.5% while the input power is in the range of −22 dBm to 3 dBm in GSM1800 band. The solar panel collects solar energy and directly connects the output to the DC booster.

The cold start voltage of the direct current (DC) booster, regulator and power manager circuit is 330 mV [10]. The DC booster circuit harvests energy from the rectifier circuit, charges the supercapacitor, and stops to charge when the voltage is up to the threshold. The threshold can be determined by setting the external resistors of the DC booster chip.

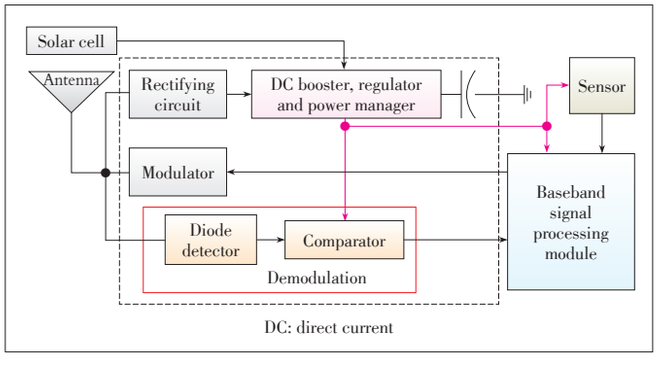

▲Figure 1. The proposed wireless energy-harvesting UHF WSN tag scheme.

The modulator controls the state of impedance matching by using gate-controlled metal oxide semiconductor (MOS). The microcontroller unit (MCU) outputs low level signal to make the impedance match and outputs high level signal to make the impedance mismatch. The WSN tag backscatters the RF signal to the reader, and the reader determines whether the reply signal of the tag is high or low according to the reflecting RF energy. The demodulator circuit consists of a diode detector and a comparator. The demodulation circuit uses the Schottky diode. The comparator uses the low voltage comparator chip.

The baseband signal processor implements the ISO/IEC 18000-6C protocol standard, and the detailed design process is described in section 3. The temperature sensor is used to detect temperature in the ambient environment. The temperature sensor can operate at a supply voltage as low as 1.5 V, while operating over the wide temperature range of −50 ℃ to +150 ℃. The temperature sensor delivers an output voltage that is inversely proportional to the measured temperature, and its low supply current makes it ideal for battery-powered systems as well as general temperature sensing applications [11]. In the WSN tag, the gain selects (GS) of the temperature sensor are both set to zero, so the voltage output can be approximately expressed as follows.

$$V=(-5.50\ \text{mV}/^{\circ}C)\times T+1035\ \text{mV}. \quad (1)$$

3 WSN Tag Implementation

In this paper, the onboard MSP430FR5969 microcontroller is responsible to achieve a WSN Tag [12]. The MCU has ultra-low power consumption features, which is widely used in the pre-research of low-power systems. The WSN tag achieves the ISO/IEC18000-6C protocol standard and can be identified by Impinj R420 reader.

The most difficult aspect of a WSN tag is to meet the timing requirement and reduce the power consumption at the same time. It is essential to have a high efficient programming method for the low power requirements. The proposed system reduces MCLK and operates alternately between the low power mode and the active mode to improve the tag performance. The WSN tag supports all the mandatory commands specified in the ISO/IEC 18000-6C protocol and adds a low speed mode (less than 40 kbit/s) to the general ISO/IEC18000-6C protocol. Simultaneously, the WSN tag extends Miller coding function [13]. The low-speed mode is used to reduce power consumption, so that the main clock operating frequency is lower. The extended miller subcarriers can reduce interference. The WSN tag protocol implementation flow chart is shown in **Fig. 2**.

In the RX_IN module in Fig. 2, the delimiter of input signal from the reader needs be detected, and the delimiter is at a low

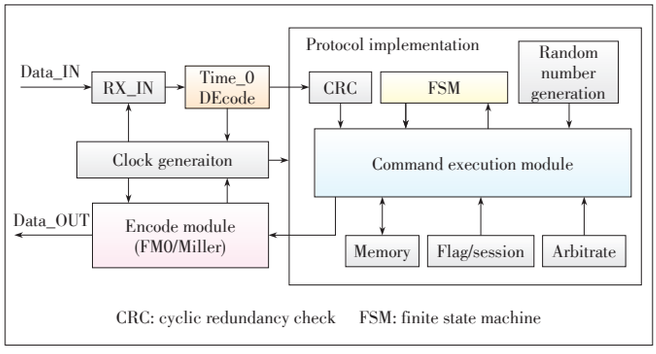

▲Figure 2. MCU achieving RFID tag protocol.

level and kept about 12.5 μs. The MCU will execute Timer_0 module when the active delimiter is detected. The Timer_0 module achieves decoding function by timer interrupt, and the MCU will start working according to the command received. The Timer_0 module is configured as a rising edge trigger to receive the input signal. The MCU will trigger the interrupt when the rising edge is detected. The interrupt routine uses the current counter value minus the value of the previous counter value to indicate the time interval between two input signals at the rising edge. In the Timer_0 interrupt routine, the time interval of two adjacent rising edges will be frequently used to determine the level of input data. The Timer_0 module decodes the forward link data, extracts the forward link rate and Rtcal/Trcal length, and provides the relevant data for the execution module. If the downlink link rate is lower than 40 kbit/s, the MCLK frequency of the MCU can be set to lower for reducing power consumption according to the length of data0.

The command execution module implements all the other functions of the WSN tag, including cyclic redundancy check (CRC), finite state machine (FSM) implementation, random number generation, arbitration module, command processing, interrupt control, timing control, working mode switching, and so on. In this paper, the sensing command of detecting the ambient temperature and humidity has been implemented. The sensing functions are very important for a WSN tag; the tag collects various sensing information and replies the information to the reader, which may analyze the sensing information to get the specific environment information.

The random number generation module generates the 16 bits pseudo-random number for the communication reliability between tags and readers. The CRC16 of the {PC+ XPC + UII} calculates at power-up which is used as the seed of the pseudo-random number. The {PC+ XPC + UII} varies in different tags, so the seeds are different too. The pseudo-random number generation algorithm also provides the pseudo-random number for the handling signal. The encoding module encodes and transmits reply data. The MCU can configure a variety of clock frequency to support the different backscatter link frequency by calling the clock generation module. At the same time, the WSN tag supports the forward and backscatter rates less than 40 kbit/s and also supports extension miller subcarrier (the Miller sequence would contain exactly 2, 4, 8, 16, 32, 64, 128 or 256 subcarrier cycles per bit). The clock generation module may set the MCU clock cycles. The highest master clock frequency, MCLK, is 16 MHz. The MCU can quickly change its MCLK frequency through its registers base on the backscatter-link frequency (BLF) parameter.

3.1 Sensing Function

The custom sensing command is used to collect almost all sensory information, including temperature information, humidity information, pressure information, and other information. **Table 1** shows the formats of the custom sensing commands and **Table 2** shows its reply formats.

The command field is defined as 0xE001. The WSN field is a parameter of the custom sensing command, and its value represents the type of sensing information. That the WSN is 1 indicates the tag will collect temperature information, and that the WSN is 2 indicates the tag will collect humidity information.

The WrEn field indicates whether the WSN tag collects the sensing information or not, and whether it writes the information collected to memory or not. If WrEn is 2'b00, it indicates that the WSN tag does not collect sensing information, reads the sensing information base on the address of the WSN tag distribution and returns sensing information to the reader. If WrEn is 2'b01, it indicates that the WSN tag does not collect sensing information, reads the sensing information base on the address of the wordPtr field and returns sensing information to the reader. If WrEn is 2'b10, it indicates that the WSN tag collects the sensing information, writes the sensing information to the assigned address by the WSN tag and returns the information to the reader. When WrEn is 2'b11, it indicates that the WSN tag collects the sensing information, writes the sensing information to the address of WordPtr field and returns the sens-

▼Table 1. The sensor command formats

	Bits	Description
Command	16	0xE001
WSN	16	0=RFU, 1=temperature, 2=humidity
RFU	16	0x0
WrEn	2	00=fix read, 01=read 10=fix write, 11=write
WordPtr	8	Word address pointer
RN16	16	Handle
CRC16	16	Checksum

▼Table 2. Tag replies to the sensor commands

	Header	WSN Data	RN16	CRC16
Bits	1	16	16	16
Description	0	Data	Handle	Checksum

ing information to the reader.

The WordPtr field indicates the address where the WSN tag writes the information collected to the memory. RN16 field is a 16-bit tag-authentication number. CRC16 field is the CRC check code for ensuring communication reliability. The custom sensing command has a total of 90 bits. The sensing information collected directly by the sensor connects to the analog to digital converter (ADC) of the MCU through analog input pin (the different sensing functions connect different input pins). ADC converts the input analog signal into the digital output (N_{ADC}) and stores N_{ADC} in the corresponding registers. The ADC supports 12-bit analog-to-digital conversion, and the ADC conversion formulas for N_{ADC} are shown as follows.

$$N_{ADC} = 4096 \times \frac{(V_{in+} + \frac{1}{2}LSB) - V_{R-}}{V_{R+} - V_{R-}}, \quad (2)$$

$$1LSB = \frac{V_{R+} - V_{R-}}{4096}. \quad (3)$$

Fig. 3 shows the execution of the custom sensing command. When receiving the sensing command, the MCU will jump to the subroutine and then verify the CRC-16 and 16-bit tag-authentication number (handle). If the CRC-16 and handle both pass the validation, the MCU will continue to execute this subroutine, otherwise it will terminate the process directly. The WSN field is used to select different functions of the wireless sensor network. The WrEn is used to select reading and writing. Finally, if the WSN tag passes the validation, it replies to the custom sensing command (Table 2), otherwise the WSN tag remains silent.

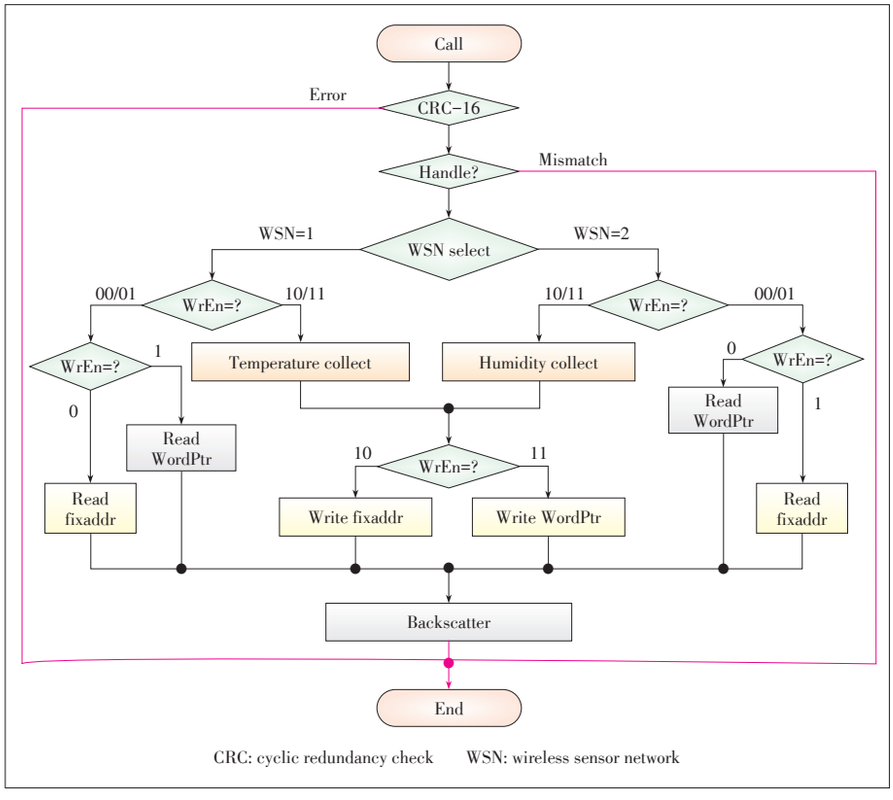

▲Figure 3. The execution of the sensing command.

3.2 Miller Coding

The MCU realizes miller coding to meet the ISO/IEC18000-6C protocol standard. The miller coding rules are defined as follows. The original symbol "1" does not convert at the beginning and conducts conversion at the center point. The original symbol "0" is divided into a single "0" or a continuous "0" to be treated differently. When a single "0" appears, the electrical level before 0 is unchanged, even if the electrical level does not convert at the symbol boundary and is meta-intermediate. For the continuous "0", the electrical level converts at the border of two consecutive "0".

Firstly, the program encodes the miller preamble according to the TRext value of Query commands. When TRext is 0, the program sends the number of four times M values square waves; when TRext is 1, the program sends the number of sixteen times M values square waves. Secondly, the program adds to a string of 0100111_b at the end of square waves. The miller coding uses the shortest instruction to meet the timing requirement, and the jump range of the JMP instruction must be fewer than 512 words to avoid using extra clock cycles for the instruction. The MCU must separate two subcarrier sequences from other subcarrier sequences, because the two subcarrier sequences have only two subcarriers which are not possible to encode all bits as other subcarrier sequences encoding with five clock cycles. The loop jump needs to determine the number of subcarriers and the jump needs two clock cycles, but the program must determine to send 1 or 0 level in five clock cycles. Thus, it is necessary to distinguish two subcarrier sequences from other subcarrier sequences for meeting the timing requirement.

The miller coding is shown in **Fig. 4**. When the main program jumps to the miller coding through a jump command, the program must first configure the specific output ports and specific MCLK according to the BLF. Then, the program jumps to M2 (two subcarriers) module when the M value specified in the Query command is one, otherwise it jumps to Mx (more subcarriers than two subcarriers) module. The TRext specified in the Query command determines the number of pilot tone sent. The program jumps to M_byte1_bit0 if the

bits_cnt (bits_cnt is zero for the entire byte, vice versa) is zero, otherwise jumps to Send_byte1_bit1. Taking miller value 2 as an example, **Fig. 5** shows the encoded miller preamble.

The WSN tag expands the M values specified by the ISO/IEC18000-6C protocol standard, and the expanded M values shall be confirmed according to the custom command. For simplicity and compatibility, the target (Target = 101 and 110) of the select command is used to select different M values. The custom parameters are shown in **Table 3**.

4 Realization and Testing of Wireless Energy Harvest ER Ultra High Frequency IoT Tag

The proposed WSN tag was tested with a commercially available UHF RFID reader. The functions of the energy harvesting, ISO/IEC18000-6C protocol and temperature sensing were tested. The tested results are basically consistent with the theoretical analysis. The both front and back of the WSN tag circuit board are shown in **Fig. 6**.

4.1 Testing of Energy Harvesting

The WSN tag combines RF energy and solar energy for cellular IoT applications. The test of the energy harvesting performance was conducted in a wireless environment. The gain of transmitting antenna was 12 dBi, and the R420 reader provided 30 dBm transmit power. The gain of receiving antenna was 8 dBi. The two antennas kept 1 m away. The energy harvesting circuit can be charged in the wireless environment. The voltage of the super capacitor could reach 5.09 V within 24 s. The WSN tag can also turn solar energy into electricity by a solar panel, and the time of charging the supercapacitor up to 4.2 V is about 15 m.

4.2 Testing of Temperature Sensing

The temperature sensor was fixed to work in the mode which the gain selects are zero. The temperature sensing performance was tested in a high-low temperature test chamber from −30°C to 60°C with

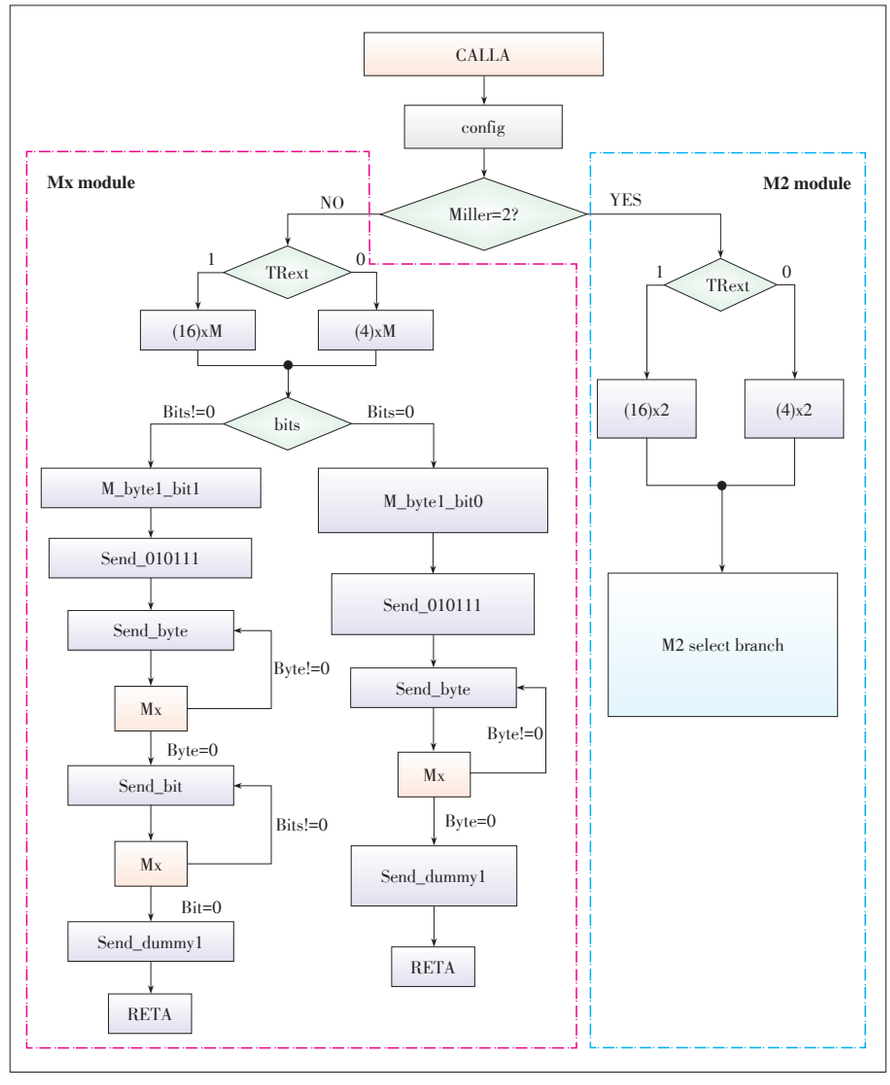

▲Figure 4. Miller coding.

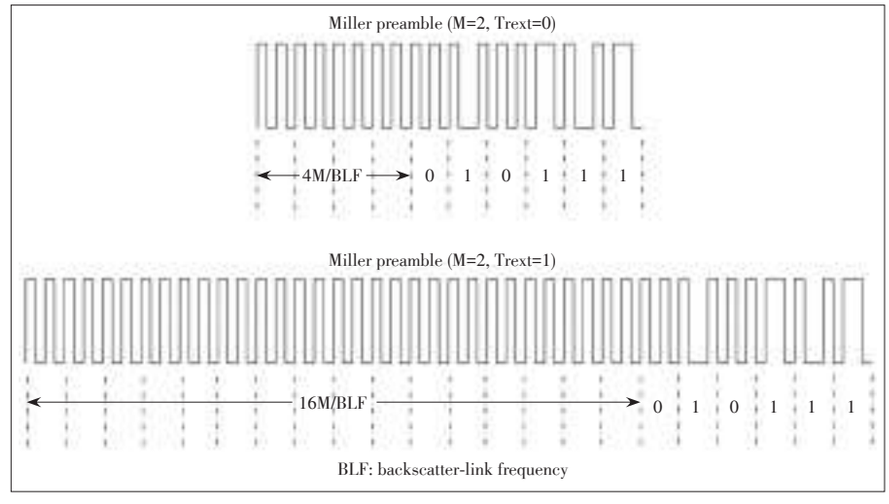

▲Figure 5. The encoded miller preamble (M=2).

▼Table 3. The compatibility table of the expanded M values

Target	M	Encode
3'bxxx	2'b00	FM0
3'b0xx	2'b01	M2
	2'b10	M4
	2'b11	M8
3'b101	2'b01	M16
	2'b10	M32
	2'b11	M64
3'b110	2'b01	M128
	2'b10	M256

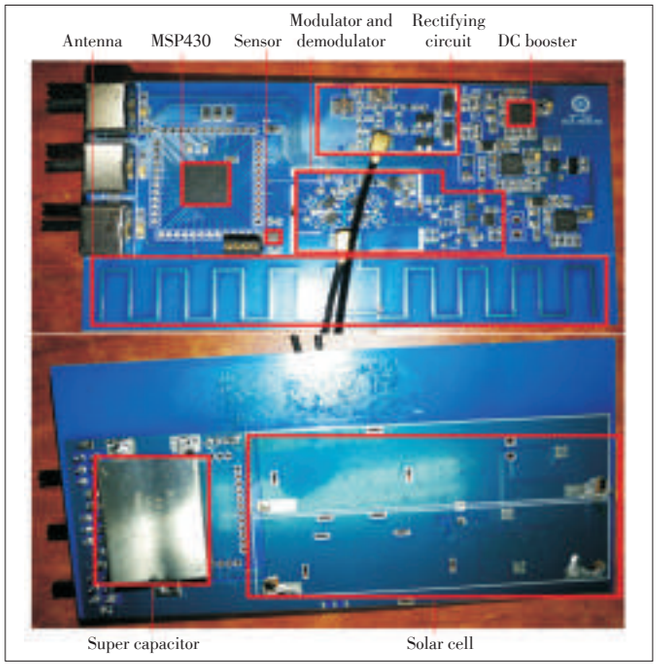

▲Figure 6. The circuit board of the WSN tag.

a step of 5°C. The test environment of WSN tag temperature is shown in **Fig. 7**. A self-designed UHF RFID reader was used for custom sensing command.

Fig. 8 compares the real temperature and test temperature. The horizontal axis represents N_{ADC} produced by the ADC, the vertical axis represents the temperature. We use the inverse transform of generating a N_{ADC} value to calculate the ambient temperature according to (1) and (2). From this figure, the test temperature is basically consistent with the real temperature.

4.3 Testing of Tag Protocol Performance

The distance within which the R420 reader can inventory the WSN tag successfully can be calculated by the friss electromagnetic wave propagation formula. The antennas of the reader and tag were placed on stands 2.4 m above the floor. The sensitivity of R420 reader is -82 dBm. The power transmitted

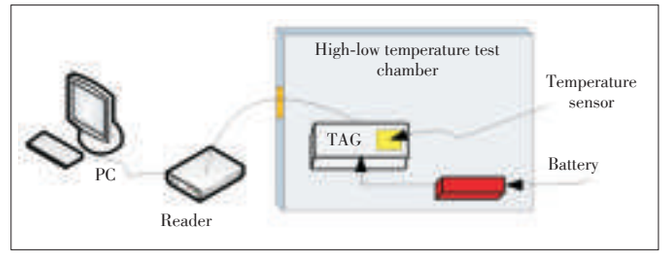

▲Figure 7. The test environment of WSN tag temperature.

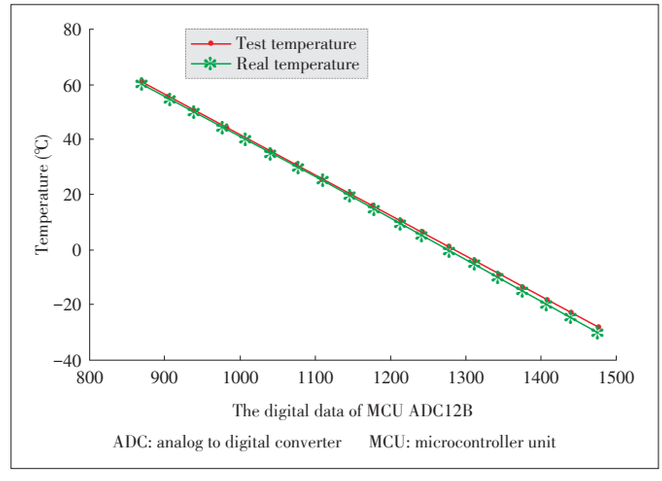

▲Figure 8. The contrast of test temperature and real temperature.

is 30 dBm by the R420 reader, and the line loss L_{loss} is 1 dB. The gain of transmit antenna G_1 is 9 dBi, and the gain of tag antenna G_2 is 1 dBi. The sensitivity of tag, P_e, is −32 dBm, and the operating frequency is 920 MHz. The two antennas are both circular polarization, so the polarization loss, G_3, is 0 dB. The loss of the backscatter, G_4, is −6 dB. The distance within which the WSN tag can receive the available signal from the reader can be calculated by the following Friss equation:

$$P_e = P_1 - L_{loss} + G_1 + G_2 + G_3 + 10\lg\left(\frac{\lambda}{4\pi r_1}\right)^2. \quad (4)$$

Therefore, r_1 = 116 m. Similarly, by the Friss equation, P_3 is the power reader received from the backscatter of the WSN tag. Accordingly, it is possible to calculate the distance r_2 within which the reader can receive available reply signals by (5).

$$P_3 = P_1 - 2L_{loss} + G_4 + 2(G_1 + G_2 + G_3) + 10\lg\left(\frac{\lambda}{4\pi r_2}\right)^4. \quad (5)$$

Therefore, r_2 = 32.68 m. **Table 4** shows the test distances in various modes of the reader, and some test distances are obviously beyond the theoretical distances, which are due to the influence of multipath effects.

5 Conclusions

The wireless energy-harvested WSN tag has been developed

▼Table 4. Test distances in various modes

Reader mode	R->T (kbit/s)	T->R (kbit/s)	r_2 (m)	r_1 (m)
Autoset dense reader	≈70	≈426.66	19	91.2
Autoset static	≈70	≈426.66	20	93.8
Max throughput	≈70	≈426.66	23	90.9
Hybrid mode	≈70	≈426.66	27	94.9
Dense reader M=4(1)	≈50	≈320	33	96.4
Dense reader M=4(2)	≈70	≈320	35.2	96.4
Dense reader M=8	≈70	≈320	36.5	97.4

in circuit board (Fig. 6). Reducing power and obtaining renewable energy are main advantages of the WSN tag. This paper presents the relevant wireless energy harvesting, common tag protocol, miller coding, extended miller coding and sensing functions. The test results of energy harvesting are consistent with the theoretical values. The rectifier efficiency reaches 39% when the rectifier circuit has input of -14 dbm and output voltage of 360 mV that is greater than 330 mV, which meets the condition of the DC Booster circuit cold start. The WSN tag successfully implements the common ISO/IEC 18000-6C protocol standard, and the sensitivity of the WSN tag is up to -32 dBm. The WSN tag also implements low speed mode for saving power. The extensional miller coding has first been implemented in the assembler. In the future, we plan to design multi-band RF energy harvesting system, to implement more applications of the WSN tag for the cellular IoT.

References

[1] S. T. Hsieh, "RFID medical information system: a system implementation on MSP430 platform," in *International Conference on Consumer Electronics, Communications and Networks (CECNet)*, Xian Ning, China, 2011, pp. 1-4. doi: 10.1109/CECNET.2011.5768332.
[2] Y. S. Lin, Z. Y. Guo, Y. S. Huang, and C. H. Yeh, "A low-power UHF passive RFID transponder chip in 0.18 μm CMOS," in *IEEE Wireless Power Transfer Conference (WPTC)*, Taipei, China, 2017, pp. 1-5. doi:10.1109/WPT.2017.7953802.
[3] H. Reinisch, M. W. flecker, S. Gruber, et al., "A multifrequency passive sensing tag with on-chip temperature sensor and off-chip sensor interface using EPC HF and UHF RFID technology," *IEEE Journal of Solid-State Circuits*, vol. 46, no. 12, pp. 3075-3088, Dec. 2011. doi: 10.1109/JSSC.2011.2167548.
[4] S. Q. Geng, L. G. Hou, J. H. Wang, et al., "Design of RFID active tag system based on MSP430," *IET 2nd International Conference on Wireless, Mobile and Multimedia Networks (ICWMMN 2008)*, Beijing, China, 2008, pp. 139-142. doi: 10.1049/cp:20080956.
[5] T. Skaik, "A quad-band rectifier design with improved matching bandwidth for RF energy harvesting applications," in *International Conference on Promising Electronic Technologies (ICPET)*, Deir El-Balah, Palestine, 2017, pp. 82-86. doi: 10.1109/ICPET.2017.21.
[6] X. Li, J. Wang, X. Wu, and H. Zhao, "A dual-band integrated wireless energy harvesting system," in *2017 International Applied Computational Electromagnetics Society Symposium (ACES)*, Suzhou, China, 2017, pp. 1-2.
[7] A. Mouapi, N. Hakem, and N. Kandil, "High efficiency rectifier for RF energy harvesting in the GSM band," in *2017 IEEE International Symposium on Antennas and Propagation & USNC/URSI National Radio Science Meeting*, San Diego, USA, 2017, pp. 1617-1618. doi: 10.1109/APUSNCURSINRSM.2017.8072851.
[8] P. Mhatre, R. Duche, S. Nawale, and P. Patil, "RF power harvesting system for RFID applications in multiband systems," in *6th International Conference on Computing, Communication and Networking Technologies (ICCCNT)*, Denton, USA, 2015, pp. 1-5. doi: 10.1109/ICCCNT.2015.7395226.
[9] S. Jung, D. Y. H. Chun, W. Kim, et al., "UWB sensor chip measurement system implementation using labview and MCU board," in *ICTC 2011*, Seoul, Korea, 2011, pp. 649-651. doi: 10.1109/ICTC.2011.6082679.
[10] Q. Zhang, T. Lin, and J. Yang, "The acquisition and analysis of vibration energy signal generated by magnetic shape memory alloys," in *29th Chinese Control and Decision Conference (CCDC)*, Chongqing, China, 2017, pp. 7019-7022. doi: 10.1109/CCDC.2017.7978447.
[11] C. Boyer and S. Roy, "Backscatter communication and RFID: coding, energy, and MIMO analysis," *IEEE Transactions on Communications*, vol. 62, no. 3, pp. 770-785, Mar. 2014. doi: 10.1109/TCOMM.2013.120713.130417.
[12] A. Sample, D. Yeager, P. Powledge, and J. Smith, "Design of a passively powered, programmable sensing platform for UHF RFID systems," in *Proc. 2007 IEEE International Conference on RFID*, Grapevine, USA, 2007, pp. 149-156. doi: 10.1109/RFID.2007.346163.
[13] M. A. Khan, M. Sharma, and R. B. Prabhu, "FSM based FM0 and Miller encoder for UHF RFID tag emulator," in *IEEE International Advance Computing Conference.*, Patiala, India, 2009, pp. 1317-1322. doi: 10.1109/IADCC.2009.4809207.

Manuscript received: 2017-09-07

Biographies

LI Gang (ligang1986718@163.com) received his M.E. degree from Chengdu University of Technology, China in 2012. He has five years of research in communication integrated circuits. He has currently been pursuing his Ph.D. degree at School of Communication and Information Engineering, University of Electronic Science and Technology of China (UESTC), China since 2016. His research interests include RFID, wireless communication networks, cognitive radio networks, and information security.

XU Rui (xurui_uestc@163.com) is currently pursuing his master's degree at School of Communication and Information Engineering, UESTC, China. His research interests include programmed algorithm and embedded system, and RFID and IoT.

LI Zhenbing (thomaslizhenbing@163.com) is currently pursuing his Ph.D. degree at School of Communication and Information Engineering, UESTC, China. His research interests include RFID and IoT, and RF circuit and system.

ZHOU Jie (jie.zhou1994@hotmail.com) is currently pursuing his master's degree at School of Communication and Information Engineering, UESTC, China. His research interests include RFID and IoT, and RF circuit and system.

LI Jian (uestclijian@163.com) is an associate research fellow at School of Communication and Information Engineering, UESTC, China. His research interests include RFID, IoT, wireless communication systems and networks, and RF circuit and system.

WEN Guangjun (wgj@uestc.edu.cn) received his B.Sc. and the M. E. degrees from Chongqing University, China in 1986 and 1992, respectively, and his Ph.D. degree from UESTC, China in 1998. From July 1986 to February 1995, he was with Chongqing University as a lecturer. He was with UESTC from July 1998 to May 2000, and then with Electronics and Telecommunication Research Institute, Korea from May 2000 to May 2001, as a postdoctoral fellow. He was with Nanyang Technological University, Singapore, as a research fellow from May 2001 to September 2002. He worked for VS Electronic Pte Ltd (Singapore) and Sumitomo Electric Group (Yokohama, Japan) as a senior RF design engineer from September 2002 to August 2005. Since January 2004, he has been a professor with UESTC. His research interests include radio frequency integrated circuits and systems for various wireless communication systems, analysis and design of RFID tag and reader, circuit components and antennas design for the internet of things. He has authored or co-authored more than 200 journal papers and presented more than 120 conference papers.

DOI: 10.3969/j.issn.1673-5188.2018.01.004
http://kns.cnki.net/kcms/detail/34.1294.TN.20180201.1556.002.html, published online February 1, 2018

Exploiting Correlations of Energy and Information: A New Paradigm of Energy Harvesting Communications

GONG Jie[1] and ZHOU Sheng[2]
(1. School of Data and Computer Science, Sun Yat-sen University, Guangzhou 510006, China;
2. Department of Electronic Engineering, Tsinghua University, Beijing 100086, China)

Abstract

For deployment flexibility and device lifetime prolonging, energy harvesting communications have drawn much attention recently, which however, encounter energy domain randomness in addition to the channel state randomness and traffic load randomness. The three-dimensional randomness makes the resource allocation problem extremely difficult. To resolve this, we exploit the inherent correlations of energy arrival and information. The correlations include self correlations of energy profiles and mutual correlations between energy and information in both time and spatial domains. The correlations are explicitly explained followed by a state-of-art survey. Candidate mechanisms exploiting the correlations for the ease of resource allocation are introduced along with some recent progress. Finally, a case study is presented to illustrate the performance of the proposed algorithm.

Keywords

energy harvesting; wireless communications; spatial and temporal correlations; resource allocation

1 Introduction

With the rapid growth of mobile multimedia traffic requirements, wireless networks tend to be deployed more and more densely, resulting in more and more energy consumption. At the same time, with the emergence of Internet of Things [1] and wearable devices [2], large quantities of wireless sensors are appearing, causing stringent requirement on flexibility of deployment and cruising ability. By gathering energy from ambient environment (solar, wind, radio waves and so on) to power wireless devices, energy harvesting communication system is one of the candidate technologies to reduce CO2 emission and support flexible and sustainable wireless communications. Nowadays, the energy harvesting technology is drawing much attention from industrial community. For instance, China Mobile has deployed 13,000 renewable energy powered base stations (BSs) by May 2017 [3], and Powercast is developing wireless power harvesters [4]. It is expected that energy harvesting technology will be widely used in the future wireless networks.

A key feature of the ambient energy is that the energy arrival is random, leading to unstable power supplies. Thus, in addition to channel fading and traffic load variation, another dimension of randomness, the unstable power input needs to be considered, which makes the design of energy harvesting communications extremely difficult. Conventionally, the problem is mainly studied by two ways of simplifications. The first is to assume that all the dynamics (energy arrival, data arrival and channel fading) are known in advance, and the resource allocation can be optimized with offline global information [5]–[10]. The advantage of offline analysis is that structural properties can be found. However, since the non-causal information cannot be accurately predicted in reality, the offline results can hardly be used in causal systems. The other way is to consider only one or two types of randomness. For instance, one can analyze the system capacity in non-fading AWGN channel [11], [12], or optimize the resource allocation with constant energy arrival rate [13]–[15]. Nevertheless, the design with three-dimensional randomness is still an open problem.

In the real environment, the three-dimensional randomness is neither independent nor purely random, but is closely correlated with one another. For instance, real data shows that the solar energy arrival is quite stable and changes slowly in sunny day [16], while the network traffic load varies drastically [17], and the peak energy arrival rate and the peak traffic load appear in different time periods. On one hand, the correlation property can be utilized to simplify the problem formulation; on the other hand, it may cause other problems. Specifically, the stable energy arrival can be viewed semi-static. Hence, the

This paper is supported by the National Natural Science Foundation of China under grant Nos. 61771495 and 61571265.

randomness in energy domain can be omitted, while the mismatch between energy arrival and traffic load may severely degrade the system performance.

In this paper, we investigate a new paradigm of studying the energy harvesting communications by exploiting the inherent correlations between energy and information. We mainly focus on two types of correlations: 1) Self correlation of energy arrival process; 2) mutual correlation between energy and information. A thorough description on these correlations and state-of-art survey are given, based on which potential mechanisms based on them are discussed. In addition, a case study is provided to illustrate the importance of correlation properties.

The rest of the paper is organized as follows. Section 2 describes the correlation properties. Section 3 proposes some correlation-aware mechanisms. A case study is given in Section 4. Finally, Section 5 concludes the paper.

2 Inherent Correlations of Energy and Information

A typical application scenario of energy harvesting technology in heterogeneous cellular networks is depicted in **Fig. 1**. It can be seen that the macro BS is plugged into power grid with stable power supply to provide a basic network coverage. A supplementary solar panel is connected to reduce the grid power consumption. The small BSs 1 and 2 are powered by solar power and wind power, respectively. Some low-power mobile devices that are located close to the BSs can harvest energy from the radio signal, i.e., wireless power transfer. In real systems, the energy arrival process should be characterized by temporal and spatial correlations with itself as well as with network traffic. In this paper, the correlations are mainly discussed based on the cellular scenario as in Fig. 1. Nevertheless, the properties and algorithms are not limited to this case. They can also be extended to any other energy harvesting communication scenarios.

2.1 Self Correlations of Energy Arrival

The energy arrival process in real systems can be viewed as a "semi-static" stochastic process due to the embedded self correlations. The term "semi-static" means that the energy arrival keeps constant to some extent or is known by some mechanisms. Such a property can be used to reduce the complexity of the resource allocation design. The self correlations are discussed in both time domain and spatial domain as detailed in the following.

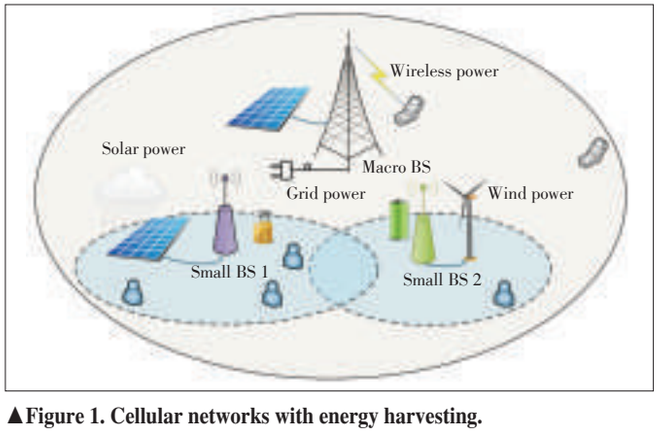

▲Figure 1. Cellular networks with energy harvesting.

2.1.1 Temporal Self Correlation

Based on the solar radiation data collected by the Measurement and Instrumentation Data Center (MIDC) [16], it is observed that the outdoor solar power in sunny days is quite stable, i.e., the energy arrival is strongly correlated in time domain (correlation coefficient ≈ 1). The energy arrival rate only changes at a long time scale following a predictable profile. When the energy harvester harvests energy from radio signals, the energy arrival process is predictable and even controllable by information exchange in the control plane. If the correlation properties are properly modeled, the complexity of resource allocation can be reduced.

The temporal self-correlation has been exploited in the literature. Define an energy harvesting frame as a set of consecutive slots during which the energy arrival rate keeps constant. In a single energy harvesting frame, power allocation and scheduling policies have been proposed for relay networks [13] and distributed networks [14]. For multiple energy harvesting frames, the outage minimization problem has been studied in [18]. However, there is a lack of a general framework to formulate the self correlations in energy harvesting communications. In fact, in wireless power transfer, the energy arrival may change in each slot, but it is self correlated from power transmitter side. It is also possible that the wireless channel is static such as line-of-sight (LOS) links, while the energy arrival rate varies rapidly. In this case, the channel state is strongly self correlated, which can also be taken advantage of.

2.1.2 Spatial Self Correlation

In the multi-node case, the self correlation exists not only in the time domain, but also in the spatial domain. The energy arrivals in different nodes may be different due to either diverse types of energy harvesters (e.g., solar v.s. wind) or various environments (e.g., solar power in cloudy day). The spatial energy distribution is modeled and analyzed in [19] which shows significant impact of spatial correlation on the network performance such as coverage. In this case, cooperation among nodes becomes quite important for coverage guarantee and energy-efficiency enhancement.

Some simple cases have been studied considering the spatial correlation of energy arrivals. For a two-node communication link with correlated energy harvesting transmitter and receiver, the optimal transmission policy is found in [20]. When two BSs cooperatively serve the cell-edge users, how they adapt the conventional network MIMO scheme to the spatial

correlated case is considered in [15]. It can be seen that some nice results are obtained in these simple cases. However, the solutions cannot be applied to cases with multi-node directly, where a node's decision depends on its neighbors' states, while its neighbors also depend on their neighbors, and so on. Hence, the high complexity of solving such problems due to the coupling effect over the network is a major challenge.

2.2 Mutual Correlations between Energy and Information

The classic Shannon's formula $R=\log_2(1+P/N)$ describes the basic relation between energy and information. However, it is only for a single link with additive white Gaussian noise (AWGN) channel, and considers greedy source and constant transmit power. In reality, burstiness exists in both the data traffic and the energy arrival. The amount of traffic that can be carried by a certain amount of energy depends on both temporal and spatial relations between energy arrival and traffic requirement.

2.2.1 Temporal Mutual Correlation

By drawing the 24 hour traffic profile based on [21] and the renewable power profile based on [22] together in **Fig. 2**, it can be seen that they do not match with each other in the time domain. The peak power meets a medium traffic load, while the peak traffic even meets zero power. Such a negative correlation between power and traffic may have severe impact on the wireless communication if the harvested energy is not smartly allocated to satisfy the traffic requirement.

Large battery is a promising solution. It has been proved that with ergodic energy arrival process, if the battery capacity is sufficiently large, the randomness in the energy domain is wiped out, and the system is equivalent to the one with the average power constraint [11], [23]. However, the battery capacity is limited in practice due to hardware constraints and expensive cost. Even if a large battery is equipped without financial limitation, the imperfections during charging and discharging as well as the limited lifetime will become an inevitable problem. With limited battery capacity, how to dynamically match harvested energy with traffic requirement needs some novel techniques.

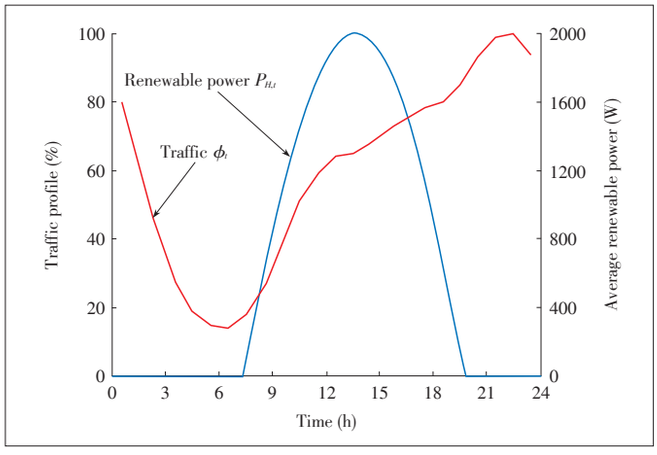

▲Figure 2. Traffic profile and renewable power profile over time.

2.2.2 Spatial Mutual Correlation

The spatial mutual correlation can be illustrated by the example in Fig. 1. There are three users in small BS 1's coverage, but only one in small BS 2's. When the weather becomes cloudy and windy, BS 1 may be deficient in energy while BS 2 may be over charged. In this case, the traffic distribution mismatches the energy distribution in space. The users in BS 1's coverage may be out of service, while BS 2's battery may overflow. The negative correlation effect in spatial domain also degrades the service performance.

By jointly considering the traffic requirement and the energy profile, wireless resource allocation problem and dynamic BS sleeping problem are studied in [24] and [25], respectively. However, these works assume that the energy arrivals are identical in all the nodes, i.e., uniform energy distribution over space. For non-uniform distribution, the system needs to be redesigned from network planning to resource allocation, both of which should be traffic aware.

3 Exploiting Correlations for Energy Efficient Communications

As shown in the previous section, the correlations inside the energy arrival process and between energy and traffic profiles are of significant impact on energy harvesting communications. Some of them can be utilized to simplify the problem, while some others should be carefully handled to eliminate the passive impact, both requiring novel algorithm design. As a starting point, this section presents some potential mechanisms to exploit the correlation properties.

3.1 Low-Complexity Resource Management Based on Temporal Correlation

If the channel fading and the energy arrival are viewed as purely random process, a two-dimensional randomness results in high complexity for transmission policy optimization. Exploiting temporal correlation can potentially reduce the complexity. For instance, when the change of energy arrival rate is slower than the channel fading, a two-stage power allocation algorithm can be applied to decouple the two-dimensional randomness as shown in **Fig. 3**. In particular, when the energy arrival rate keeps constant, an inner sub-problem adjusts the power allocation according to the channel fading only. The period with constant energy arrival rate is called energy harvesting frame. Then an outer problem deals with energy management among frames considering the change of energy arrival rate. As a consequence, the energy arrival and the channel fading are decoupled. Hence, the complexity is greatly reduced. Similarly, the two-stage algorithm can also be applied to the

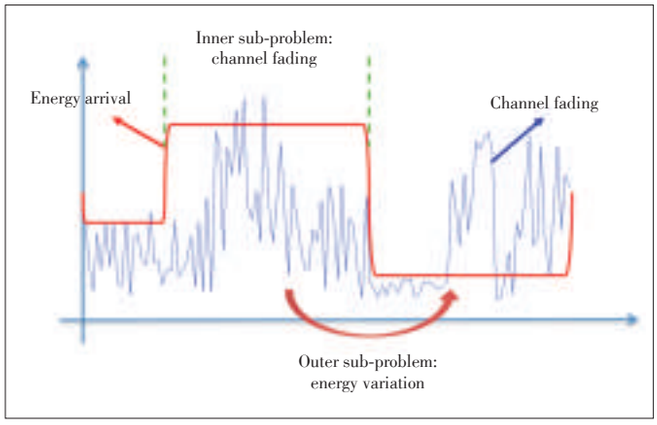

▲Figure 3. Two-stage power allocation algorithm for decoupling channel fading with energy variation.

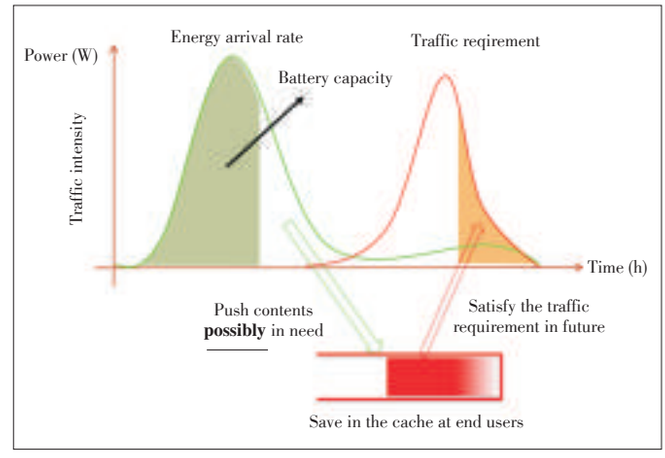

▲Figure 4. Solving energy-information mismatch problem via proactive caching and push.

case in which the channel state varies slower than the energy arrival.

For the case in which energy arrival and channel fading changes in the same time scale, such as simultaneous wireless information and power transfer (SWIPT) [26], the two-stage algorithm is infeasible. Nevertheless, good news is that the transmit power is controllable. Thus, through information exchange between transmitter and receiver, the harvested energy well adapts to the wireless channel. Since the wireless power transfer is usually of low efficiency, it is mainly adopted with sufficiently strong channel gain. The information transmission is still possible in medium or even poor channel conditions. Taking the advantage of correlation between energy transfer and channel fading, the energy harvesting efficiency can be enhanced.

3.2 Energy-Aware Content Caching and Push

We now focus on how to deal with the negative temporal correlation between energy and information. The energy profile and the traffic profile usually mismatch, and the limited battery capacity is not sufficient to wipe out energy domain randomness. Thus, the storage ability in information domain should be taken into account, i.e., content caching. As shown in **Fig. 4**, the energy profile (green curve) and the traffic requirement (red curve) mismatch in the time domain, and the battery capacity is limited. When the battery is full, the continuously arrived energy can be used to push contents possibly needed in the future to the end users. Later, when the actual traffic demand is generated, part of it can be satisfied by the users' local cache. Thus, the barrier built up by the limited battery is broken, and the energy is "moved" from now to the future. Based on content caching and push mechanism, we have proposed a framework, namely GreenDelivery [27], to enable efficient content delivery with energy harvesting based small cells. In addition, content push policy for a single cell has been designed in [28].

Although GreenDelivery well exploits the correlation between energy and information, the study on caching-aided energy harvesting communications is still in its infancy. Lots of problems need to be further examined. Firstly, the content caching schemes strongly depend on the statistic information of content popularity and long-term energy arrival process. Online algorithms are needed to accurately learn and predict the content popularity as well as energy statistics. Secondly, content caching consumes both energy and storage space of the devices. When the practical caching cost is accounted, the performance gain we can get may be reduced. The conditions on which an expected performance gain is achievable should be clarified. Finally, in a network with multiple cells, how BSs cooperate to reduce the content caching cost and improve file hitting probability over asymmetric energy and traffic distribution needs to be studied. This problem is actually related to how to exploit the spatial correlation between energy information, which will be further discussed later.

3.3 Joint Transceiver Design with Energy Harvesting

In multi-hop relay networks, the relay nodes not only receive but also transmit data, and they may be powered wirelessly for deployment flexibility. As shown in **Fig. 5**, the relay node maintains two buffers: data buffer and energy buffer. Both data transmission and receiving consumes energy, while the spectral efficiency of data transmission is strongly related to channel state. Thus, the transceiver module should be jointly designed and optimized so that data buffer, energy buffer and channel state are well managed. Intuitively, data should be transmitted when the channel is good. If the data buffer is almost empty, the relay node needs to receive data from the source. Otherwise, the good channel state may not be fully utilized as there is no data to transmit. Either half-duplex (HD) or full-duplex (FD) mode is applicable in the relay nodes. The FD mode is expected to achieve a higher spectral efficiency compared with the HD mode, but consumes more energy due to the additional signal processing circuits for self-interference can-

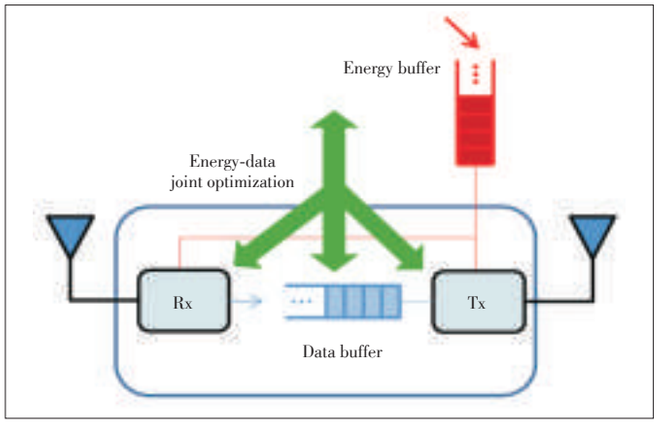

▲Figure 5. Joint transceiver optimization for balancing the data queue and the energy queue.

cellation. In summary, the energy arrival process and the channel fading are correlated temporally via the controllable data buffers (by controlling the transceiver's working mode). Similarly, different nodes are also correlated spatially.

Transmission policy optimization has been studied in [29] for a simple multi-hop topology, i.e., the system is composed of a source node, a relay node, and a destination node. A tradeoff between HD and FD is observed by exploiting the temporal correlation between energy buffer and channel states of the two hops. For a generalized multi-hop network, how to exploit the correlation between nodes spatially is a challenge issue.

3.4 Dynamic Network Planning and Traffic Offloading

Conventional network planning determines the locations of BSs based on the expected average traffic load requirement as well as deployment and operation costs. For the energy harvesting communications, the deployment should be re-designed considering the energy distribution and the randomness of energy arrivals. First of all, a heterogeneous network topology where macro BSs are plugged into power grid to guarantee a stable network coverage, and small BSs can be powered by any energy source, is a necessity. Secondly, the planning of small BSs depends on the correlations between the energy and traffic. If the energy harvesting devices are deployed independent to the BSs and connect to the small BSs via power lines, the energy and traffic profiles are decoupled. Conventional network planning can be applied by additionally considering the deployment cost of power lines. If the energy harvesting devices are equipped on each BS, which can reduce the cost for deploying power lines, joint traffic-energy-aware network planning should be designed. For instance, the BSs should be density deployed when either the traffic load is high or the energy arrival rate is low so that the spectral resources and the available energy amount are sufficient.

Due to the dynamics of energy arrival and traffic load, the nodes in the network may need the help of neighbor nodes when the energy is insufficient and the traffic load is high. Traffic offloading [30] is a candidate solution to realize the neighborhood cooperation. As shown in **Fig. 6**, the traffic offloading is based on energy-aware cell zooming [31]. When the energy profile and the traffic profile do not match for the two BSs, the BS with lower energy shrinks its coverage and the other with higher energy expands its coverage. As a result, the energy is "moved" from the cell on the right to the one on the left, and all the users can be served with sufficient energy. This is an efficient mechanism to transform the negative correlation between energy and traffic into a positive correlation over the space.

4 Case Study: Two-Stage Power Allocation with Semi-Static Energy Arrival

In this section, we present a case study to show how time correlations can be utilized to simplify the algorithm corresponding to Section 3.1. In particular, we consider a single link where the transmitter is powered by the energy harvested from ambient environment. It is assumed that the change of energy arrival rate is slower than the channel fading, i.e., the energy arrival rate changes every N ($N \geqslant 1$) fading blocks, i.e., an energy harvesting frame. The timeline of energy profile is shown in **Fig. 7**, where the time slot is denoted by (k, n) with k representing index of frames and n representing index of fading blocks in each frame, E_k is the energy arrival rate in frame k, $B_{k,n}$ is the battery energy state in slot (k, n), and $P_{k,n}$ is the transmit power. The channel gain in slot (k, n) is denoted as

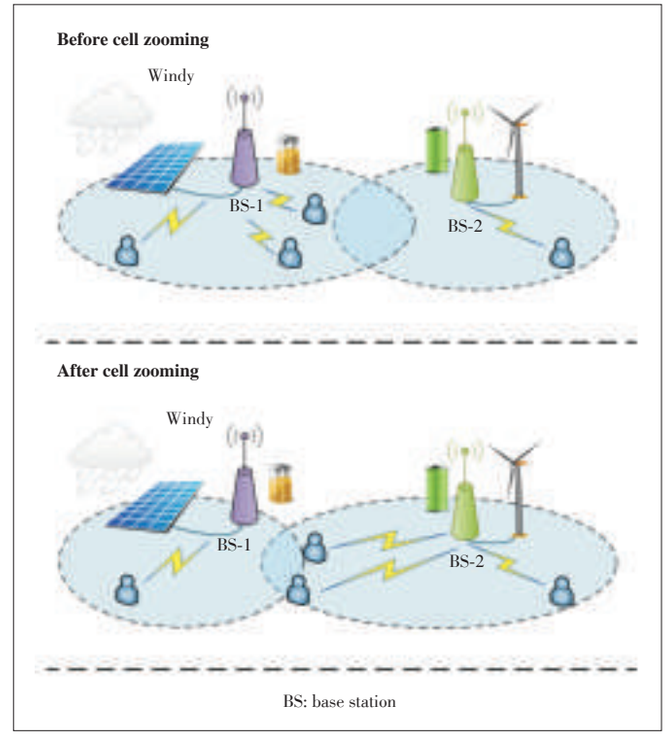

▲Figure 6. Energy-aware cell zooming for realizing traffic offloading.

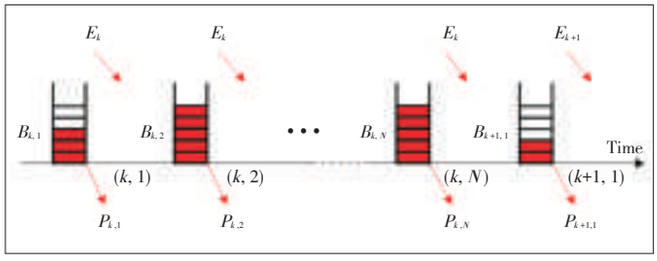

▲Figure 7. Timeline of energy profile.

$\gamma_{k,n}$. Thus, the battery energy state evolves as

$$B_{k,n+1}=\min\{B_{k,n}-P_{k,n}+E_k,B_{\max}\}, \quad (1)$$

where $B_{k,N+1}=B_{k+1,1}$, and $B_{\max}$ is the battery capacity. The data rate is related to the transmit power and the channel gain, denoted as $r(P_{k,n},\gamma_{k,n})$. We aim to maximize the average data rate by optimizing the power allocation, i.e.,

$$\max \lim_{K\to\infty}\frac{1}{KN}E\left[\sum_{k=1}^{K}\sum_{n=1}^{N}r(P_{k,n},\gamma_{k,n})\right]. \quad (2)$$

The problem can be formulated as a Markov decision process (MDP) and solved by dynamic programming (DP) approach [32]. The DP algorithm deals with a set of MDP problems which can be divided into stages. In each stage, the system state $x_k\in S$ dynamically changes under the influence of control action u_k and random parameter w_k embedded in the system, and the reward function $g_k(x_k,u_k,w_k)$ is additive over time. The objective is to maximizing the average reward function $\lim_{K\to\infty}(1/K)\sum_{k=1}^{K}g_k(x_k,u_k,w_k)$ by optimizing the state-dependent control policies $u_k=\mu_k(x_k)$, $k=1,...,K$. Theoretical results show that a scalar λ and a vector $h=\{h(i)|i\in S\}$ satisfy Bellman's equation

$$\lambda+h(i)=\max_{u\in U(i)}\left[E_w(g(i,u,w)+\sum_{j\in S}p_{i,j}(u)h(j)\right], \quad (3)$$

where $p_{i,j}(u)$ is the transition probability from state i to state j under action u. Then λ is the optimal average reward and can be solved by value iteration based on the following equation

$$h^{(k+1)}(i)=\max_{u\in U(i)}\left[E_w(g(i,u,w)+\sum_{j\in S}p_{i,j}(u)h^{(k)}(j)\right]-\lambda^{(k)}, \quad (4)$$

where $\lambda^{(k)}=\max_{u\in U(s)}\left[E_w(g(s,u,w)+\sum_{j\in S}p_{s,j}(u)h^{(k)}(j)\right]$ for a fixed state s. It converges to the optimal average reward λ.

In our problem, the system state includes the battery energy state $B_{k,n}$, channel state $\gamma_{k,n}$, energy arrival rate E_k, and the number of slots since the last change of energy arrival rate. The control action is the power allocation $P_{k,n}$, and the per-stage reward is the data rate $r(P_{k,n},\gamma_{k,n})$. By directly applying the above DP algorithm, the problem can be solved. However, it can be seen that the state space would be huge if the energy harvesting frame is long, which results in the curse of dimensionality problem. To resolve this, we exploit the correlation feature in time domain to reduce the computational complexity.

The original problem can be decoupled into two sub-problems, finite horizon power allocation in each energy harvesting frame, and infinite horizon energy management among frames. If the initial battery state and the terminal battery state are given, the optimal power allocation in a frame is irrelevant to the other frames since the energy arrival rate is known and fixed. In this sense, we can formulate an inner problem of finite horizon power allocation within a frame. On the other hand, given the expected per-frame reward obtained by solving the inner problem, the optimization among frames can be formulated as an outer problem that determines the initial/terminal battery energy of each frame, which is equivalent to determining the optimal amount of energy to be used in each frame. The inner and outer problems can be solved by finite horizon DP algorithm and infinite horizon DP algorithm, respectively. The system state of the inner problem includes battery state and channel state, and that of the outer problem includes battery state, channel state, and energy arrival rate. By comparison, the state space of the inner and outer problems are much smaller than the DP optimal one. The algorithm to solve the inner and outer problems sequentially is termed as two-stage DP algorithm.

We run some numerical simulations to evaluate the performance of the proposed two-stage DP algorithm. Consider a binary system settings, i.e., both the channel gain and the energy/power take only two values, $\gamma_{k,n}\in\{0,1\}$, $E_k\in\{0,1\}$, and $P_{k,n}\in\{0,1\}$. The channel fading is assumed independently and identically distributed (i.i.d.), and the channel state is good ($\gamma_{k,n}=1$) with probability p = 0.7, and is bad ($\gamma_{k,n}=0$) with probability $1-p$ = 0.3. In good channel state, the data rate with a unit of power is $r(1,1)=r_1$. In bad state, the data rate is $r(1,0)=r_0$. If the transmit power is zero, the data rate is zero. One unit of energy is harvested with probability q = 0.7, and there is no energy arrival with probability $1-q$ = 0.3.

The comparison of the two-stage DP algorithm and the DP optimal algorithm is shown in **Fig. 8**. It can be found that there is a performance gap between the two algorithms when N is small, which gradually vanishes as N becomes larger. Specifically, the gap is neglected when $N\geqslant 20$. As N increases, the average rate reduces for both of the algorithms, and converges to a fixed point as shown by the red dashed line. The result demonstrates that the proposed low-complex algorithm well approaches the DP optimal algorithm. In addition, it is interesting to note that the average rate with small value of N is larger than that with large value of N. As smaller value of N refers to more randomness in energy arrival process, it shows that the randomness actually helps to improve the overall performance

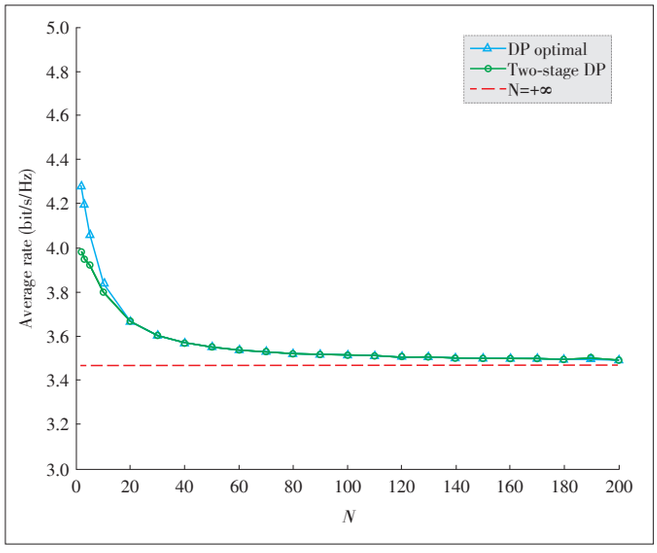

▲**Figure 8. Performance comparison of the two-stage DP algorithm and the DP optimal algorithm.**

by the concept of opportunistic scheduling. As both energy arrival and channel fading are random, there are more opportunities that good channel state meet sufficient energy arrival.

5 Conclusions

This paper discussed the inherent correlations of energy and information, which can be exploited to facilitate the resource allocation for energy harvesting communications. The temporal self correlation of energy arrival process results in a semi-static energy profile so that joint-energy-channel-aware power allocation can be decoupled. With the spatial correlation, neighboring nodes can help each other. The negative correlation due to the mismatch between energy and traffic in temporal domain can be effectively resolved via the content caching technique. In the spatial domain, the mismatch problem can be relieved by energy aware traffic offloading. In summary, the correlations between energy and information are key features for characterizing the three-dimensional randomness. Accurately modeling and properly using the correlations would be a feasible path to realize intelligent resource allocation in energy harvesting wireless communications.

References

[1] L. Atzori, A. Iera, and G. Morabito, "The internet of things: a survey," *Computer Networks*, vol. 54, no. 15, pp. 2787–2805, Oct. 2010.
[2] http://wearable.ofweek.com/2016-05/ART-8110-5006-29092330.html
[3] C. I, "5G, a marathon," Global 5G Summit (invited talk), Shanghai, China, Jul. 2017.
[4] Powercast. *Powercast* [Online]. Available: http://www.powercastco.com
[5] O. Ozel, K. Tutuncuoglu, J. Yang, S. Ulukus, and A. Yener, "Transmission with energy harvesting nodes in fading wireless channels: optimal policies," *IEEE Journal on Selected Areas in Communications*, vol. 29, no. 8, pp. 1732–1743, Aug. 2011. doi: 10.1109/JSAC.2011.110921.
[6] J. Gong, S. Zhou, and Z. Niu, "Optimal power allocation for energy harvesting and power grid coexisting wireless communication systems," *IEEE Transactions on Communications*, vol. 61, no. 7, pp. 3040–3049, Jul. 2013. doi: 10.1109/TCOMM.2013.05301313.120705.
[7] M. A. Antepli, E. Uysal-Biyikoglu, and H. Erkal, "Optimal packet scheduling on an energy harvesting broadcast link," *IEEE Journal on Selected Areas in Communications*, vol. 29, no. 8, pp. 1721–1731, Feb. 2011. doi: 10.1109/JSAC.2011.110920.
[8] J. Yang and S. Ulukus, "Optimal packet scheduling in a multiple access channel with energy harvesting transmitters," *Journal of Communications and Networks*, vol. 14, no. 2, pp. 140–150, Apr. 2012. doi: 10.1109/JCN.2012.6253062.
[9] C. Hu, J. Gong, X. Wang, S. Zhou, and Z. Niu, "Optimal green energy utilization in MIMO systems with hybrid energy supplies," *IEEE Transactions on Vehicular Technology*, vol. 64, no. 8, pp. 3675–3688, Aug. 2015. doi: 10.1109/TVT.2014.2354677.
[10] A. Minasian, S. ShahbazPanahi, and R. S. Adve, "Energy harvesting cooperative communication systems," *IEEE Transactions on Wireless Communications*, vol. 13, no. 11, pp. 6118–6131, Nov. 2014. doi: 10.1109/TWC.2014.2320977.
[11] O. Ozel and S. Ulukus, "Achieving AWGN capacity under stochastic energy harvesting," *IEEE Transactions on Information Theory*, vol. 58, no. 10, pp. 6471–6483, Oct. 2012. doi: 10.1109/TIT.2012.2204389.
[12] V. Jog and V. Anantharam, "An energy harvesting AWGN channel with a finite battery," in *IEEE International Symposium on Information Theory*, Honolulu, USA, Jun. 2014, pp. 806–810. doi: 10.1109/ISIT.2014.6874944.
[13] C. Huang, J. Zhang, P. Zhang, and S. Cui, "Threshold-based transmissions for large relay networks powered by renewable energy," in *IEEE Global Communications Conference*, Atlanta, USA, Dec. 2013, pp. 1921–1926. doi: 10.1109/GLOCOM.2013.6831355.
[14] H. Li, C. Huang, S. Cui, and J. Zhang, "Distributed opportunistic scheduling for wireless networks powered by renewable energy sources," in *IEEE International Conference on Computer Communications*, Toronto, Canada, Apr. 2014, pp. 898–906. doi: 10.1109/INFOCOM.2014.6848018.
[15] J. Gong, S. Zhou, and Z. Zhou, "Networked MIMO with fractional joint transmission in energy harvesting systems," *IEEE Transactions on Communications*, vol. 64, no. 8, pp. 3323–3336, Aug. 2016. doi: 10.1109/TCOMM.2016.2589267.
[16] NREL. *Measurement and Instrumentation Data Center (MIDC)* [Online]. Available: http://www.nrel.gov/midc
[17] D. Willkomm, S. Machiraju, J. Bolot, and A. Wolisz, "Primary user behavior in cellular networks and implications for dynamic spectrum access," *IEEE Communications Magazine*, vol. 47, no. 3, pp. 88–95, Mar. 2009. doi: 10.1109/MCOM.2009.4804392.
[18] C. Huang, R. Zhang, and S. Cui, "Optimal power allocation for outage probability minimization in fading channels with energy harvesting constraints," *IEEE Transactions on Wireless Communications*, vol. 13, no. 2, pp. 1074–1087, Feb. 2014. doi: 10.1109/TW.2013.121813.130953.
[19] K. Huang, M. Kountouris, and V. O. K. Li, "Renewable powered cellular networks: energy field modeling and network coverage," *IEEE Transactions on Wireless Communications*, vol. 14, no. 8, pp. 4234–4247, Aug. 2015. doi: 10.1109/TWC.2015.2418262.
[20] S. Zhou, T. Chen, W. Chen, and Z. Niu, "Outage minimization for a fading wireless link with energy harvesting transmitter and receiver," *IEEE Journal on Selected Areas in Communications*, vol. 33, no. 3, pp. 496–511, Mar. 2015. doi: 10.1109/JSAC.2015.2391951.
[21] G. Auer, V. Giannini, I. Godor, et al., "Cellular energy efficiency evaluation framework," in *IEEE Vehicular Technology Conference*, Yokohama, Japan, May 2011, pp. 1–6. doi: 10.1109/VETECS.2011.5956750.
[22] M. Gorlatova, A. Wallwater, and G. Zussman, "Networking low-power energy harvesting devices: measurements and algorithms," in *Proc. IEEE International Conference on Computer Communications*, Shanghai, China, Apr. 2011, pp. 1602–1610. doi: 10.1109/INFCOM.2011.5934952.
[23] J. Gong, S. Zhou, Z. Zhou, and Z. Niu, "Policy optimization for content push via energy harvesting small cells in heterogeneous networks," *IEEE Transactions on Wireless Communications*, vol. 16, no. 2, pp. 717–729, Feb. 2017. doi: 10.1109/TWC.2016.2628789.
[24] T. Han and N. Ansari, "On optimizing green energy utilization for cellular networks with hybrid energy supplies," *IEEE Transactions on Wireless Communications*, vol. 12, no. 8, pp. 2872–2882, Apr. 2013. doi: 10.1109/TCOMM.2013.051313.121249.
[25] J. Gong, J. Thompson, S. Zhou, and Z. Niu, "Base station sleeping and resource allocation in renewable energy powered cellular networks," *IEEE Transactions on Communications*, vol. 62, no. 11, pp. 3801–3813, Nov. 2014. doi: 10.1109/TCOMM.2014.2359883.

[26] I. Krikidis, S. Timotheou, S. Nikolaou, et al., "Simultaneous wireless information and power transfer in modern communication systems," *IEEE Communications Magazine*, vol. 52, no. 11, pp. 104–110, Nov. 2014. doi: 10.1109/MCOM.2014.6957150.
[27] S. Zhou, J. Gong, Z. Zhou, W. Chen, and Z. Niu, "GreenDelivery: proactive content caching and push with energy-harvesting-based small cells," *IEEE Communications Magazine*, vol. 53, no. 4, pp. 142–149, Apr. 2015. doi: 10.1109/MCOM.2015.7081087.
[28] J. Gong, S. Zhou, Z. Zhou, and Z. Niu, "Policy optimization for content push via energy harvesting small cells in heterogeneous networks," *IEEE Transactions on Wireless Communications*, vol. 16, no. 2, pp. 717–729, Feb. 2017. doi: 10.1109/TWC.2016.2628789.
[29] J. Gong and X. Chen, "Throughput maximization of hybrid full-duplex/half-duplex relay networks with energy harvesting," in *IEEE Global Communications Conference*, Washington D.C., USA, Dec. 2016, pp. 1–6. doi: 10.1109/GLOCOM.2016.7842328.
[30] S. Zhang, N. Zhang, S. Zhou, et al., "Energy-aware traffic offloading for green heterogeneous networks," *IEEE Journal on Selected Areas in Communications*, vol. 34, no. 5, pp. 1116–1129, May 2016. doi: 10.1109/JSAC.2016.2520244.
[31] Z. Niu, Y. Wu, J. Gong, and Z. Yang, "Cell zooming for cost-efficient green cellular networks," *IEEE Communications Magazine*, vol. 48, no. 11, pp. 74–79, Nov. 2010. doi: 10.1109/MCOM.2010.5621970.
[32] D. P. Bertsekas, *Dynamic Programming and Optimal Control*. Belmont, USA: Athena Scientific, 2005.

Manuscript received: 2017-11-21

Biographies

GONG Jie (gongj26@mail.sysu.edu.cn) received his B.S. and Ph.D. degrees in Department of Electronic Engineering in Tsinghua University, China in 2008 and 2013, respectively. From July 2012 to January 2013, he visited Institute of Digital Communications, University of Edinburgh, UK. From July 2013 to October 2015, he worked as a postdoctorial scholar in Department of Electronic Engineering in Tsinghua University. He is currently an associate research fellow with School of Data and Computer Science, Sun Yat-sen University, China. He was a co-recipient of the Best Paper Award from IEEE Communications Society Asia-Pacific Board in 2013. He was selected as the IEEE Wireless Communications Letters (WCL) Exemplary Reviewer in 2016. His research interests include cloud RAN, energy harvesting technology and green wireless communications. He published more than 50 scientific papers.

ZHOU Sheng (sheng.zhou@tsinghua.edu.cn) received the B.E. and Ph.D. degrees in electronic engineering from Tsinghua University, China in 2005 and 2011, respectively. From January to June 2010, he was a visiting student at the Wireless System Lab, Department of Electrical Engineering, Stanford University, USA. From November 2014 to January 2015, he was a visiting researcher in Central Research Lab of Hitachi Ltd., Japan. He is currently an associate professor with the Department of Electronic Engineering, Tsinghua University. His research interests include cross-layer design for multiple antenna systems, mobile edge computing, and green wireless communications. He has published more than 150 scientific papers.

DOI: 10.3969/j.issn.1673-5188.2018.01.005
http://kns.cnki.net/kcms/detail/34.1294.TN.20180212.1116.002.html, published online February 12, 2018

Recent Advances of Simultaneous Wireless Information and Power Transfer in Cellular Networks

LIU Binghong, PENG Mugen, and ZHOU Zheng
(Beijing University of Posts and Telecommunications, Beijing 100876, China)

Abstract

As a promising solution to alleviating the energy bottleneck in wireless devices with limited battery capacity, simultaneous wireless information and power transfer (SWIPT) techniques have been widely researched in cellular networks. To further improve the spectral and energy efficiency of wireless information and power transfer, the combination of SWIPT and new techniques in cellular networks has drawn much attention recently. In this paper, we comprehensively survey the key techniques for SWIPT, the combination of SWIPT and new techniques in cellular networks, challenges and open issues. The key techniques for SWIPT including traditional power splitting, time switching, etc., and joint receiving and transmitting techniques such as eigenchannels and mixed signals are provided in detail. Furthermore, the applications of SWIPT to recent techniques such as SWIPT-assisted non-orthogonal multiple access, SWIPT-assisted device-to-device communication, and SWIPT-assisted full-duplex communication, are comprehensively summarized in this paper. The potential open issues including the management of dynamic harvested energy, trading between wireless power transfer and traffic offloading, and effects of the mode switching at energy harvesting devices, are outlined as well.

Keywords

SWIPT; non-orthogonal multiple access; device-to-device communication; full-duplex communication

1 Introduction

Limited device battery life has always been a key consideration in the energy-constrained wireless network and largely confines the performance of the network. In order to prolong the battery life, a sustainable power supply has to be considered. In the near-field communication, techniques such as inductive coupling and magnetic resonance coupling contribute to high power density and conversion efficiency. However, because of the non-radiative property, the power transfer distance of these techniques is limited. As a result, in the far-field communication, the radio frequency (RF) signal is chosen as a continuous and stable power supply. Recently, the dual use of RF signals including information transmitting and power delivering has been studied. Simultaneous wireless information and power transfer (SWIPT) [1] is an emerging technology to utilize RF signals to transmit information and energy concurrently and offers a promising solution to above problems.

In recent years, attention on SWIPT in mobile communication networks has been growing significantly. For instance, in [2], a two-user Multiple-Input Single-Output (MISO) interference channel with SWIPT is discussed, in which different transmission strategies are proposed to maximize the achievable sum rate. And in [3], multiuser Multiple-Input Multiple-Output (MIMO) systems with SWIPT are studied. There are two scenarios, including separated information decoding (ID) and energy harvesting (EH) receivers and co-located ID and EH receivers, and optimal transmission strategies are proposed to achieve different tradeoffs between maximal information rate and energy transfer for the separated scenario. In addition, in [4], SWIPT is also applied into broadband wireless systems. In this system, the integration of SWIPT and microwave power transfer has been considered as a convenient power supply, freeing the wireless devices from the limited battery capacities. The optimization of power control for different system configurations (i.e. single-user/multiple-user and downlink/uplink information transfer) is studied and the optimal algorithm is used to sequentially allocate required decoding power for mobile devices in ascending order until all the budgeted power is spent.

Nowadays, to further improve the transmission performance, the combination of SWIPT and 5G key techniques has been considered to improve the spectral efficiency (SE) and energy efficiency (EE). As a key technique for the 5G wireless net-

work, massive MIMO is used to satisfy the demand for the ever-increasing data traffic and enhance the spectral efficiency and radiated energy efficiency. Therefore, the surveys [5] and [6] investigate the existing work of massive MIMO with SWIPT. In particular, [5] describes the general architecture of distributed massive MIMO, including receiver/transmitter design and beamforming in the uplink/downlink. Then, it proposes future directions based on interference management and power allocation. Furthermore, the survey [6] introduces relay in MIMO SWIPT networks and investigate different network topologies with single and multiple users.

The existing surveys about SWIPT to 5G key techniques involve massive MIMO and relaying [5], [6]. However, surveys about combination of SWIPT with key techniques in 5G networks such as non-orthogonal multiple access (NOMA), device-to-device (D2D) and full-duplex (FD) are still open. Therefore, to fill in this gap, we provide a comprehensive survey about the applications of SWIPT with the key techniques for 5G networks in this paper.

The contributions of this work are three-folds, which are summarized as follows:

- A comprehensive survey on SWIPT techniques is presented, besides the popular receiving techniques for SWIPT, such as power splitting, time switching and antenna switching. Recent advantages on joint transmitting and receiving techniques for SWIPT based on the designs of Eigen-channels or mixed signals are also concluded.
- The 5G key techniques that have been applied to SWIPT are comprehensively surveyed in this paper. In particular, as shown in **Table 1**, SWIPT with NOMA, with D2D communication, and with FD communication are illustrated respectively, which improve the SE and EE of communication in cellular networks.
- The future directions and open problems related to SWIPT in cellular networks are identified, as the management of dynamic harvested energy, trading between wireless power transfer and traffic offloading, and effects of the mode switching at energy harvesting devices, which are vital for the future development of SWIPT.

The rest of this survey is organized as follows. Section 2 introduces practical techniques to realize SWIPT, including receiver design techniques and joint transmitter and receiver design techniques. Section 3 discusses the combination of SWIPT and some 5G key techniques including NOMA, D2D and FD based on the realizing technologies mentioned in Section 2. Section 4 provides some future challenges and open issues. Finally, Section 5 concludes the survey.

▼Table 1. Contributions of survey

Aspects	Survey papers	Contributions
Realizing techniques for SWIPT	[7], [8]	Surveys about wireless energy transfer technology, its applications, and three types of practical SWIPT receivers.
	[9]	A survey about receiving and transmitting techniques, and resource allocation for SWIPT.
	[10]	A hybrid receiver design to maximize the achievable rate in relay channels.
	This Article	A comprehensive survey on techniques for SWIPT, including receiving techniques and joint transmitting and receiving techniques.
SWIPT with NOMA	[12], [13]	Performance analysis on SWIPT with NOMA for single user pair.
	[14], [15]	Performance analysis on SWIPT with NOMA for multiple user pairs.
	[16], [17]	Performance analysis on NOMA with wireless powered relay.
	This Article	A comprehensive survey of NOMA with SWIPT, including pairing schemes, with/without relay, relaying protocols, the node and receiving techniques for SWIPT.
SWIPT with D2D	[18], [19]	Techniques for wireless powered D2D communication.
	[20]–[22]	Techniques for wireless powered D2D relay.
	This Article	A comprehensive survey of D2D with SWIPT, including with/without relay, receiving techniques for SWIPT and relaying protocols.
SWIPT with FD	[24]–[28]	Transmission schemes for two-phase FD relaying systems with SWIPT.
	[29], [30]	Transmission schemes for one-phase FD uplink and downlink communications with SWIPT.
	This Article	A comprehensive survey of two types of FD, including with/without relay, relaying protocols, the node and receiving techniques for SWIPT.

D2D: device-to-device NOMA: non-orthogonal multiple access
FD: full-duplex SWIPT: simultaneous wireless information and power transfer

2 Techniques for SWIPT

In SWIPT systems, dual use of RF signals is exploited to simultaneously transmit information and energy. Therefore, the receiver of SWIPT has to be split into EH receiver and ID receiver to deal with the information and energy respectively. This section considers practical receiver designs for SWIPT. Furthermore, based on techniques at the receiver, joint transmitting and receiving techniques are proposed, which can improve the performance of energy harvesting and information decoding by designing the transmitted channel or signal.

2.1 Receiving Techniques for SWIPT

Practical receiver design techniques include power splitting (PS), time switching (TS) and antenna switching (AS) [7] (**Fig. 1**). These three techniques split the RF signal resources from the energy domain, the time domain and the space domain respectively.

2.1.1 Power Splitting

As shown in Fig. 1a, the PS receiver consists of a EH receiver and an ID receiver. By using PS ratio ρ, the PS receiver splits the received signal $y(t)$ into two streams with different

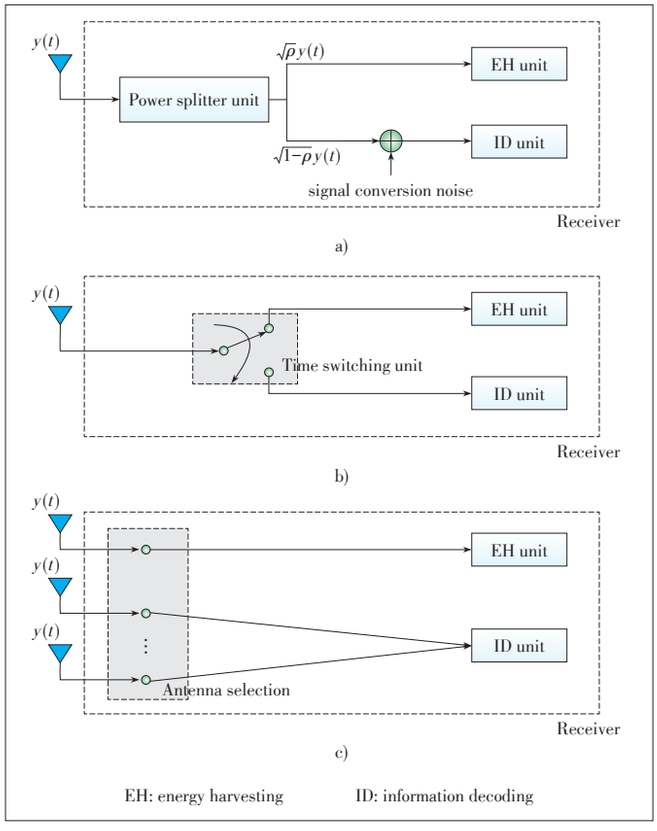

▲Figure 1. Receiving techniques for SWIPT, including a) power splitting, b) time switching and c) antenna switching.

power, namely $\sqrt{\rho}\,y(t)$ and $\sqrt{1-\rho}\,y(t)$. One is used for harvesting energy at the EH receiver, while the other is used for decoding information at the ID receiver at the same time. It should be noted that there is a signal conversion noise added to the ID receiver, which is produced by RF band to baseband conversion. Different rate-energy trade-offs can be achieved by adjusting the PS ratio ρ.

2.1.2 Time Switching

In this case, the transmitter divides the transmission block into two orthogonal time slots based on the TS factor. One slot is used for data transmission and the other is used for power transmission. At each time slot, the transmitter can optimize its transmission waveforms to achieve better transmission for information or energy.

2.1.3 Antenna Switching

There are multiple antennas at the AS receiver. These antennas are divided into two groups, one group for information decoding and the other for energy harvesting [8]. To decide the optimal assignment of the antenna elements for information decoding and energy harvesting, the solution of an optimization problem in each communication frame is required. Furthermore, antenna switching can be regarded as a special case of power splitting, which the PS ratio at each antenna is binary.

Based on the techniques mentioned above, a comprehensive SWIPT architecture, i.e., the hybrid time-switching/power-splitting (TS/PS) energy harvesting receiver or the hybrid time-switching/antenna-switching (TS/AS) energy harvesting receiver and the hybrid power-splitting/antenna-switching (PS/AS) [9] can be further considered.

2.2 Joint Transmitting and Receiving Techniques for SWIPT

In this section, we mainly focus on the design of the transmitter, including decomposing the transmission channel into multiple sub-channels: eigenchannels and using mixed-signals for transmission (**Fig. 2**).

2.2.1 Eigenchannels

As referred in [10], the communication link is decomposed into multiple eigenchannels, which can be used either to convey information or to transfer energy. As shown in Fig. 2a, at the output of each eigenchannel, there is a switch that switches the channel output either to the information decoding receiver or to the energy harvesting receiver.

2.2.2 Mixed Signals

There is an information signal X_I sent to the ID receiver and an energy signal X_E sent to the EH receiver. The mixed signal includes both of them. Then we can perform the beamforming for the mixed transmission signal to achieve better performance at the ID and EH receivers. To be more specific, by designing the mixed signal at the transmitter, i.e. using the pseudo random signal as the energy signal, which is known by the

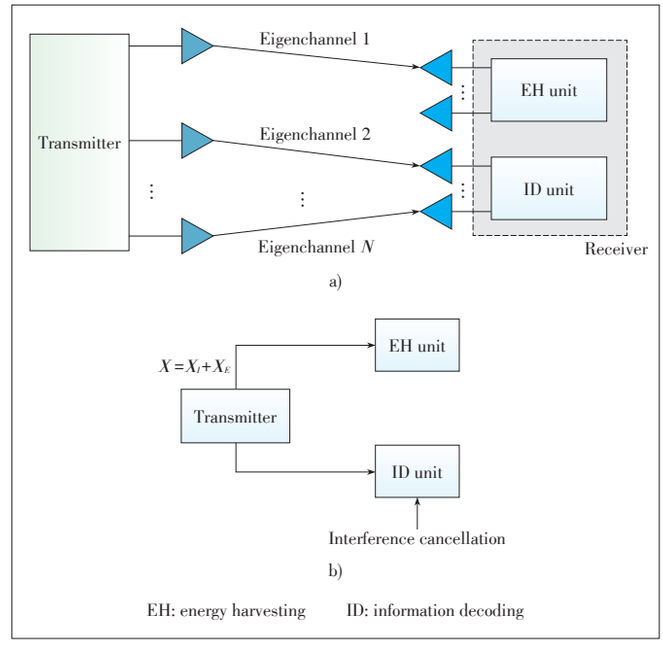

▲Figure 2. Joint transmitting and receiving techniques for SWIPT.

receiver, the ID receiver can use successive interference cancellation (SIC) to remove the energy signal. Meanwhile, the information signal can also be used as a source of energy, which increases the energy harvested at the EH receiver and enhances its performance.

3 Combination of SWIPT and Recent Techniques in Cellular Networks

Except for massive MIMO, recent techniques in cellular networks include NOMA, D2D and full-duplex, which contribute to the enhancement of spectrum efficiency and network capacity. NOMA is to realize multiple access in the power domain. D2D is used to provide proximity services and enable the establishment of high data rate peer-to-peer (P2P) links. And full-duplex allows device to transmit and receive on the same frequency concurrently. However, devices involved in all of these techniques are faced with a limited battery capacity, which leads to a constrained performance. Therefore, the combination of SWIPT and 5G key techniques has a promising prospect in the future network.

3.1 SWIPT with Non-Orthogonal Multiple Access

Non-orthogonal multiple access has been considered as an emerging technology for the 5G network [11], which improves the SE by superposing multiple users in power domain. In NOMA systems, the near NOMA user acts as a relay to help transmit information for the far NOMA user, which shorten the lifetime of the energy-constrained near NOMA users. As a result, cooperative NOMA with SWIPT (SWIPT-CNOMA) is proposed, so that the near user can harvest energy from received signals and then use the harvested energy rather than its own energy to assist the information transmission for the far NOMA user.

In SWIPT-CNOMA, a near user and a far user are chosen to pair. Then there is a two-phase transmission. In the first transmission phase, the access point (AP) broadcasts superposed signals to both of the two users. The near user adopts power splitting scheme to use the part of the received signal for energy harvesting and the rest for information decoding. Particularly, based on SIC, the near user first decodes the message of the far user and then subtracts it from its observation to decode its own information. While the far user just keeps the received signal for jointly decoding in the second phase. In the second phase, the far user forwards the message decoded in the first phase to the weak user by its harvested energy. At the end of the second phase, the far user decodes the message jointly based on the signals received from AP and the near user using maximal-ratio combination (MRC).

Hence, in the following paragraphs, we will introduce three kinds of NOMA with SWIPT (**Fig. 3** and **Table 2**), the first two types are about user pairing including single user pair and mul-

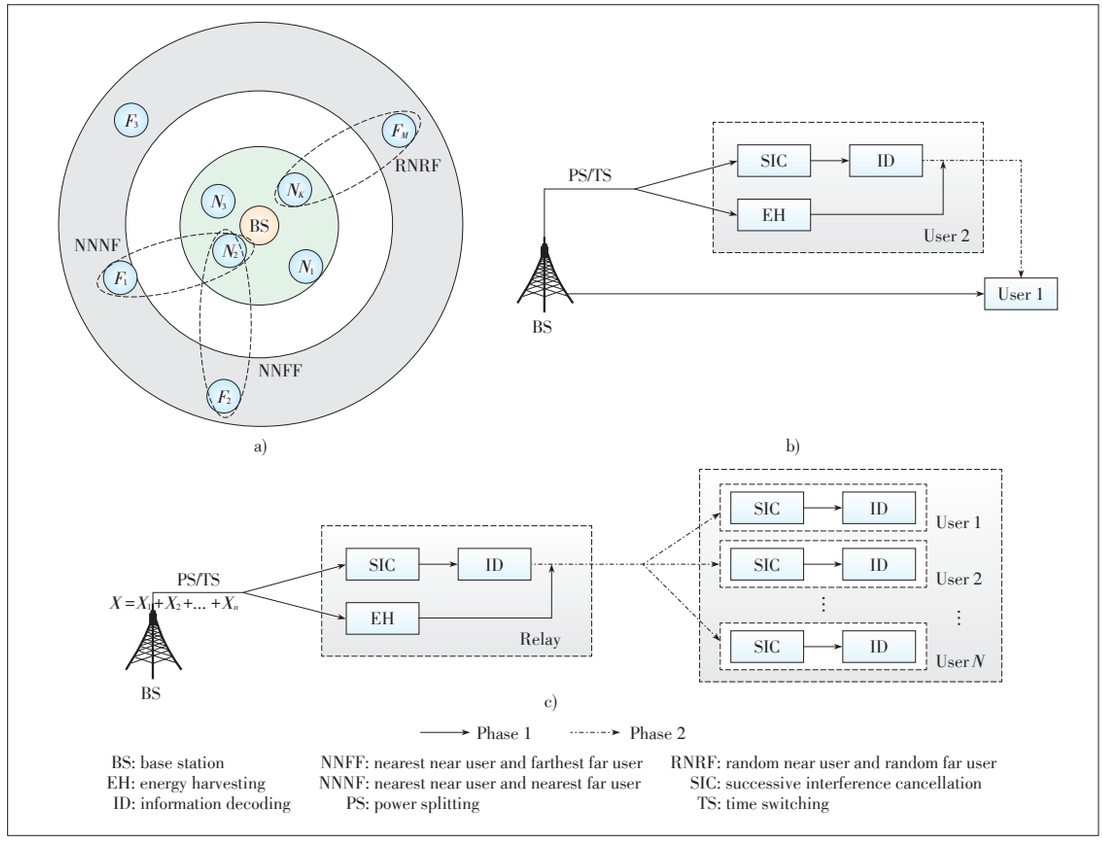

Figure 3. ▶ SWIPT with NOMA: a) pairing schemes for near and far users; b) transmission scheme for NOMA with wireless powered relaying at the near user; c) transmission scheme for NOMA with the EH relay.

▼Table 2. Summary of SWIPT with NOMA

Literature	System model	Transmission protocol	SWIPT technique	Design objective (far/near)
Y. Xu et al. [12]	One BS with single user pair	NOMA with wireless powered DF relaying at the near user	PS at the near user	Maximization of the data rate
N. T. Do et al. [13]	One BS with single user pair	NOMA with wireless powered DF relaying at the near user	Hybrid TS/PS at the near user	Closed-form approximate expressions for the outage probability
Y. Liu et al. [14]	One source with multiple user-pairs	NOMA with wireless powered DF relaying at the near user	PS at the near user	Outage probability and system throughput
Y. Ye et al. [15]	One BS with multiple user-pairs	NOMA with wireless powered DF relaying at the near user	PS at the near user	Ensure target data rates of the relay and the far user are realized prior to harvesting energy
Z. Zhang et al. [16]	One source, an energy-harvesting relay and a user group (2 users)	NOMA with wireless powered DF relaying at the energy-harvesting relay	PS at the energy-harvesting relay	Performance analysis of the outage probability and SNR
W. Han et al. [17]	One BS, an energy-harvesting relay and a user group (multiple users)	NOMA with wireless powered DF relaying at the energy-harvesting relay	PS at the energy-harvesting relay	Performance of the outage probability

BS: base station
DF: decode-and-forward
NOMA: non-orthogonal multiple access
PS: power splitting
SNR: signal-noise ratio
SWIPT: simultaneous wireless information and power transfer
TS: time switching

tiple user pairs, the last is about users with relay.

3.1.1 Single User Pair

In the case of single user pair, there only exists one near-far user pair. Specifically, considering a downlink MISO transmission system in [12]. To achieve the maximization of the near user's data rate while satisfying the far user's QoS requirement, the corresponding transmitting beamformers and PS ratio have to be optimized. Demonstrated by simulation, the proposed SWIPT-CNOMA strategy outperforms the existing SWIPT orthogonal multiple access (OMA) strategy, thus marking it a promising candidate for enabling high throughput in IoT and mMTC scenarios.

The author in [13] also considers the situation of single user pair. Furthermore, it takes the impact of the wireless AP with multiple antennas on the transmission performance into consideration. When the source is equipped with multiple antennas, [13] proposes two transmit antenna selection schemes to reduce the complexity of precoding design at the transmitter. The first scheme is selecting an antenna that provides the strongest channel condition of the channel from the AP to the far user. The second scheme is selecting an antenna that maximizes the gain of the channel from the base station (BS) to the near user. The transmission divides into two phases. Different from [12], in the first phase, the near user adopts hybrid time switching and power splitting technologies to obtain information and energy simultaneously, which provides higher flexibility than the conventional power splitting scheme. To be more specific, in the first transmission phase, the AP broadcasts the superposed signals to users, which contain information of the near and far users. In particular, for a near user, the block time T is divided into two sub-blocks. In the first sub-block, the near user harvests energy from its received signal. In the second sub-block, the near user simultaneously utilizes the received power for energy harvesting and information decoding, while the far user just keeps the received signal for jointly decoding in the second phase. The second transmission phase is similar to the process referred in [12]. The authors derive tight closed-form approximate expressions for the outage probability (OP) of near and far users and analyze diversity order of two antenna selection schemes. The results demonstrate that at the high SRN region, the first antenna selection scheme outperforms the second and vice-versa, which exactly reflects the characteristics of the two proposed schemes.

3.1.2 Multiple User Pairs

Considering the situation of multiple user pairs, users are divided into two groups: near users and far users, based on their distance from the BS. Therefore, different near-far user pairing schemes have to be chosen. The work in [14] proposes three user selection schemes based on the user distance from the BS:

- Random near user and random far user (RNRF) selection scheme, in which both the near and far users are randomly selected from the two groups. The advantage of RNRF is that it does not require the knowledge of instantaneous channel state information (CSI).
- Nearest near user and nearest far user (NNNF) selection scheme, in which a near user and a far user closest to the BS are selected from the two groups. This scheme can enable the selected near user to harvest more energy and minimize the outage probability of both the near and far users.
- Nearest near user and farthest far user (NNFF) selection, in which a near user that is closest to the BS is selected and a far user that is farthest from the BS is selected. The transmission in this paper is similar to [12]. The authors derive closed-form expressions for the outage probability and system throughput of three user selection schemes to evaluate the performance. The results confirm that NNNF outperforms other two schemes with the lowest outage probability and the highest throughput for both the near and far users.

The work in [15] also considers the situation of multiple user pairs and the user selection scheme is based on the RNRF scheme referred in [14], which does not need instantaneous CSI and can be easy of implementation. The authors mainly discuss the PS ratio in the first transmission phase. The previous PS protocol in [12] sets that in the first phase, as long as the decoding correctness of far users' information is guaranteed, the rest of the signal is totally used for energy harvesting at the near user (namely the EH relay), which may result that the near user may not be able to decode its own information correctly. Therefore, the new proposed PS protocol sets the PS ratio to firstly ensure the decoding correctness of both near users' information and far users' information at the near user, then use the rest signal for energy harvesting. The impact of the proposed PS protocol for far users on the outage probability of both near and far NOMA users is studied. Simulation results show that comparing with the existing PS protocol in [12], the proposed PS protocol can greatly reduce the outage probability of the near users and enhance system throughput. Meanwhile, it does not affect the outage performance of far users.

3.1.3 Users with Relay

Besides the traditional multiple access scenarios, the combination of SWIPT and NOMA is applied into cooperative non-orthogonal multiple access scenarios, which mainly considers that the source node is far from users and the EH relay is introduced to provides service for users.

The work in [16] considers a situation that a source node communicates with two users through an energy harvesting relay. The transmission is divided into two phases. In the first phase, the source uses superposition coding to combine two independent signals of near and far users, and the relay receives information and energy from the source simultaneously. Specifically, firstly the relay uses part of the signal for harvesting energy and the rest for decoding information. In the information decoding process, based on SIC, the relay first decodes the far users' information and then, decodes the near user information. In the second phase, the relay uses the energy harvested from the first phase to simultaneously serve two users through NOMA. Specifically, based on decode-and-forward (DF) protocol, the relay transmits the superposed signals to two users. Then the far user will directly decode its own information and the near user will decode the far users' information based on SIC and then decode its own information. In this paper, the effect of power allocation on SWIPT-CNOMA has been investigated. The results show that compared with traditional OMA with SWIPT, NOMA can efficiently lower the outage probability and obtain the same diversity gain.

Similar to the study in [16], [17] considers a source communicating with a group of users through an EH relay. Existing works are mostly focused on single-antenna system and Rayleigh fading channels. However, the work in [17] mainly investigates the impact of multiple antennas and Nakagami-m fading channels on transmission performance of the NOMA EH relay, in which the multiple-antenna technology is used to improve the performance of information and energy transmission. The paper introduces Nakagami-m distribution because it is better at modeling empirical data than Rayleigh distribution. The transmission can also be divided into two phases, while the relay uses the amplify-and-forward (AF) protocol to forward information. To be more specific, in the first phase, the source is equipped with multiple antennas. The transmit antenna that maximizes the channel gain between the source and the relay is chosen for transmitting the superposed signal to the relay, which enhances the performance of the system. On the basis of PS protocol, the received signals at the EH relay are split into two parts, one for harvesting energy and the other for processing information. In the second phase, based on NOMA, the relay uses the energy harvested from the first phase to broadcast the superposed signal. Because the user is equipped with multiple antennas, so the received signals are combined with the rule of MRC. Then, users decode the signals using the optimal order for SIC, which is in the order of the increasing channel gain, where users with better channel conditions are required to decode the signals for others before decoding their own. The paper concentrates on the outage performance of NOMA-EH relaying networks and derives closed-form expressions for the outage probability. Finally, simulation results demonstrate that the worst relay location for both NOMA-EH and OMA-EH relaying networks is the half-way point between users and the BS. Furthermore, it is shown that NOMA-EH outperforms OMA-EH with better performance of outage probability and EE. Meanwhile, NOMA can provide better user fairness and SE since more users can be served at the same time.

3.2 SWIPT with D2D Communications

D2D communication, which provides proximate services by establishing direct links between devices rather than through the BS, has emerged as a key technology for future 5G system to solve the conflict between the limited network bandwidth and the growing demands of users. However, the growing demand for higher data rate and ubiquitous mobile services have caused a high-energy consumption in mobile devices with limited battery capacities, which becomes a bottleneck of the network lifetime. SWIPT enables the receivers to harvest RF energy from the transmitters to extend their lifetimes and improve the EE. What's more, the traditional harmful noise and interference can also be exploited as a source of energy to improve the EE. Therefore, the SWIPT with D2D (**Fig. 4** and **Table 3**) has been proposed, facilitating the deployment of D2D networks by prolonging the network lifetime.

In the following paragraphs, we will talk about SWIPT with D2D mainly from three aspects. Firstly, we will analyze the performance of the energy harvesting-based D2D communications. Then, we will discuss the performance of D2D user equipment relay. Finally, we will investigate the security issue

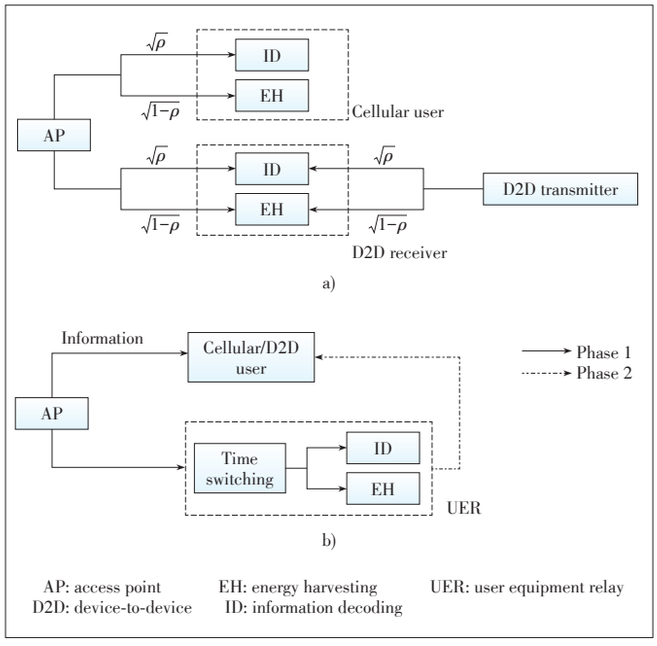

▲**Figure 4. SWIPT with D2D: a) wireless powered UE communications; b) wireless powered relaying at the D2D transmitter.**

in cooperative D2D communications with SWIPT.

3.2.1 Energy Harvesting-Based D2D Communications

The performance of the energy harvesting-based D2D communications are discussed based on two aspects: the outage probability and the EE performance.

The work in [18] analyzes cognitive and energy harvesting-based D2D communication in cellular networks from the perspective of the outage probability. In this paper, there are multiple macro BSs, multiple cellular users and multiple D2D pairs, in which D2D users can reuse downlink (DL) resource blocks (RBs) occupied by cellular UEs to enhance the system SE. All D2D transmitters are powered by energy harvested from the ambient interference caused by the simultaneous cellular transmissions in the network (i.e., downlink and uplink transmissions), and then use one of the channels allocated to cellular UEs to communicate with the corresponding receivers. Considering the power-hungry characteristic of the user equipment, D2D users with SWIPT communicate with each other only when they harvest enough energy. The authors in [18] propose two spectrum access policies for cellular communication in the uplink or downlink and use tools from stochastic geometry to evaluate the performance of the proposed communication system model with general path-loss exponent in terms of outage probability for D2D and cellular UEs. The results show that energy harvesting can be a reliable alternative to power cognitive D2D transmitters while achieving acceptable performance.

The study in [19] aims to address joint power control and spectrum resource allocation problem in SWIPT-based energy-harvesting D2D underlay networks from the perspective of the EE. In this paper, there are only one BS, multiple users and multiple D2D pairs. Each user can harvest energy from the received desired signals, interference signals and noise. As a result of downlink spectrum reusing, a cellular user can scavenge energy from the BS and the D2D transmitter using the same channel, while a D2D receiver can harvest energy from its corresponding D2D transmitter and the BS. The D2D users with SWIPT can communicate with each other as long as they harvest energy, which improves the EE performance. The purpose of this work is to maximize the EE performance of D2D links and the amount of energy harvested at cellular UEs by designing an efficient resource allocation mechanism. Hence, a joint optimization problem of power control and partner selection between D2D pairs and cellular UEs has to be considered. Simulation results demonstrated that the EH-based energy-efficient stable matching algorithm can achieve the best EE performance under all of the considered scenarios.

3.2.2 User Equipment Relay

Except for the functionality that users in the D2D pair can

▼**Table 3. Summary of SWIPT with D2D**

Literature	Mode	Scenario	SWIPT technique	Design objective
A. H. Sakr et al. [18]	Wireless powered user equipment communication	Multiple macro BSs, multiple users and multiple D2D users	TS at the D2D transmitter	Performance evaluation of the outage efficiency
Z. Zhou et al. [19]	Wireless powered user equipment communication	One BS, multiple cellular users and multiple D2D users	PS at the D2D transmitter	Performance analysis of the energy efficiency
H. H. Yang et al. [20]	Wireless powered DF relaying at the D2D transmitter	Multiple APs, cellular users, D2D users, where the idle D2D transmitter acts as the relay	TS at the D2D transmitter	Performance analysis of the outage probability
R. Atat et al. [21]	Wireless powered DF relaying at the D2D transmitter	One BS, cellular users, D2D users, where the idle D2D transmitter acts as the relay, along with MTC devices	TS at the D2D transmitter	Performance analysis of the spectral efficiency
R. I. Ansari et al. [22]	Wireless powered DF relaying at the D2D transmitter	One BS, cellular users, D2D users, where the idle D2D transmitter acts as the relay	TS at the D2D transmitter	Performance evaluation of the outage probability

AP: access point
BS: base station
D2D: device-to-device
DF: decode-and-forward
PS: power splitting
SWIPT: simultaneous wireless information and power transfer
TS: time switching

communicate directly with each other, D2D UEs can also act as a relay for UEs by cooperative transmission and traffic offloading. Therefore, the concept of mobile user equipment relay (UER) has been introduced to support D2D communications for enhancing communication reliability. However, as the UER needs to use its own power for data transmission of other UEs, relaying information in D2D communication may be undesirable for the UER and UEs are not obligated to provide energy for the UER. Therefore, SWIPT is introduced for energy compensation. Namely, the UER harvests energy from APs and relays information of other UEs in D2D communication using only the harvested energy.

The work in [20] considers a D2D communication provided EH heterogeneous cellular network (HCN), where APs are capable of performing wireless power transfer and UEs can harvest energy from nearby APs. Specifically, the UER can harvest energy from the RF signal transmitted by nearby wireless APs and then store it. When the harvested energy has been accumulated to a certain threshold, the UER will be chosen to achieve the best performance based on the best UER selection strategy. By introducing the EH region (EHR) and modeling the status of harvested energy using Markov chain, the network outage probability is derived in close form to measure the performance of a D2D communication provided EH HCN. The results show that by exploiting EH-D2D communication, the energy can be saved by turning off some APs while maintaining a certain level of expected outage probability. The results also show that there exist the optimal AP transmit power which increases with EH efficiency, and the optimal offloading bias which decreases compared to an HCN without EH-D2D communication.

Considering the future 5G networks, there are massive numbers of machine-type communication (MTC) devices to be scheduling and powering. Offloading MTC traffic onto D2D communication links can better manage radio resources and reduce MTC devices energy consumption. However, it requires D2D users to use their own limited energy to relay MTC traffic. Therefore, the study in [21] proposes using D2D communication to offload MTC traffic and exploiting RF energy harvesting for powering D2D relay transmission. A cellular network consists of cellular users, MTC devices and D2D relays, where D2D users and cellular users (CUs) share the licensed uplink spectrum, while MTC devices use orthogonal spectrum resources. Specifically, to lower MTC devices energy consumption and improve the transmission performance, the EH-D2D user can serve as a D2D relay, which is able to access a fraction of the spectrum occupied by cellular users, to help relay the information of MTC devices to the BS. To protect cellular users, the spectrum available to D2D users needs to be reduced, which limits the number of D2D transmissions, but increases the amount of time that D2D users can spend harvesting energy to support MTC traffic. The authors in [21] analyze the average MTC SE, the average cellular SE and the weighted proportional-fairness SE, in which the last one is used to show the balance between efficiency and fairness among D2D and cellular transmitters. Simulation results have shown that a small spectrum partition factor, combined with an adequate number of available channels in the network, can achieve 1) a balance and fairness in weighted SE among D2D and cellular users that are sharing the spectrum, 2) a higher D2D transmission probability, and 3) a relatively high MTC and D2D SE in a dense cellular environment.

The work in [22] proposes a SWIPT-based cooperative D2D network, where the D2D pairs are distributed in a circular area. Energy-constrained D2D networks calls for multi-hop communications. Therefore, the authors introduce the dual-hop D2D network when the destination is spatially distant from the transmitter. In the system architecture, there are multiple idle D2D nodes between the source and the destination. To be more specific, the idle D2D node can serve as relay to forward the message to the destination using the cooperative DF mechanism. It can also serve as the energy harvesting node to harvest energy from RF signals transmitted by nearby transmitters. A transmission flow mechanism encompassing energy harvesting and decode-and-forward nodes is devised for end-to-end transmission. The results show that for a larger distance between D2D communication nodes, dual-hop D2D network is more suitable for reliable end-to-end communication.

3.2.3 Security

In the cooperative D2D communication with SWIPT, there exist multiple idle D2D users who need to harvest energy from the D2D transmitter signals and store the harvested energy for future use. However, the idle D2D users may decode the cellular message without permission instead of harvesting energy, which results in cellular message security problem. Therefore, in addition to meeting the energy harvesting requirements of the idle D2D users, the cooperative D2D communication system with SWIPT should be optimally designed to guarantee the cellular message security in the presence of potential eavesdropping of the idle D2D users.

The work in [23] considers cooperation between a cellular downlink communication and a D2D communication. The cellular downlink communication system consists of a source and a CU, while the D2D communication system has a pair of D2D users (DUs). There exists multiple idle DUs. The source transmits the confidential message to the CU, the D2D transmitter (DT) transmits a non-confidential message to the desired DU and assists the source to transmit the confidential message to the CU. To be more specific, the paper considers a two-phase transmission. At the first phase, the source transmits a signal to all the receivers. The DT amplifies the received cellular signal at different receive antennas using MRC receiver. At the second phase, the DT concurrently transmits both the cellular confidential message and its own message to the CU and to the desired DU. The paper aims to design secure beamforming

schemes to maximize the D2D users' data rate while guaranteeing the secrecy rate requirements of the cellular users and the minimum required amounts of power transferred to the idle D2D users. Simulation results demonstrate that comparing with the two-suboptimal secure beamforming scheme, the proposed optimal secure beamforming scheme in [23] achieves a significant data rate of the desired DU while provides a high secrecy rate for the cellular users and facilitates the efficient power transfer for the idle DUs.

3.3 SWIPT with Full-Duplex Communication

Recently, FD communication has become a viable option for next generation wireless communication networks. In contrast to conventional half-duplex (HD) transmission, FD communication allows devices to transmit and receive simultaneously on the same frequency, thus potentially doubling the SE. However, the self-interference caused by the own transmit signal impairs the simultaneous signal reception in FD systems severely. In fact, the self-interference can also serve as a vital energy sources for RF energy harvesting. As a result, when considering the self-interference as well as EH, FD SWIPT systems (**Fig. 5** and **Table 4**) have been proposed.

There are mainly two types of FD SWIPT systems; one is FD relaying systems and the other is FD systems.

In FD relaying SWIPT systems, there is a source node communicating with a destination node with the assistance of a SWIPT FD relay node. The FD relay node receives signal from the source node and concurrently transmits information using a portion of the harvested energy. The energy harvested for the relay node comes from the source node and the self-interference link.

The work [24] employs DF protocol and PS for the relay.

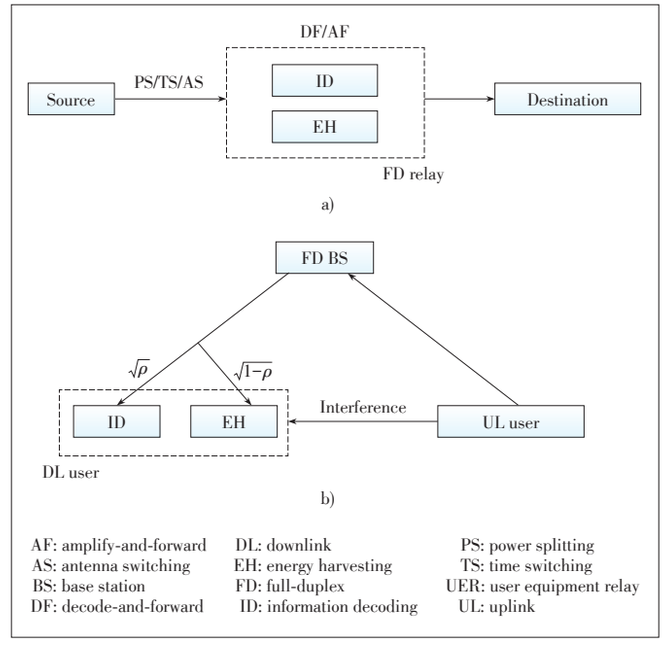

▲**Figure 5. SWIPT with full-duplex: a) transmission schemes for two-phase FD relaying systems with SWIPT; b) transmission schemes for one-phase FD uplink and downlink communications with SWIPT.**

The relay node splits its received signal into two components for energy harvesting and information decoding, respectively, and forwards the decoded information using a portion of the harvested energy. To maximize the end-to-end transmission rate, the PS ratio and energy consumption proportion at the relay have been jointly optimized. Demonstrated by simulations, increasing the number of transmit antennas at both the source node and the relay node can increase the transmission rates of

▼**Table 4. Summary of SWIPT with full-duplex**

Literature	Transmission scheme	System model	SWIPT technique	Design objective
I. Orikumhi et al. [28]	Two-phase DF	Multiple FD relay nodes, one HD source node and one HD destination node	TS at the FD relay nodes	Management of the degrading effect of the inter-relay-interference on the ID receiver and optimization of the ID and EH receivers
L. Zhao et al. [24]	Two-phase DF	One FD relay node, one HD source and one HD destination	PS at the FD relay	Maximization of the end-to-end transmission rate
H. Liu et al. [25]	Two-phase DF	One FD relay node, one HD source and one HD destination	PS at the FD relay	Maximization of the end-to-end signal-to-interference-plus-noise ratio and optimization the outage probability
Y. Zeng et al. [26]	Two-phase AF	One FD relay node, one HD source and one HD destination	TS at the FD relay	Optimization of power allocation and beamforming design
L. Zhang et al. [27]	Two-phase AF	One FD relay node, one HD source and one HD destination	TS at the FD relay	Minimization of the MSE
S. Leng et al. [29]	One-phase transmission	One FD BS and multiple HD users	PS at HD users	The trade-off between uplink transmit power minimization, downlink transmit power minimization, and total harvested energy maximization.
M. M. Zhao et al. [30]	One-phase transmission	Multiple FD RRHs and multiple HD users	PS at HD users	Minimization of the total power consumption

AF: amplify-and-decode
BS: base station
DF: decode-and-forward
EH: energy harvesting
FD: full-duplex
HD: half-duplex
ID: information decoding
MSE: mean-squared-error
PS: power splitting
RRH: remote radio head
SWIPT: simultaneous wireless information and power transfer
TS: time switching

FD relay systems.

The study in [25] extends the work in [24] by considering the power management of relay-harvested energy. The traditional power management is the harvest-use model, in which the harvested energy has been fully used up for relay transmission. Although the harvest-use model is easy to implement, it is not an efficient technology of power management. Therefore, in [25], the authors consider the situation that storing part of the harvested energy for future usage is good for practical scenarios, and propose a new harvest-use-store model. The results show that the harvest-use-store model outperforms the harvest-use model.

Different from the work in [24], [26] employs a new two-phase protocol for AF based SWIPT. In the first phase, information is transmitted from the source to the relay. In the second phase, the received signal at the relay is amplified and forwarded to the destination, and concurrently, dedicated energy signals are sent from the source to the relay for energy harvesting, which possesses the advantage of uninterrupted information transmission since no time switching or power splitting is needed at the relay for energy harvesting. The simulation results show a significant throughput gain achieved by this two-phase proposed design over the existing time switching based relay protocol.

The study in [26] investigates the design of robust non-linear transceivers in the face of realistic imperfect CSI. The relay node uses the same AF protocol as [26] and TS protocol. In the first phase, the source node transmits information to the relay node, and in the second phase, the relay node harvest energy from the source node and transmits information to the destination node. The proposed nonlinear transceiver relies on a Tomlinson-Harashima (TH) precoder along with an AF relaying matrix and a linear receiver, where the TH precoder is composed of a feedback matrix and a source precoding matrix. The simulation results show that the robust design advocated is capable of alleviating the effects of CSI errors, hence improving the robustness of the system over that of the corresponding linear designs.

The work in [24]–[27] all considers the system with only one relay, while the authors in [28] study the FD relay SWIPT system with multiple relays, which bring about the inter-relay-interference. However, the IRI can serve as an additional source of energy to the relay. Namely, the relay can use energy harvested from the source node and gleaned from self-interference and IRI links. To manage the degrading effect of the IRI on the ID receiver, maximum channel gain transmit antenna selection scheme is proposed at the relay to transmit information to the destination node. In addition, precoding matrices which optimize the ID and EH receivers are jointly designed. The simulated results show that although IRI could be a degrading factor from the information viewpoint, it can be properly managed and exploited for energy harvesting at the relay while maintaining the end-to-end data rate.

In FD SWIPT systems comprising a FD BS and multiple HD users, the BS transmits information and energy simultaneously to receivers and receive information transmitted by HD users.

The work in [29] deals with receivers, where ID receivers and EH receivers are separated, namely some HD users serve as ID receivers and some serve as EH receivers. To study the trade-off between uplink transmit power minimization, downlink transmit power minimization, and total harvested energy maximization, a multi-objective optimization framework has been proposed. Numerical results reveal the improved power efficiency facilitated by FD in SWIPT systems compared to traditional HD systems.

Differently, the authors in [30] study joint transceiver design for a FD cloud radio access network with SWIPT considering integrated receivers. The design aims to minimize the total power consumption with both uplink and downlink quality of service constraints and energy harvesting constraints.

4 Open Problems and Future Directions

SWIPT causes many challenging problems. In the following, we will discuss some of the research challenges and potential solutions.

4.1 Management of Dynamic Harvested Energy

Based on the investigation about SWIPT, we find out that the energy harvested by the energy-harvesting receiver arrives dynamically. Therefore, the available energy at the receiver can be changed over time. As referred in [25], the traditional power management: harvest-and-use model is not an efficient utilization of harvested energy, so that the authors in [25] propose a new harvest-use-store model to store part of the harvested energy in a battery group for future usage. However, the battery capacity is limited, which may lead to two situations:

- Overflowing when there is too much energy stored in the battery;
- Lacking of energy for the following slot when there is too little energy stored in the battery.

Thus, further research on the problems that when to store the energy and how much energy to store is still needed.

Intuitively, the problems proposed above are related to the channel condition. If the channel condition is better in the next slot, we can choose to store more harvested energy in the battery and vice versa. A recent work in [31] considers utilizing statistical properties of CSI to design a scheme of power management.

4.2 Trading Between Wireless Power Transfer and Traffic Offloading

The abilities (including computing, storage and communications) of edge intelligent UEs in the cellular network can be exploited to resolve the network congestion. Specifically, the transmission task can be offloaded on edge intelligent UEs or

small BSs. However, existing works usually assume that edge UEs and small BSs are willing to perform this offloading. Actually, the offloading will consume energy of edge UEs which are energy-hungry and degrade the gain brought about by traffic offloading. Then, the edge UEs may not be willing to use their limited power to perform the offloading. Hence, the paper [32] proposes the issue of making a tradeoff between the amount of RF energy needed for the offloading and the price at which edge UEs are willing to participate in the traffic offloading.

4.3 Effect of Mode Switching

There are some wireless powered access points in the network, such as PICO BSs. Based on the time switching technology of SWIPT, they can switch between the energy harvesting mode and the information transmission mode in different part of a time slot. Therefore, access points involved in the information transmission may be different during different time, which leads to the topology change of the wireless access network. Hence, the transmission and resource allocation in cellular network have to be dynamic and adaptive, which need to be further investigated.

5 Conclusions

A comprehensive survey on recent advantages of SWIPT in next generation cellular networks is presented in this paper. Firstly, we provide an overview of popular techniques that realizing SWIPT. Then, we survey the combination of the SWIPT techniques with NOMA techniques, with D2D communication techniques and with FD communication techniques. Finally, we discuss the future research directions for SWIPT in next generation cellular networks.

References

[1] Y. Ma, M. Peng, and Z. Zhao, "Optimization of simultaneous wireless information and power transfer in cloud radio access networks," in *Proc. 2016 IEEE Vehicular Technology Conference (VTC Spring)*, Nanjing, China, 2016, pp. 1–5. doi: 10.1109/VTCSpring.2016.7504391.
[2] C. Shen, W. Li, and T. Chang, "Simultaneous information and energy transfer: a two-user MISO interference channel case," in *Proc. 2012 IEEE Global Communications Conference (GLOBECOM)*, Anaheim, USA, 2012, pp. 3862–3867. doi: 10.1109/GLOCOM.2012.6503719.
[3] R. Zhang and C. K. Ho, "MIMO broadcasting for simultaneous wireless information and power transfer," *IEEE Transactions on Wireless Communications*, vol. 12, no. 5, pp. 1989–2001, May 2013. doi: 10.1109/TWC.2013.031813.120224.
[4] K. Huang and E. Larsson, "Simultaneous information and power transfer for broadband wireless systems," *IEEE Transactions on Signal Processing*, vol. 61, no. 23, pp. 5972–5986, Dec. 2013. doi: 10.1109/TSP.2013.2281026.
[5] F. Yuan, S. Jin, Y. Huang, et al., "Joint wireless information and energy transfer in massive distributed antenna systems," *IEEE Communications Magazine*, vol. 53, no. 6, pp. 109–116, Jun. 2015. doi: 10.1109/MCOM.2015.7120025.
[6] Z. Ding, C. Zhong, D. Wing Kwan Ng, et al., "Application of smart antenna technologies in simultaneous wireless information and power transfer," *IEEE Communications Magazine*, vol. 53, no. 4, pp. 86–93, Apr. 2015. doi: 10.1109/MCOM.2015.7081080.
[7] S. Bi, C. K. Ho, and R. Zhang, "Wireless powered communication: opportunities and challenges," *IEEE Communications Magazine*, vol. 53, no. 4, pp. 117–125, Apr. 2015. doi: 10.1109/MCOM.2015.7081084.
[8] R. Zhang and C. K. Ho, "MIMO broadcasting for simultaneous wireless information and power transfer," *IEEE Transactions on Wireless Communications*, vol. 12, no. 5, pp. 1989–2001, May 2013. doi: 10.1109/TWC.2013.031813.120224.
[9] Z. Zhou, M. Peng, Z. Zhao, and Y. Li, "Joint power splitting and antenna selection in energy harvesting relay channels," *IEEE Signal Processing Letters*, vol. 22, no. 7, pp. 823–829, Jul. 2015. doi: 10.1109/LSP.2014.2369748.
[10] I. Krikidis, S. Timotheou, S. Nikolaou, et al., "Simultaneous wireless information and power transfer in modern communication systems," *IEEE Communications Magazine*, vol. 52, no. 11, pp. 104–110, Nov. 2014. doi: 10.1109/MCOM.2014.6957150.
[11] Z. Ding, M. Peng, and H. Vincent Poor, "Cooperative non-orthogonal multiple access in 5G systems," *IEEE Communication Letters*, vol. 19, no. 8, pp. 1462–1465, Aug. 2015. doi: 10.1109/LCOMM.2015.2441064.
[12] Y. Xu, C. Shen, Z. Ding, et al., "Joint beamforming design and power splitting control in cooperative SWIPT NOMA systems," in *Proc. 2017 IEEE International Conference on Communications (ICC)*, Paris, France, 2017. doi: 10.1109/ICC.2017.7996560.
[13] N. T. Do, D. Benevides da Costa, T. Q. Duong, and B. An, "Transmit antenna selection schemes for MISO-NOMA cooperative downlink transmissions with hybrid SWIPT protocol," in *Proc. 2017 IEEE International Conference on Communications (ICC)*, Paris, France, 2017. doi: 10.1109/ICC.2017.7997005.
[14] Y. Liu, Z. Ding, M. Elkashlan, and H. V. Poor, "Cooperative non-orthogonal multiple access with simultaneous wireless information and power transfer," *IEEE Journal on Selected Areas in Communications*, vol. 34, no. 4, pp. 938–953, Apr. 2016. doi: 10.1109/JSAC.2016.2549378.
[15] Y. Ye, Y. Li, D. Wang, and G. Lu, "Power splitting protocol design for the cooperative NOMA with SWIPT," in *Proc. 2017 IEEE International Conference on Communications (ICC)*, Paris, France, 2017. doi: 10.1109/ICC.2017.7996751.
[16] Z. Yang, Z. Ding, P. Fan, and N. Al-Dhahir, "The impact of power allocation on cooperative non-orthogonal multiple access networks with SWIPT," *IEEE Transactions on Wireless Communications*, vol. 16, no. 7, pp. 4332–4343, July. 2017. doi: 10.1109/TWC.2017.2697380.
[17] W. Han, J. Ge, and J. Men, "Performance analysis for NOMA energy harvesting relaying networks with transmit antenna selection and maximal-ratio combining over Nakagami-m fading," *IET Communications*, vol. 10, no. 18, pp. 2687–2693, Dec. 2016. doi: 10.1049/iet-com.2016.0630.
[18] A. H. Sakr and E. Hossain, "Cognitive and energy harvesting-based D2D communication in cellular networks: stochastic geometry modeling and analysis," *IEEE Transactions on Communications*, vol. 63, no. 5, pp. 1867–1880, May 2015. doi: 10.1109/TCOMM.2015.2411266.
[19] Z. Zhou, C. Gao, C. Xu, et al., "Energy-efficient stable matching for resource allocation in energy harvesting-based device-to-device communications," *IEEE Access*, vol. 5, pp. 15184–15196, 2017. doi: 10.1109/ACCESS.2017.2678508.
[20] H. H. Yang, J. Lee, and T. Q. S. Quek, "Heterogeneous cellular network with energy harvesting-based D2D communication," *IEEE Transactions on Wireless Communications*, vol. 15, no. 2, pp. 1406–1419, Feb. 2016. doi: 10.1109/TWC.2015.2489651.
[21] R. Atat, L. Liu, N. Mastronarde, and Y. Yi, "Energy harvesting-based D2D-assisted machine-type communications," *IEEE Transactions on Communications*, vol. 65, no. 3, pp. 1299–1302, Mar. 2017. doi: 10.1109/TCOMM.2016.2639507.
[22] R. I. Ansari, S. A. Hassan, and C. Chrysostomou, "A SWIPT-based device-to-device cooperative network," in *Proc. 2017 24th International Conference on Telecommunications (ICT)*, Limassol, Cyprus, 2017. doi: 10.1109/ICT.2017.7998285.
[23] L. Jiang, C. Qin, X. Zhang, and H. Tian, "Secure beamforming design for SWIPT in cooperative D2D communications," *China Communications*, vol. 14, no. 1, pp. 20–33, Jan. 2017. doi: 10.1109/CC.2017.7839755.
[24] L. Zhao, X. Wang, and T. Riihonen, "Transmission rate optimization of full-duplex relay systems powered by wireless energy transfer," *IEEE Transactions on Wireless Communications*, vol. PP, no. 99, pp. 1–1. doi: 10.1109/TWC.2017.2723564.
[25] H. Liu, K. J. Kim, K. S. Kwak, and H. Vincent Poor, "Power splitting-based SWIPT with decode-and-forward full-duplex relaying," *IEEE Transactions on Wireless Communications*, vol. 15, no. 11, pp. 7561–7577, Nov. 2016. doi: 10.1109/TWC.2016.2604801.

[26] Y. Zeng and R. Zhang, "Full-duplex wireless-powered relay with self-energy recycling," *IEEE Wireless Communications Letters*, vol. 4, no. 2, pp. 201–204, April. 2015. doi: 10.1109/LWC.2015.2396516.
[27] L. Zhang, Y. Cai, M. Zhao, B. Champagne, and L. Hanzo, "Nonlinear MIMO transceivers improve wireless-powered and self- interference-aided relaying," *IEEE Transactions on Wireless Communications*, vol. PP, no. 99, pp. 6953–6966, 2017. doi: 10.1109/TWC.2017.2734772.
[28] I. Orikumhi, C. Y. Leow, and Z. Ding, "Wireless information and power transfer in MIMO virtual full duplex relaying system," *IEEE Transactions on Vehicular Technology*, vol. PP, no. 99, pp. 11001– 11010, 2017. doi: 10.1109/TVT.2017.2720460.
[29] S. Leng, D. W. K. Ng, N. Zlatanov, and R. Schober, "Multi-objective resource allocation in full-duplex SWIPT systems," in *Proc. 2016 IEEE International Conference on Communications (ICC)*, Kuala Lumpur, Malaysia, 2016. doi: 10.1109/ICC.2016.7510760.
[30] M. M. Zhao, Q. Shi, Y. Cai, and M. J. Zhao, "Joint transceiver design for full-duplex cloud radio access networks with SWIPT," *IEEE Transactions on Wireless Communications*, vol. 16, no. 9, pp. 5644–5658, Sept. 2017. doi: 10.1109/TWC.2017.2712693.
[31] Z. Zhou, M. Peng, Z. Zhao, W. Wang, and R. S. Blum, "Wireless-powered cooperative communications: power-splitting relaying with energy accumulation," *IEEE Journal on Selected Areas in Communications*, vol. 34, no. 4, pp. 969–982, Apr. 2016. doi: 10.1109/JSAC.2016.2544559.
[32] X. Lu, P. Wang, D. Niyato, D. I. Kim, and Z. Han, "Wireless networks with RF energy harvesting: a contemporary survey," *IEEE Communications Surveys and Tutorials*, vol. 17, no. 2, pp. 757– 789, 2015. doi: 10.1109/COMST.2014.2368999.

Manuscript received: 2017-12-17

Biographies

LIU Binghong (2013210720@bupt.edu.cn) received the B.S. degree in communication engineering from Beijing University of Posts and Telecommunications (BUPT), China in 2017. She is currently pursuing the Ph.D. degree at BUPT. Her research interests include energy harvesting and fog radio access networks.

PENG Mugen (pmg@bupt.edu.cn) received the B.E. degree in electronics engineering from Nanjing University of Posts & Telecommunications, China in 2000, and the Ph.D. degree in communication and information system from the Beijing University of Posts & Telecommunications (BUPT), China in 2005. Afterward, he joined BUPT, and became a full professor with the School of Information and Communication Engineering, BUPT, in October 2012. During 2014, he was also an Academic Visiting Fellow at Princeton University, USA. He is leading a research group focusing on wireless transmission and networking technologies in the Key Laboratory of Universal Wireless Communications (Ministry of Education), BUPT. He has authored/coauthored more than 60 refereed IEEE journal papers and over 200 conference proceeding papers. His research interests include wireless communication theory, radio signal processing and convex optimizations, with particular interests in cooperative communication, radio network coding, self-organization networking, heterogeneous networking, and cloud communication.

ZHOU Zheng (nczhouzheng@gmail.com) received the B.S. degree in information engineering from Beijing University of Posts and Telecommunications (BUPT), China in 2012. He is currently pursuing the Ph.D. degree at BUPT. His research interests include simultaneous information and power transfer and cloud radio access networks.

DOI: 10.3969/j.issn.1673-5188.2018.01.006
http://kns.cnki.net/kcms/detail/34.1294.TN.20180329.1124.002.html, published online March 29, 2018

Secure Beamforming Design for SWIPT in MISO Full-Duplex Systems

Alexander A. Okandeji[1], Muhammad R. A. Khandaker[2], WONG Kai-Kit[2], ZHANG Yangyang[3], and ZHENG Zhongbin[4]

(1. Department of Electrical and Computer Engineering, Ighinedion University Okada, PMB 0006, Benin city, Edo State, Nigeria;
2. Department of Electronic and Electrical Engineering, University College London, WC1E 7JE, United Kingdom;
3. Kuang-Chi Institute of Advanced Technology, Shenzhen 518057, China;
4. East China Institute of Telecommunications, China Academy of Information and Communications Technology, Shanghai 200001, China)

Abstract

This paper investigates the problem of bi-directional secure information exchange for a multiple-input single-output (MISO) broadcast channel in presence of potential and external eavesdroppers capable of decoding the confidential messages. Specifically, a multi-antenna base station (BS) simultaneously sends wireless information and power to a set of dual-antenna mobile stations (MSs) using power splitters (PSs) in the downlink and receives information in the uplink in full-duplex (FD) mode. We address the joint design of the receiver PS ratio and the transmit power at the MSs, the artificial noise covariance, and the beamforming matrix at the BS in order to guarantee the individual secrecy rate and energy harvesting constraints at each receiver, and the signal-to-interference plus noise ratio (SINR) at the BS and MSs. Using semidefinite relaxation (SDR) technique, we obtain solution to the problem with imperfect channel state information (CSI) of the self-interfering channels. Simulation results are presented to demonstrate the performance of our proposed scheme.

Keywords

physical layer security; full-duplex; SWIPT; energy harvesting

1 Introduction

Since the continuous operation of wireless devices is mostly constrained by the limited capacity of their power sources, radio frequency (RF) energy harvesting (EH) has been identified as a promising technique to power future wireless devices. Technically, RF signals that carry information can also be used as a vehicle for transporting energy at the same time. For this reason, the study of simultaneous wireless information and power transfer (SWIPT) has attracted huge interest from industrial and academic communities [1]–[7]. Effectively, wireless data and energy access can be made available to mobile users through the application of SWIPT, which in turn gives mobile users great convenience. SWIPT technology has been practically deployed in wireless communication networks. For example, [8] considered the practical deployment of SWIPT in a wireless sensor network mounted at a remote and difficult-to-access location, and powered only by a battery with limited operation time. Recharging or replacing the battery may be inconvenient, and often attract huge cost. Consequently, electromagnetic energy emanating from numerous radio and television broadcasting in the environment may serve as an opportunistic as well as greener alternative for harvesting energy to power such devices.

SWIPT was first introduced in [9] to describe the trade-off between the rates at which energy and dependable information is transmitted over a noisy channel and thus, a capacity energy function was proposed. A key assumption in [9] was the possibility of the receiver capable of simultaneously decoding information and harvesting energy from the same received signal. However, this assumption does not hold in practice as practical circuits for harvesting energy from the received signal are not able to decode information directly. Consequently, to facilitate wireless information and power transfer at the receiver, the work done in [10] proposed two practical receiver architecture designs for SWIPT, namely time switching (TS) and power splitting (PS). Specifically, in the TS design architecture, the receiver switches over time to achieve information decoding and energy harvesting, while with PS, the receiver splits the receive signal into two streams of different power in order to decode information and harvest energy separately. It was shown in [10] that PS generally achieves better performance than TS as the TS receiver architecture scheme, in general, can be regarded as a special form of PS with only a binary split power ra-

tio. In this paper, we focus on the PS design architecture.

Conventionally, half-duplex (HD) communication modes, in which the transmission and reception of radio signals occur over orthogonal time or frequency resources in order to avoid crosstalk, have been employed for wireless communications. Recent advances, however, suggest full-duplex (FD) communications that allow simultaneous transmission and reception of signals over the same radio channel in order to maximally use the limited available spectral resource [11], [12]. The key challenge to achieve FD communications is the presence of self-interference (SI). Thus, for wireless communication systems to communicate in FD mode, the generated SI must be significantly suppressed, if not cancelled completely, to receiver's noise floor [13]. Digital SI cancellation (SIC) for FD wireless systems was studied in [14]. Authors in [14] demonstrated the possibility of achieving SIC of 70 dB and 76 dB for antenna separation and digital cancellation at 20 cm and 40 cm spacing, respectively, between interfering antennas. It suffices to say therefore that radios can work in FD if SI can be significantly suppressed. Interestingly, the study of FD systems brings a new opportunity for SWIPT in FD systems [1], [7]. In particular, authors in [1] investigated the end-to-end sum-rate maximization approach for SWIPT in FD system while maintaining the energy harvesting threshold at each node by optimizing the receive power splitter and transmit power at each node. In contrast, [7] investigated the joint optimization of the transmit power at the source nodes and the two-way relay beamforming matrix for SWIPT with a FD MIMO amplify and forward (AF) relay employing PS, where the achievable sum-rate is maximized subject to energy harvesting and individual power constraints.

Wireless communication networks are susceptible to eavesdropping; however, SWIPT systems are more susceptible to eavesdropping due to the inherent characteristics of SWIPT and the open nature of wireless channel. The security issue in SWIPT systems is therefore a critical issue that needs to be addressed. Existing works on communication security have adopted the cryptographic technique. Although this technique may guarantee communication security to some degree in the application layer, the suitability of these technique on SWIPT systems is not guaranteed since it requires complex encryption/decryption algorithms and key distribution [15]. Alternatively, physical-layer (PHY) security has been identified to perfectly guarantee secure wireless information transmission against eavesdropping by using the physical properties of wireless channels such as fading and interference [16], [17]. In this context, artificial noise (AN), injected into the transmitted signal, is used to confuse the eavesdropper [18].

The fundamental study of the integration of PHY security and SWIPT was first considered in [15]. In particular, authors in [15] investigated the joint design of the beamforming vectors and power allocation to maximize the secrecy rate or the total harvested energy under a multi-user multiple-input single-output (MISO) SWIPT scenario. The work done in [19] proposed a robust secure transmission scheme which minimises the total transmit power in a multi-user MISO SWIPT system. In contrast, authors in [20] and [21] extended the study of PHY security into a multiple-input multiple-output (MIMO) broadcast SWIPT system. To maximise the secrecy rate in a MIMO SWIPT scenario, [20] investigated the secure transceiver beamforming design while ensuring efficient energy harvesting. On the other hand, authors in [21] considered the harvested energy maximization approach subject to secure information transmission by designing the transmit covariance.

In contrast to existing works, this paper considers the novel integration of SWIPT, FD technology and PHY security. In particular, this paper extends the secure HD MISO SWIPT communication scenario in [22] to the FD case, where the harvested energy at the MSs is utilized to send feedback information to the BS. We aim to minimize the end-to-end transmit power for SWIPT in FD MISO systems (**Fig. 1**) while satisfying the secrecy rate at each MSs, and the QoS requirements for each MS by optimizing jointly the receive PS ratio and the transmit power at the MSs, the beamforming matrix at the BS, and the AN covariance matrix. Specifically, we assume perfect CSI, which is accomplished from fine estimation by transmitting dedicated training symbols at the receiver, for the uplink and downlink channels for the MISO SWIPT system. In contrast, loop channels are assumed to be imperfect due to the fact that the distribution of SI channels are unknown. Also, SI channel measurement results obtained in [23] indicate that the SI channel has a multipath nature. Specifically, it was shown in [23] that multiple paths arising from SI channel measurements are known to have higher power relative to the line of sight (LOS) path. Consequently, there is the need to suppress SI with multiple path nature, through the use of an adaptive cancellation technique whose measurement can be used to cancel both the LOS path and the delayed version of the same, which is not the objective

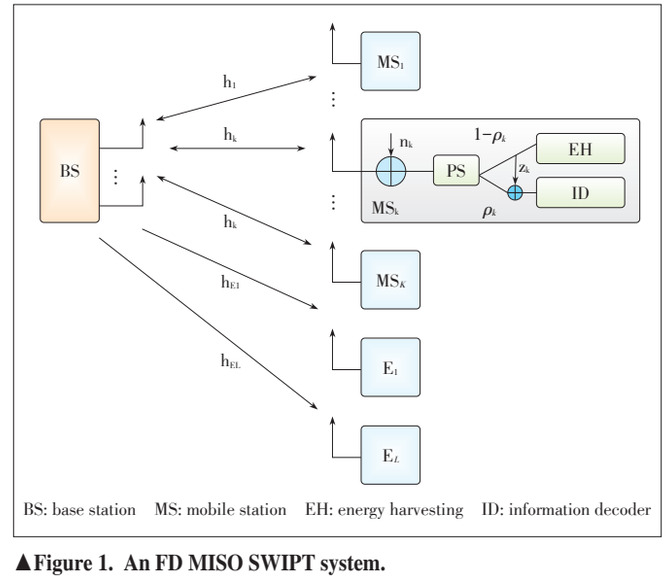

▲Figure 1. An FD MISO SWIPT system.

to be achieved in this work. Nonetheless, for convenience, SI channels can be modelled as Gaussian channels [7]. Accordingly, due to insufficient knowledge of the SI channel, a deterministic model for channel uncertainties is considered, where the magnitude of the estimation error as well as the SI power is bounded. Since the problem is non-convex, we propose an alternating optimization approach.

We denote scalars by non-bold letters and boldface lowercase letters are used to represent vectors, while boldface uppercase letters are used for matrices. For a square matrix $\mathbf{A}$, $\mathrm{Tr}(\mathbf{A})$, $\mathrm{Rank}(\mathbf{A})$, $\mathbf{A}^T$ and $\mathbf{A}^H$ denote its trace, rank, transpose and conjugate transpose, respectively, while $\mathbf{A}\succeq 0$ means that $\mathbf{A}$ is a positive semidefinite matrix. Also, $\mathbf{I}_n$ denotes an $n\times n$ identity matrix, $\|\cdot\|$ returns the Euclidean norm. The distribution of a circularly symmetric complex Gaussian (CSCG) random vector with mean μ and covariance matrix $\mathbf{C}$ is denoted by $\mathcal{CN}(\mu,\mathbf{C})$. Finally, $\mathbb{C}^{m\times n}$ denotes the space of $m\times n$ complex matrices.

2 System Model and Problem Statement

2.1 System Model

In this paper, we consider the end-to-end transmit power minimization approach for secure SWIPT in a MISO FD system where the BS simultaneously transmits K independent confidential messages to K dual-antenna (one for transmission, one for reception) receivers in the downlink, in the presence of L external single-antenna eavesdroppers, and receives information in the uplink in FD mode. In addition to the external eavesdroppers, each receiver attempts to eavesdrop messages intended for other receivers. Hence we call them potential eavesdroppers. To ensure secure information transmission, AN is superimposed to the transmitted signal to confuse these potential as well as the external eavesdroppers. We denote the number of transmit and receive antennas at the BS, respectively, as N_t and N_r, and each MS uses an identical pair of transmitter and receiver antennas for signal transmission and reception. In the downlink transmission, the BS performs transmit beamforming to send information to the receivers while the MSs, using the harvested energy from the received signal, send feedback to the BS in the uplink with transmit power $P_{\mathrm{up},k}, k=1,...,K$. Therefore, the complex baseband signal transmitted at the BS is expressed as

$$x=\sum_{k=1}^{K}\mathbf{a}_k s_k+\mathbf{b}, \tag{1}$$

where $s_k\sim\mathcal{CN}(0,1)$ denotes the confidential message intended for the kth receiver, $\mathbf{a}_k\in\mathbb{C}^{N_t\times 1}$ denotes the corresponding precoding vector. $\mathbf{b}\in\mathbb{C}^{N_t\times 1}$ is the AN vector modelled as $\mathbf{b}\sim\mathcal{CN}(0,\mathbf{V})$, where $\mathbf{V}=\mathbf{b}\mathbf{b}^H$ denotes the covariance matrix of $\mathbf{b}$. For convenience, we use $\mathcal{K}=\{1,\ldots,K\}$, $\mathcal{L}=\{1,\ldots,L\}$ and $\mathcal{M}_k=\{1,\ldots,k-1,k+1,\ldots,K\}$ to denote the index set of receivers, external eavesdroppers, and receivers except the kth receiver, respectively. The received signal at the kth receiver and lth external eavesdropper can be expressed as

$$y_k=\mathbf{h}_{\mathrm{dl},k}^H\mathbf{x}+h_{\mathrm{SI},k}m_k+z_k,\forall k, \tag{2}$$

$$y_{e,l}=\mathbf{g}_l^H\mathbf{x}+n_{e,l},\forall l, \tag{3}$$

where $\mathbf{h}_{\mathrm{dl},k}\in\mathbb{C}^{1\times N_t}$ and $\mathbf{g}_l\in\mathbb{C}^{1\times N_t}$ represent the channel vectors from the BS to the kth receiver, and from the BS to the lth external eavesdropper, respectively, and m_k denotes the information bearing symbol transmitted by MS_k. The antenna noises at the kth receiver and the lth external eavesdropper are modelled as $z_k\sim\mathcal{CN}(0,\sigma_k^2)$ and $n_{e,l}\sim\mathcal{CN}(0,\sigma_{e,l}^2)$. We assume each receiver adopts the PS scheme to coordinate the process of information decoding and energy harvesting. Specifically, a ρ portion of the received signal power is split to the information decoder (ID) while the remaining $(1-\rho)$ portion is split to the EH. Accordingly, the signal split to the ID of MS_k is given by

$$y_k^{\mathrm{ID}}=\sqrt{\rho_k}\left(\underbrace{\mathbf{h}_{\mathrm{dl},k}^H\mathbf{a}_k s_k}_{\text{desired signal}}+\underbrace{\sum_{j\neq k}^{K}\mathbf{h}_{\mathrm{dl},k}^H\mathbf{a}_j s_j}_{\text{interfering signal}}+\underbrace{\mathbf{h}_{\mathrm{dl},k}^H\mathbf{b}}_{\text{artificial noise}}+\underbrace{h_{\mathrm{SI},k}m_k}_{\text{self interference}}+z_k\right)+z_{a,k},\forall k. \tag{4}$$

where $z_{a,k}\sim\mathcal{CN}(0,\sigma_{a,k}^2)$ denotes the additional processing noise introduced by the ID of the kth receiver. Consequently, the signal-to-interference plus noise ratio (SINR) at the ID of the kth receiver can be expressed as

$$\Gamma_k=\frac{\rho_k\left|\mathbf{h}_{\mathrm{dl},k}^H\mathbf{a}_k\right|^2}{\rho_k\left(\sum_{j\neq k}\left|\mathbf{h}_{\mathrm{dl},k}^H\mathbf{a}_j\right|^2+\mathrm{Tr}(\mathbf{h}_{\mathrm{dl},k}^H\mathbf{h}_{\mathrm{dl},k}\mathbf{V})+\left|h_{\mathrm{SI},k}\right|^2P_{\mathrm{up},k}+\sigma_k^2\right)+\sigma_{a,k}^2}. \tag{5}$$

Also, the signal received at the EH of the kth receiver can be written as

$$y_k^{\mathrm{EH}}=\sqrt{1-\rho_k}\left(\sum_{j=1}^{K}\mathbf{h}_{\mathrm{dl},k}^H\mathbf{a}_j s_j+\mathbf{h}_{\mathrm{dl},k}^H\mathbf{b}+h_{\mathrm{SI},k}m_k+z_k\right),\forall k. \tag{6}$$

Then, the energy harvesting rate (i.e., power) at the kth EH can be expressed as [22]

$$Q_k=\eta_k(1-\rho_k)\left(\sum_{j=1}^{K}\left|\mathbf{h}_{\mathrm{dl},k}^H\mathbf{a}_j\right|^2+\mathbf{h}_{\mathrm{dl},k}^H\mathbf{V}\mathbf{h}_{\mathrm{dl},k})+P_{\mathrm{up},k}\left|h_{\mathrm{SI},k}\right|^2+\sigma_k^2\right), \tag{7}$$

where η_k is the energy conversion efficiency which for notational simplicity is assumed to be unity throughout this paper.

Meanwhile, the received signal at the BS can be written as

$$y^{\mathrm{BS}}=\underbrace{\sum_{k=1}^{K}\mathbf{h}_{\mathrm{ul},k}m_k}_{\text{desired signal}}+\underbrace{\sum_{j=1}^{K}\mathbf{H}_{\mathrm{SI,BS}}\mathbf{a}_j s_j}_{\text{self interference}}+\mathbf{n}_{\mathrm{BS}}, \tag{8}$$

where $\mathbf{h}_{\mathrm{ul}}$ is the channel vector from the MS to the transmit antennas at the BS and $\mathbf{n}_{\mathrm{BS}}$ denotes the additive white Gaussian noise (AWGN) vector at the BS modelled as $\mathbf{n}_{\mathrm{BS}}\sim\mathcal{CN}(0,\sigma_{BS}^2\mathbf{I})$. To equalize the uplink signal from MS_k, we assume that the BS applies a receive beamformer $\mathbf{w}_k$ expressed as given in [24]

$$s_k^{\mathrm{UL}}=\mathbf{w}_k^H\mathbf{h}_{\mathrm{ul},k}m_k+\mathbf{w}_k^H\sum_{j\neq k}^{K}\mathbf{h}_{\mathrm{ul},j}m_j+\mathbf{w}_k^H\sum_{j=1}^{K}\mathbf{H}_{\mathrm{SI,BS}}\mathrm{a}_j+\mathbf{w}_k^H\mathbf{n}_{\mathrm{BS}}. \tag{9}$$

Therefore, the SINR at the BS for the kth user's signal can be written as [24]

$$\Gamma_k^{\mathrm{BS}}=\frac{P_{\mathrm{up},k}\left|\mathbf{w}_k^H\mathbf{h}_{\mathrm{ul},k}\right|^2}{\sum_{j\neq k}^{K}P_{\mathrm{up},j}\left|\mathbf{w}_k^H\mathbf{h}_{\mathrm{ul},j}\right|^2+\sum_{j=1}^{K}\left|\mathbf{w}_k^H\mathbf{H}_{\mathrm{SI,BS}}\mathbf{a}_j\right|^2+\sigma_{BS}^2\left\|\mathbf{w}_k\right\|^2}. \tag{10}$$

As in [22], we also assume that the legitimate receivers themselves may attempt to overhear the signals transmitted to other receivers and we want to guarantee secrecy against any such attempt. As such, we denote the received SINR which corresponds to the signal transmitted for the kth receiver at the mth potential eavesdropper and the lth external eavesdropper as

$$\Gamma_{m,k}=\frac{\left|\mathbf{h}_{\mathrm{dl},m}^H\mathbf{a}_k\right|^2}{\sum_{j\neq k}\left|\mathbf{h}_{\mathrm{dl},m}^H\mathbf{a}_j\right|^2+\mathbf{h}_{\mathrm{dl},m}^H\mathbf{V}\mathbf{h}_{\mathrm{dl},m}+P_{\mathrm{up},m}\left|h_{\mathrm{SI},m}\right|^2+\sigma_m^2},\forall k,\forall m, \tag{11}$$

and

$$\Gamma_l^k=\frac{\left|\mathbf{g}_l^H\mathbf{a}_k\right|^2}{\sum_{j\neq k}\left|\mathbf{g}_l^H\mathbf{a}_j\right|^2+\mathbf{g}_l^H\mathbf{V}\mathbf{g}_l+\sigma_{e,l}^2},\forall k,\forall l. \tag{12}$$

In this work, the communication security is considered from the viewpoint of individual security [25], [26]. Consequently, the achievable individual secrecy rate at the kth receiver is given as [22]

$$R_k=\left[\log_2(1+\Gamma_k)-\log_2\left(1+\max_{\forall m,\forall l}\left\{\Gamma_{m,k},\Gamma_l^k\right\}\right)\right]^+, \tag{13}$$

where $[x]^+=\max(0,x)$.

2.2 Modelling the SI

Due to the insufficient knowledge of the SI channel, it is impossible to completely eliminate residual SI (RSI). For this reason, we consider a deterministic model for imperfect SI channels. In particular, the actual SI channels $h_{\mathrm{SI},k}$ and $\mathbf{H}_{\mathrm{SI,BS}}$ are assumed to respectively lie in the neighbourhood of the estimated channels $\hat{h}_{\mathrm{SI},k}$ and $\hat{\mathbf{H}}_{\mathrm{SI,BS}}$ that are available at the corresponding nodes. Therefore, the actual channels due to imperfect channel estimates can be modelled as

$$h_{\mathrm{SI},k}=\hat{h}_{\mathrm{SI},k}+\triangle h_{\mathrm{SI},k}, \tag{14a}$$

$$\mathbf{H}_{\mathrm{SI,BS}}=\hat{\mathbf{H}}_{\mathrm{SI,BS}}+\triangle\mathbf{H}_{\mathrm{SI,BS}}, \tag{14b}$$

where $\triangle h_{\mathrm{SI},k}$ and $\triangle\mathbf{H}_{\mathrm{SI,BS}}$ represent the channel uncertainties assumed to be bounded as

$$\left|\triangle h_{\mathrm{SI},k}\right|=\left|h_{\mathrm{SI},k}-\hat{h}_{\mathrm{SI},k}\right|\leqslant\epsilon_1, \tag{15a}$$

$$\left\|\triangle\mathbf{H}_{\mathrm{SI,BS}}\right\|=\left\|\mathbf{H}_{\mathrm{SI,BS}}-\hat{\mathbf{H}}_{\mathrm{SI,BS}}\right\|\leqslant\epsilon_2, \tag{15b}$$

for some $\epsilon_1,\epsilon_2\geqslant 0$. It is worth noting that the bounding values $\{\epsilon_k\}$ are dependent on the accuracy of the CSI estimates. Consequently, to efficiently define the worst-case SI level, we modify (14a) and (14b) using the triangle inequality and the Cauchy-Schwarz inequality, respectively [27]. It follows from (14a) and (14b) that

$$\left|h_{\mathrm{SI},k}\right|^2=\left|\left(\hat{h}_{\mathrm{SI},k}+\triangle h_{\mathrm{SI},k}\right)\right|^2\leqslant\left(\left|\hat{h}_{\mathrm{SI},k}\right|+\left|\triangle h_{\mathrm{SI},k}\right|\right)^2\leqslant\left|\hat{h}_{\mathrm{SI},k}\right|^2+\epsilon_1^2+2\epsilon_1\left|\hat{h}_{\mathrm{SI},k}\right|, \tag{16a}$$

$$\begin{aligned}&\left\|\mathbf{H}_{\mathrm{SI,BS}}\mathbf{a}_k\right\|^2\leqslant\left\|\mathbf{H}_{\mathrm{SI,BS}}\right\|^2\left\|\mathbf{a}_k\right\|^2=\\&\left\|\hat{\mathbf{H}}_{\mathrm{SI,BS}}+\triangle\mathbf{H}_{\mathrm{SI,BS}}\right\|^2\left\|\mathbf{a}_k\right\|^2\leqslant\\&\left(\left\|\hat{\mathbf{H}}_{\mathrm{SI,BS}}\right\|+\left\|\triangle\mathbf{H}_{\mathrm{SI,BS}}\right\|\right)^2\left\|\mathbf{a}_k\right\|^2\leqslant\\&\left(\left\|\hat{\mathbf{H}}_{\mathrm{SI,BS}}\right\|^2+\epsilon_2^2+2\left\|\hat{\mathbf{H}}_{\mathrm{SI,BS}}\right\|\epsilon_2\right)\left\|\mathbf{a}_k\right\|^2.\end{aligned} \tag{16b}$$

Note that in the absence of statistical information about the error, we use ϵ_k to represent the minimal knowledge of the upper-bound of the channel error which is sufficient enough to describe the error. Thus from (16a) and (16b), we obtain

$$\max_{\left|\triangle h_{\mathrm{SI},k}\right|\leqslant\epsilon_1}\left|h_{\mathrm{SI},k}\right|^2\leqslant\left|\hat{h}_{\mathrm{SI},k}\right|^2+\epsilon_1^2+2\epsilon_1\left|\hat{h}_{\mathrm{SI},k}\right|, \tag{17a}$$

$$\max_{\left\|\triangle\mathbf{H}_{\mathrm{SI,BS}}\mathbf{a}_k\right\|\leqslant\epsilon_2}\left\|\mathbf{H}_{\mathrm{SI,BS}}\mathbf{a}_k\right\|^2\leqslant\left(\left\|\hat{\mathbf{H}}_{\mathrm{SI,BS}}\right\|^2+\epsilon_2^2+2\left\|\hat{\mathbf{H}}_{\mathrm{SI,BS}}\right\|\epsilon_2\right)\left\|\mathbf{a}_k\right\|^2. \tag{17b}$$

In addition, it holds that

$$\left|\left(\hat{h}_{\mathrm{SI},k}+\triangle h_{\mathrm{SI},k}\right)\right|^2\geqslant\left(\left|\hat{h}_{\mathrm{SI},k}\right|-\left|\triangle h_{\mathrm{SI},k}\right|\right)^2\geqslant\left|\hat{h}_{\mathrm{SI},k}\right|^2+\epsilon_1^2-2\left|\hat{h}_{\mathrm{SI},k}\right|\epsilon_1. \tag{18}$$

Here, we assume, in general, that $\left|\hat{h}_{\mathrm{SI}}\right|\geqslant\left|\triangle h_{\mathrm{SI}}\right|$ implies that the error $\left|\triangle h_{\mathrm{SI}}\right|$ is sufficiently small relative to the estimate or the estimate is not meaningful. Consequently,

$$\min_{\left|\triangle h_{\mathrm{SI},k}\right|\leqslant\epsilon_1}\left|h_{\mathrm{SI},k}\right|^2\geqslant\left|\hat{h}_{\mathrm{SI},k}\right|^2+\epsilon_1^2-2\left|\hat{h}_{\mathrm{SI},k}\right|\epsilon_1. \tag{19}$$

2.3 Problem Statement

In this work, we consider the case where each MS_k is char-

Secure Beamforming Design for SWIPT in MISO Full-Duplex Systems

Alexander A. Okandeji, Muhammad R. A. Khandaker, WONG Kai-Kit, ZHANG Yangyang, and ZHENG Zhongbin

acterised by strict quality of service (QoS) requirement. In particular, to ensure a continuous information transfer, the QoS constraints require that the SINR of the downlink channel at all times should be above a given threshold denoted by $\gamma_k^{\mathrm{DL}}, \forall k$. Furthermore, it is required that the harvested energy by each MS must be above a certain useful level specified by a prescribed threshold denoted by $Qk, \forall k$. In addition, for the uplink channel, we also assume that each MS is expected to send feedback to the BS and a strict QoS is required such that the SINR of the uplink channel is expected to be higher than a given threshold denoted as $\gamma_k^{\mathrm{UL}}, k=1,...,K$.

FD communication is feasible subject to the effective cancellation of SI. As an increase in transmit power causes a corresponding increase in the SI, it is important for communication nodes to transmit at optimality. To this end, our aim is to minimize the total transmit power while maintaining the achievable secrecy rate and energy harvesting constraints at each receiver as well as the non - zero uplink and downlink SINR ($\gamma^{\mathrm{UL}}>0;\gamma^{\mathrm{DL}}>0$). We achieve this by jointly designing the transmit beamforming vector ($\mathbf{a}$) at the BS, the AN covariance ($\mathbf{V}$), the uplink transmit power ($P_{\mathrm{up},k}$) and the receive PS ratio (ρ_k) at MS_k, $k=1,...,K$. Thus we formulate the optimization problem as

$$\begin{aligned}&\min_{\mathbf{a}_k,\rho_k,\mathbf{w}_k,\mathbf{V},P_{\mathrm{up},k}} \sum_{k=1}^{K}\left(\left\|\mathbf{a}_k\right\|^2+P_{up,k}\right)+\mathrm{Tr}(\mathbf{V}) \quad s.t.\\ &R_k\geqslant r_k, Q_k\geqslant \bar{Q}_k, \Gamma_k^{\mathrm{BS}}\geqslant\gamma^{\mathrm{UL}}, \forall k,\\ &\mathbf{V}\succeq 0, 0<\left\|\mathbf{a}_k\right\|^2\leqslant P_{\max}, \Gamma_k\geqslant\gamma^{\mathrm{DL}}, \forall k,\\ &0<\rho_k<1, 0<P_{\mathrm{up},k}\leqslant\min(\bar{Q}_k, P_{\max}), \forall k,\end{aligned} \tag{20}$$

where R_k and $\bar{Q}_k$, respectively, denote the required secrecy rate and the energy harvesting constraints at each receiver. Problem (20) can explicitly be written as given in (21). Problem (21) is a non-convex problem due to the coupled optimization variables in the constraints, and hence it is very difficult to solve in closed form. Thus, we solve (21) in an alternating manner.

$$\begin{aligned}&\min_{\mathbf{a}_k,\rho_k,\mathbf{w}_k,\mathbf{V},P_{\mathrm{up},k}} \sum_{k=1}^{K}\left(\left\|\mathbf{a}_k\right\|^2\right)+\mathrm{Tr}(\mathbf{V})+\sum_{k=1}^{K}P_{\mathrm{up},k}\\ &s.t.\\ &\frac{\left|\mathbf{g}_l^H\mathbf{a}_k\right|^2}{\sum_{j\neq k}\left|\mathbf{g}_l^H\mathbf{a}_j\right|^2+\mathbf{g}_l^H\mathbf{V}\mathbf{g}_l+\sigma_l^2}\leqslant\gamma_e^k, \forall k, \forall l,\\ &\frac{\rho_k\left|\mathbf{h}_{\mathrm{dl},k}^H\mathbf{a}_k\right|^2}{\rho_k\left(\sum_{j\neq k}\left|\mathbf{h}_{\mathrm{dl},k}^H\mathbf{a}_j\right|^2+\mathbf{h}_{\mathrm{dl},k}^H\mathbf{V}\mathbf{h}_{\mathrm{dl},k}+\left|h_{\mathrm{SI},k}\right|^2P_{\mathrm{up},k}+\sigma_k^2\right)+\sigma_{a,k}^2}\geqslant\gamma_k^{\mathrm{DL}}, \forall k,\\ &\frac{\left|\mathbf{h}_{\mathrm{dl},m}^H\mathbf{a}_k\right|^2}{\sum_{j\neq k}\left|\mathbf{h}_{\mathrm{dl},m}^H\mathbf{a}_j\right|^2+\mathbf{h}_{\mathrm{dl},m}^H\mathbf{V}\mathbf{h}_{\mathrm{dl},m}+\left|h_{\mathrm{SI},k}\right|^2P_{\mathrm{up},k}+\sigma_m^2}\leqslant\gamma_e^k, \forall k, \forall m,\\ &\eta_k(1-\rho_k)\left(\sum_{j=1}^{K}\left|\mathbf{h}_{\mathrm{dl},k}^H\mathbf{a}_j\right|^2+\mathbf{h}_{\mathrm{dl},k}^H\mathbf{V}\mathbf{h}_{\mathrm{dl},k}+\left|h_{\mathrm{SI},k}\right|^2P_{\mathrm{up},k}+\sigma_k^2\right)\geqslant\bar{Q}_k,\\ &\frac{P_{\mathrm{up},k}\left|\mathbf{w}_k^H\mathbf{h}_{\mathrm{ul},k}\right|^2}{\sum_{j\neq k}^{K}P_{\mathrm{up},j}\left|\mathbf{w}_k^H\mathbf{h}_{\mathrm{ul},j}\right|^2+\sum_{j=1}^{K}\left\|\mathbf{H}_{\mathrm{SI,BS}}\mathbf{a}_j\right\|^2\left\|\mathbf{w}_k^H\right\|^2+\sigma_{\mathrm{BS}}^2\left\|\mathbf{w}_k\right\|^2}\geqslant\gamma^{\mathrm{UL}}, \forall k,\\ &V\succeq 0, 0<\left\|\mathbf{a}_k\right\|^2\leqslant P_{\max},\\ &0<\rho_k<1, 0<P_{\mathrm{up},k}\leqslant\min(\bar{Q}_k, P_{\max}).\end{aligned} \tag{21}$$

It is worth noting that the upper bound of the SI at the BS and the MS_k is obtained when the source node transmits at maximum available power [24], i.e., $P_{\mathrm{up},k}=\left\|\mathbf{a}_k\right\|^2=P_{\max}$. Consequently, we denote the upper-bounds of the SI power at the BS and MS_k as $\bar{E}$ and $\bar{G}$, respectively. Thus, the optimization problem in (21) can be upper bounded as given in (22).

$$\begin{aligned}&\min_{\mathbf{a}_k,\rho_k,\mathbf{w}_k,\mathbf{V},P_{\mathrm{up},k}} \sum_{k=1}^{K}\left\|\mathbf{a}_k\right\|^2+\mathrm{Tr}(\mathbf{V})+\sum_{k=1}^{K}P_{\mathrm{up},k}\\ &s.t.\\ &\frac{\left|\mathbf{g}_l^H\mathbf{a}_k\right|^2}{\sum_{j\neq k}\left|\mathbf{g}_l^H\mathbf{a}_j\right|^2+\mathbf{g}_l^H\mathbf{V}\mathbf{g}_l+\sigma_l^2}\leqslant\gamma_e^k, \forall k, \forall l,\\ &\frac{\rho_k\left|\mathbf{h}_{\mathrm{dl},k}^H\mathbf{a}_k\right|^2}{\rho_k\left(\sum_{j\neq k}\left|\mathbf{h}_{\mathrm{dl},k}^H\mathbf{a}_j\right|^2+\mathbf{h}_{\mathrm{dl},k}^H\mathbf{V}\mathbf{h}_{\mathrm{dl},k}+\left(\left|\hat{h}_{\mathrm{SI},k}\right|^2+\epsilon_1^2+2\epsilon_1\left|\hat{h}_{\mathrm{SI},k}\right|\right)P_{\max}+\sigma_k^2\right)+\sigma_{a,k}^2}\geqslant\gamma_k^{\mathrm{DL}}, \forall k,\\ &\frac{\left|\mathbf{h}_{\mathrm{dl},m}^H\mathbf{a}_k\right|^2}{\sum_{j\neq k}\left|\mathbf{h}_{\mathrm{dl},m}^H\mathbf{a}_j\right|^2+\mathbf{h}_{\mathrm{dl},m}^H\mathbf{V}\mathbf{h}_{\mathrm{dl},m}+\left(\left|\hat{h}_{\mathrm{SI},k}\right|^2+\epsilon_1^2+2\epsilon_1\left|\hat{h}_{\mathrm{SI},k}\right|\right)P_{\max}+\sigma_m^2}\leqslant\gamma_e^k, \forall k, \forall m,\\ &\eta_k(1-\rho_k)\left(\sum_{j=1}^{K}\left|\mathbf{h}_{\mathrm{dl},k}^H\mathbf{a}_j\right|^2+\mathbf{h}_{\mathrm{dl},k}^H\mathbf{V}\mathbf{h}_{\mathrm{dl},k}+\left(\left|\hat{h}_{\mathrm{SI},k}\right|^2+\epsilon_1^2-2\epsilon_1\left|\hat{h}_{\mathrm{SI},k}\right|\right)P_{\max}+\sigma_k^2\right)\geqslant\bar{Q}_k,\\ &\frac{P_{\mathrm{up},k}\left|\mathbf{w}_k^H\mathbf{h}_{\mathrm{ul},k}\right|^2}{\sum_{j\neq k}^{K}P_{\mathrm{up},j}\left|\mathbf{w}_k^H\mathbf{h}_{\mathrm{ul},j}\right|^2+\left(\left\|\hat{\mathbf{H}}_{\mathrm{SI,BS}}\right\|^2+\epsilon_2^2+2\left\|\hat{\mathbf{H}}_{\mathrm{SI,BS}}\right\|^2\epsilon_2\right)KP_{\max}\left\|\mathbf{w}_k\right\|^2+\sigma_{\mathrm{BS}}^2\left\|\mathbf{w}_k\right\|^2}\geqslant\gamma_k^{\mathrm{UL}}, \forall k,\\ &V\succeq 0, 0<\left\|a_k\right\|^2\leqslant P_{\max},\\ &0<\rho_k<1, 0<P_{\mathrm{up},k}\leqslant\min(\bar{Q}_k, P_{\max}).\end{aligned} \tag{22}$$

To solve problem (22), first we observe that the QoS uplink constraint does not have the PS coefficient and this is because the BS does not need to harvest energy. As a consequence, problem (22) can be decomposed into two sub-problems given in (23) and (24),

$$\begin{aligned}&\min_{\mathbf{w}_k,P_{\mathrm{up},k}} \sum_{k=1}^{K}P_{\mathrm{up},k}\\ &s.t.\\ &\frac{P_{\mathrm{up},k}\left|\mathbf{w}_k^H\mathbf{h}_{\mathrm{ul},k}\right|^2}{\sum_{j\neq k}^{K}P_{\mathrm{up},j}\left|\mathbf{w}_k^H\mathbf{h}_{\mathrm{ul},j}\right|^2+\bar{E}\left\|\mathbf{w}_k\right\|^2+\sigma_{\mathrm{BS}}^2\left\|\mathbf{w}_k\right\|^2}\geqslant\gamma_k^{\mathrm{UL}}, \forall k,\\ &0<P_{\mathrm{up},k}\leqslant\min(\bar{Q}_k, P_{\max}),\end{aligned} \tag{23}$$

where $\bar{E}\triangleq\left(\left\|\hat{\mathbf{H}}_{\mathrm{SI,BS}}\right\|^2+\epsilon_2^2+2\left\|\hat{\mathbf{H}}_{\mathrm{SI,BS}}\right\|^2\epsilon_2\right)KP_{\max}$,

$\overline{G_k}\triangleq\left(\left|\hat{h}_{\mathrm{SI},k}\right|^2+\epsilon_1^2+2\epsilon_1\left|\hat{h}_{\mathrm{SI},k}\right|\right)P_{\max}$, and

$\hat{G}_k\triangleq\left(\left|\hat{h}_{\mathrm{SI},k}\right|^2+\epsilon_1^2-2\epsilon_1\left|\hat{h}_{\mathrm{SI},k}\right|\right)P_{\max}$ are the SI power associated with the energy harvesting constraints.

$$\begin{aligned}
&\min_{\mathbf{a}_k,\rho_k,\mathbf{V}} \sum_{k=1}^{K}\left\|\mathbf{a}_k\right\|^2+\mathrm{Tr}(\mathbf{V}) \quad s.t.\\
&\frac{\left|\mathbf{g}_l^H\mathbf{a}_k\right|^2}{\sum_{j\neq k}\left|\mathbf{g}_l^H\mathbf{a}_j\right|^2+\mathbf{g}_l^H\mathbf{V}\mathbf{g}_l+\sigma_l^2}\leqslant\gamma_e^k,\forall k,\forall l,\\
&\frac{\rho_k\left|\mathbf{h}_{\mathrm{dl},k}^H\mathbf{a}_k\right|^2}{\rho_k\left(\sum_{j\neq k}\left|\mathbf{h}_{\mathrm{dl},k}^H\mathbf{a}_j\right|^2+\mathbf{h}_{\mathrm{dl},k}^H\mathbf{V}\mathbf{h}_{dl,k}+\bar{G}+\sigma_k^2\right)+\sigma_{a,k}^2}\geqslant\gamma_k^{\mathrm{DL}},\forall k,\\
&\frac{\left|\mathbf{h}_{\mathrm{dl},m}^H\mathbf{a}_k\right|^2}{\sum_{j\neq k}\left|\mathbf{h}_{\mathrm{dl},m}^H\mathbf{a}_j\right|^2+\mathbf{h}_{\mathrm{dl},m}^H\mathbf{V}\mathbf{h}_{\mathrm{dl},m}+\bar{G}+\sigma_m^2}\leqslant\gamma_e^k,\forall k,\forall m,\\
&\eta_k(1-\rho_k)\left(\sum_{j=1}^{K}\left|\mathbf{h}_{\mathrm{dl},k}^H\mathbf{a}_j\right|^2+\mathbf{h}_{\mathrm{dl},k}^H\mathbf{V}\mathbf{h}_{\mathrm{dl},k}+\hat{G}+\sigma_k^2\right)\geqslant\bar{Q}_k,\\
&\mathbf{V}\geqslant 0,0<\rho_k<1,0<P_{\mathrm{up},k}\leqslant\min(\bar{Q}_k,P_{\max})\\
&0<\left\|\mathbf{a}_k\right\|^2\leqslant P_{\max}.
\end{aligned}\tag{24}$$

Note that problem (23) corresponds to optimizing the variables involved in the uplink while problem (24) corresponds to those in the downlink. We then apply semidefinite relaxation (SDR) to the sub-problems as discussed below.

3 Proposed Solution

Clearly, even with the fixed set of $\gamma_e^k,\gamma_k^{\mathrm{DL}},\gamma_k^{\mathrm{UL}},\forall k$, problem (22) is non-convex. As a result of the possibility of decomposing problem (22) into two sub-problems, namely, problems (23) and (24), we will solve problem (23) analytically and use SDR technique to solve (24).

We first proceed by solving problem (23) to determine the optimal value of $P_{\mathrm{up},k}^*$ and $\mathbf{w}_k^*$.

The optimal receiver ($\mathbf{w}_k^*$) can be defined as the Wiener filter [28]

$$\mathbf{w}_k^*=\left(\sum_{j=1}^{K}P_{\mathrm{up},j}\mathbf{h}_{\mathrm{ul},j}\mathbf{h}_{\mathrm{ul},j}^H+\left[\sigma_j^2+\sum_{j=1}^{K}\left\|\mathbf{a}_j\right\|^2\right]\mathbf{I}\right)^{-1}\times\sqrt{P_{\mathrm{up},j}}\mathbf{h}_{\mathrm{ul},j}.\tag{25}$$

For given $\mathbf{w}_k^*$, the problem (23) can be reformulated as

$$\min_{P_{\mathrm{up},k}}\sum_{k=1}^{K}P_{\mathrm{up},k}\tag{26a}$$

s.t.

$$\frac{P_{\mathrm{up},k}\left|\mathbf{w}_k^H\mathbf{h}_{\mathrm{ul},k}\right|^2}{\sum_{j\neq k}^{K}P_{\mathrm{up},j}\left|\mathbf{w}_k^H\mathbf{h}_{\mathrm{ul},j}\right|^2+\bar{E}\left\|\mathbf{w}_k\right\|^2+\sigma_{\mathrm{BS}}^2\left\|\mathbf{w}_k\right\|^2}\geqslant\gamma_k^{\mathrm{UL}},\tag{26b}$$

$$0<P_{\mathrm{up},k}\leqslant\min(\bar{Q}_k,P_{\max}),\forall k.\tag{26c}$$

Upon investigation, the optimal $P_{\mathrm{up},k}^*$ is the minimum $P_{\mathrm{up},k}$ which satisfies (26b) to equality. Consequently, optimal $P_{\mathrm{up},k}^*$ is given by

$$P_{\mathrm{up}}^*=\frac{\gamma_k^{\mathrm{UL}}\left(\bar{E}\left\|\mathbf{w}_k\right\|^2+\sigma_{\mathrm{BS}}^2\left\|\mathbf{w}_k\right\|^2\right)}{\left|\mathbf{w}_k^H\mathbf{h}_{\mathrm{ul},k}\right|^2-\gamma_k^{\mathrm{UL}}\left(\sum_{j\neq k}^{K}\left|\mathbf{w}_k^H\mathbf{h}_{\mathrm{ul},j}\right|^2\right)}.\tag{27}$$

Then, by defining $\mathbf{A}_k=\mathbf{a}_k\mathbf{a}_k^H$, $\mathbf{H}_{\mathrm{dl},k}=\mathbf{h}_{\mathrm{dl},k}^H\mathbf{h}_{\mathrm{dl},k}$ *and* $\mathbf{G}_l=\mathbf{g}_l^H\mathbf{g}_l$, problem (24) can be equivalently rewritten as

$$\begin{aligned}
&\min_{\mathbf{A}_k,\mathbf{V},\rho_k\in(0,1)}\sum_{k=1}^{K}\mathrm{Tr}(\mathbf{A}_k)+\mathrm{Tr}(\mathbf{V}) \quad s.t.\\
&\frac{\mathrm{Tr}(\mathbf{G}_l\mathbf{A}_k)}{\sum_{j\neq k}\mathrm{Tr}(\mathbf{G}_l\mathbf{A}_j)+\mathrm{Tr}(\mathbf{G}_l\mathbf{V})+\sigma_l^2}\leqslant\gamma_e^k,\forall k,\forall l,\\
&\frac{\rho_k\mathrm{Tr}(\mathbf{H}_{\mathrm{dl},k}\mathbf{A}_k)}{\rho_k\left(\sum_{j\neq k}\mathrm{Tr}(\mathbf{H}_{\mathrm{dl},k}\mathbf{A}_j)+\mathrm{Tr}(\mathbf{H}_k\mathbf{V})+\bar{G}_k+\sigma_k^2\right)+\sigma_{a,k}^2}\geqslant\gamma_k^{\mathrm{DL}},\forall k,\\
&\frac{\mathrm{Tr}(\mathbf{H}_{\mathrm{dl},m}\mathbf{A}_k)}{\sum_{j\neq k}\mathrm{Tr}(\mathbf{H}_{\mathrm{dl},m}\mathbf{A}_j)+\mathrm{Tr}(\mathbf{H}_{\mathrm{dl},m}\mathbf{V})+\bar{G}+\sigma_m^2}\leqslant\gamma_e^k,\forall k,\forall m,\\
&\eta_k(1-\rho_k)\left(\sum_{j=1}^{K}\mathrm{Tr}(\mathbf{H}_{\mathrm{dl},k}\mathbf{A}_j)+\mathrm{Tr}(\mathbf{H}_{\mathrm{dl},k}\mathbf{V})+\hat{G}_k+\sigma_k^2\right)\geqslant\bar{Q}_k,\\
&\mathbf{V}\geqslant 0,0<\left\|\mathbf{a}_k\right\|^2\leqslant P_{\max},0<P_{\mathrm{up},k}\leqslant\min(\bar{Q}_k,P_{\max}),\\
&\mathrm{rank}(\mathbf{A}_k)=1,\forall k.
\end{aligned}\tag{28}$$

Note that problem (28) is still non-convex due to the non-convex rank-one constraints and the coupled optimization variables $\mathbf{A}_k$ and ρ_k. Applying SDR technique, after dropping the rank-one constraint, problem (28) can be reformulated into the following problem:

$$\begin{aligned}
&\min_{\mathbf{A}_k,\mathbf{V},\rho_k}\sum_{k=1}^{K}\mathrm{Tr}(\mathbf{A}_k)+\mathrm{Tr}(\mathbf{V}) \quad s.t.\\
&\frac{1}{\gamma_e^k}\mathrm{Tr}(\mathbf{G}_l\mathbf{A}_k)-\sum_{j\neq k}^{K}\mathrm{Tr}(\mathbf{G}_l\mathbf{A}_j)-\mathrm{Tr}(\mathbf{G}_l\mathbf{V})\leqslant\sigma_l^2,\forall k,\forall l,\\
&\frac{1}{\gamma_k^{\mathrm{DL}}}\mathrm{Tr}(\mathbf{H}_{\mathrm{dl},k}\mathbf{A}_k)-\sum_{j\neq k}^{K}\mathrm{Tr}(\mathbf{H}_{\mathrm{dl},k}\mathbf{A}_j)-\mathrm{Tr}(\mathbf{H}_{\mathrm{dl},k}\mathbf{V})-\bar{G}_k\geqslant\sigma_k^2+\frac{\sigma_{a,k}^2}{\rho_k},\forall k,\\
&\frac{1}{\gamma_e^k}\mathrm{Tr}(\mathbf{H}_{\mathrm{dl},m}\mathbf{A}_k)-\sum_{j\neq k}^{K}\mathrm{Tr}(\mathbf{H}_{\mathrm{dl},m}\mathbf{A}_j)-\mathrm{Tr}(\mathbf{H}_{\mathrm{dl},m}\mathbf{V})-\bar{G}_k\leqslant\sigma_m^2,\forall k,\forall m,\\
&\sum_{j=1}^{K}\mathrm{Tr}(\mathbf{H}_{\mathrm{dl},k}\mathbf{A}_j)+\mathrm{Tr}(\mathbf{H}_{\mathrm{dl},k}\mathbf{V})+\hat{G}_k\geqslant\frac{\bar{Q}_k}{\eta_k(1-\rho_k)}-\sigma_k^2,\forall k,\\
&\mathbf{V}\geqslant 0,\mathbf{A}_k\geqslant 0,0<\rho_k\leqslant 1,0<P_{\mathrm{up},k}\leqslant\min(\bar{Q}_k,P_{\max}).
\end{aligned}\tag{29}$$

Clearly, from (29), both $1/\rho_k$ and $1/(1-\rho_k)$ are convex functions over ρ_k, so that problem (29) is convex and can be solved using a disciplined convex programming toolbox such as CVX [29]. Now, let $\mathbf{A}_k^*$, $\forall k$ denotes the optimal solution to problem (29). If each $\mathbf{A}_k^*$ is rank-one, it follows that the optimal solution of problem (24) can be obtained through eigenval-

ue decomposition of $\mathbf{A}_k^*$. Interestingly, as shown in Proposition 1, problem (24) always yields rank-one optimal solutions for $\mathbf{A}_k^*, \forall k$.

Proposition 1: There always exists an optimal solution A_k^* for problem (29) such that rank $(\mathbf{A}_k^*) = 1, \forall k$.

To summarise, Proposition 1 implies that the relaxation is tight, and thus the globally optimal solution of problem (24) can be obtained.

4 Numerical Examples

In this section, numerical examples are provided. In particular, the performance of the proposed joint beamforming design (Joint Opt in **Fig. 2**) for secure SWIPT in MISO FD systems is evaluated through simulations. We simulate a flat Rayleigh fading environment in which the channel fading coefficients are characterized as complex Gaussian numbers with zero mean and are independent and identically distributed, and we assume there are $K = 2$ MSs and all MSs have the same set of parameters, i.e., $\sigma_k^2 = \sigma^2$, $\delta_k^2 = \delta^2$, $\bar{Q}_k = Q$, $\gamma_k^{\mathrm{DL}} = \gamma^{\mathrm{DL}}$, $\gamma_k^{\mathrm{UL}} = \gamma^{\mathrm{UL}}$, and $y_E = -15$ dB. We also assume that 70% of the SI power has been cancelled using existing SI cancellation techniques [14]. All simulations are averaged over 1000 independent channel realizations.

In Fig. 2, we investigate the achievable secrecy sum-rate for secure SWIPT in MISO FD system versus the uplink SINR target for all MSs for fixed values of the downlink SINR ($\gamma^{\mathrm{DL}} = -5$ dB), the harvested power threshold, and the eavesdropper's SINR ($y_E = -15$ dB). Fig. 2 shows the performance comparison between the joint optimization and the fixed ρ optimization. As can be observed, an increase in the uplink SINR corresponds to a decrease in the secrecy sum-rate due to increase in transmission power which invariably increases the generated SI. However, the joint optimization scheme outperforms the fixed ρ optimization. Also, as the harvested power threshold increases, the secrecy sum-rate decreases, but the joint optimization scheme outperforms the fixed ρ optimization scheme.

In **Fig. 3**, we further investigate the achievable secrecy sum-rate for secure SWIPT in MISO FD system versus the harvested power threshold for given values of the uplink and downlink SINR. As can be observed, as the harvested power threshold increases, the secrecy sum rate increases. Technically, an increase in the harvested power allows more power to be directed to the ER of each MS, thus less power for SI, which invariably increases the secrecy sum-rate.

In **Fig. 4**, the achievable secrecy sum-rate for secure

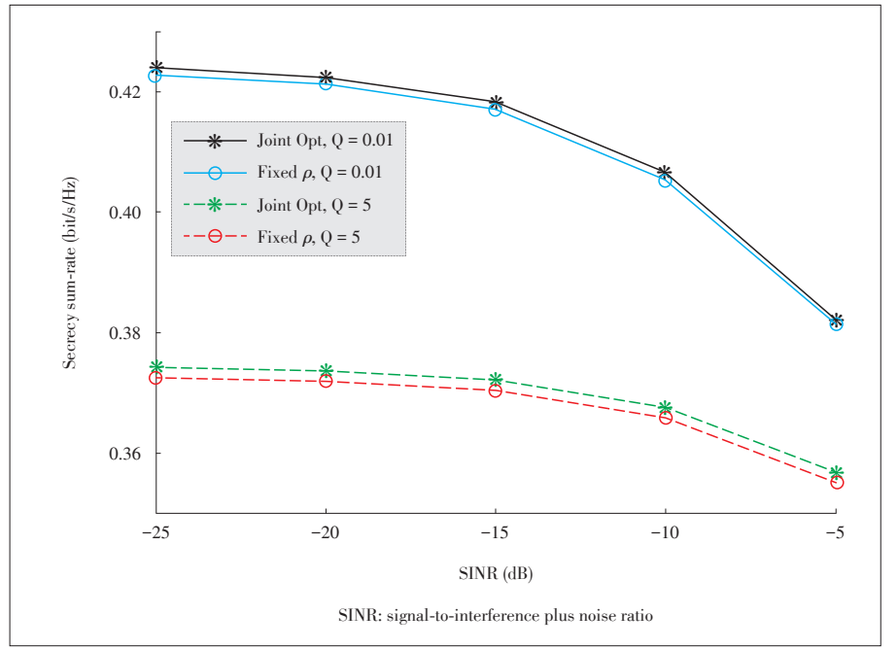

▲**Figure 2. Secrecy sum-rate versus SINR γ^{UL}.**

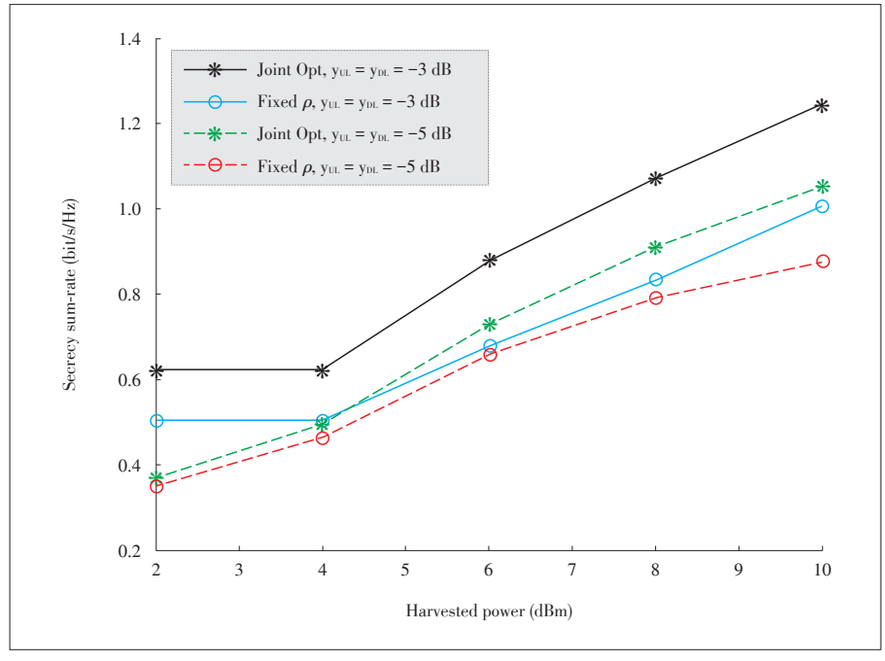

▲**Figure 3. Secrecy sum-rate versus harvested power.**

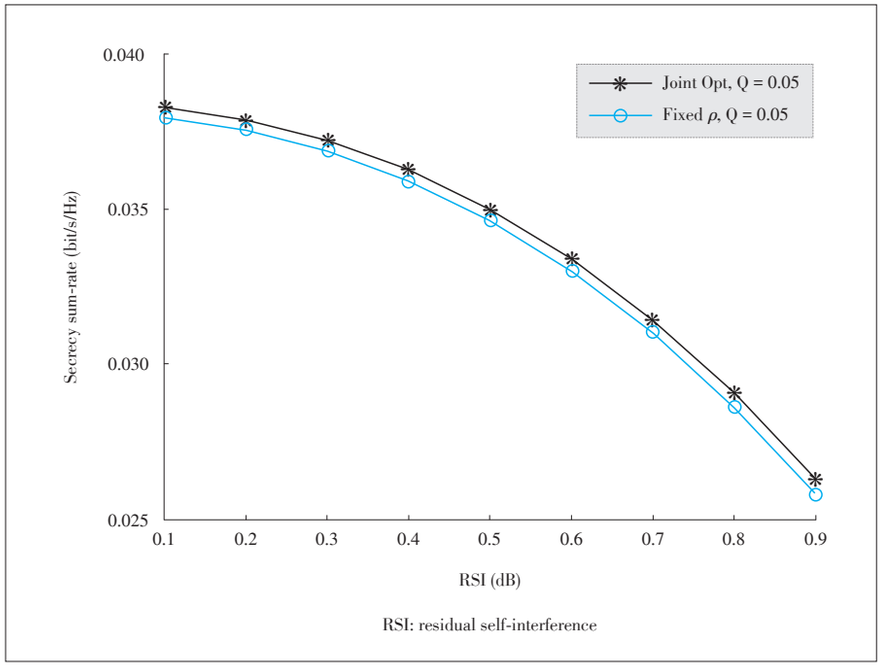

▲**Figure 4. Secrecy sum-rate versus RSI.**

SWIPT in MISO FD system versus the residual SI is investigated. In particular, we investigate the performance comparison of the proposed system for both joint optimization, and optimization with a fixed ρ. Clearly, an increase in the RSI results in a corresponding decrease in the achievable secrecy rate. However, the joint optimization scheme outperforms the optimization scheme with fixed ρ. Thus, a need for joint optimization is justified.

5 Conclusions

In this paper, we investigated the secure beamforming design for SWIPT in MISO FD system. To reduce SI and achieve secure FD transmission, the end-to-end sum transmit power has been minimized subject to the given SINR and harvested power constraints for each MS. In particular, to achieve optimal system performance, using SDR technique, we jointly optimized the transmit beamforming vector at the BS, and the received PS ratio and the transmit power at the MSs, and the AN covariance matrix. We show the need for joint optimization of system parameters through the numerical results.

References

[1] A. A. Okandeji, M. R. A. Khandaker, and K-K. Wong, "Wireless information and power transfer in full-duplex communication systems," in *Proc. IEEE International Conference on Communications*, Kuala Lumpur, Malaysia, 2016. doi: 10.1109/ICC.2016.7511169.
[2] A. A. Okandeji, M. R. A. Khandaker, and K-K. Wong, "Two-way relay beamforming optimization for full-duplex SWIPT systems," in *Proc. 24th European Signal Processing Conference*, Budapest, Hungary, 2016. doi: 10.1109/EUSIPCO.2016.7760674.
[3] J. Liao, M. R. A. Khandaker, and K. K. Wong, "Robust power-splitting SWIPT beamforming for broadcast channels," *IEEE Communications Letters*, vol. 20, no. 1, pp. 181–184, 2016. doi: 10.1109/LCOMM.2015.2498928.
[4] M. R. A. Khandaker and K. K. Wong, "SWIPT in MISO multicasting systems," *IEEE Wireless Communications Letters*, vol. 3, no. 3, pp. 277–280, 2014. doi: 10.1109/WCL.2014.030514.140057.
[5] M. R. A. Khandaker and K. K. Wong, "QoS-based multicast beamforming for SWIPT," in *Proc. IEEE SECON Workshop Energy Harvesting Communications*, Singapore, Singapore, 2014, pp. 62–67. doi: 10.1109/SECONW.2014.6979707.
[6] Q. Shi, L. Liu, W. Xu, and R. Zhang, "Joint transmit beamforming and receive power splitting for MISO SWIPT systems" *IEEE Transactions on wireless Communications*, vol. 13, no. 6, pp. 3269–3280, Jun. 2014. doi: 10.1109/TWC.2014.041714.131688.
[7] A. A. Okandeji, M. R. A. Khandaker, K-K. Wong, and Z. Zheng, "Joint transmit power and relay two-way beamforming optimization for energy harvesting full-duplex communications," in *Proc. IEEE Globecom International Workshop on Full-Duplex Wireless Communications*, Washington DC, USA, 2016. doi: 10.1109/GLOCOMW.2016.7848948.
[8] R. Zhang and C. K. Ho, "MIMO broadcasting for simultaneous wireless information and power transfer," *IEEE Transactions on wireless Communications*, vol. 12, no. 5, pp. 1989–2001, May 2013. doi: 10.1109/TWC.2013.031813.120224.
[9] L. Varshney, "Transporting information and energy simultaneously," in *Proc. IEEE International Symposium on Information Theory*, 2008, pp. 1612–1616. doi: 10.1109/ISIT.2008.4595260.
[10] X. Zhou, R. Zhang, and C. K. Ho, "Wireless information and power transfer: architecture design and rate-energy tradeoff," *IEEE Transactions on Communications*, vol. 61, no. 11, pp. 4754–4767, Nov. 2013. doi: 10.1109/TCOMM.2013.13.120855.
[11] M. Duarte, C. Dick, and A. Sabharwal, " Experiment-driven characterization of full-duplex wireless systems," *IEEE Transactions on Wireless Communications*, vol. 11, no. 12, pp. 4296–4307, Dec. 2012. doi: 10.1109/TWC.2012.102612.111278.
[12] Y. Hua, P. Liang, Y. Ma, A. C. Cirik, and Q. Gao, "A method for broadband full-duplex MIMO radio," *IEEE Signal Processing Letters*, vol. 19, no. 12, pp. 793–796, Dec. 2012. doi: 10.1109/LSP.2012.2221710.
[13] E. Ahmed and A. M. Eltawil, "All-digital self-interference cancellation technique for full-duplex systems," *IEEE Transactions on Wireless Communications*, vol. 14, no. 7, pp. 3519–3532, Jul. 2015. doi: 10.1109/TWC.2015.2407876.
[14] M. Duarte and A. Sabharwal, "Full-duplex wireless communication using off-the-shelf radios: feasibility and first result," in *IEEE ASILOMAR*, Pacific Grove, USA, 2010. doi: 10.1109/ACSSC.2010.5757799.
[15] L. Liu, R. Zhang, and K. C. Chua, "Secrecy wireless information and power transfer with MISO beamforming," *IEEE Transactions on Signal Processing*, vol. 62, no. 7, pp. 1850–1863, Apr. 2014. doi: 10.1109/TSP.2014.2303422.
[16] W.-C. Liao, T.-H. Chang, W.-K. Ma, and C.-Y. Chi, " QoS-based transmit beamforming in the presence of eavesdroppers: an optimized artificial noise-aided approach," *IEEE Transactions on Signal Processing*, vol. 59, no. 3, pp. 1317–1322, Mar. 2011. doi: 10.1109/TSP.2010.2094610.
[17] J. Zhu, R. Schober, and V.-K. Bhargava, "Secure transmission in multicell massive MIMO systems," *IEEE Transactions on Wireless Communications*, vol. 13, no. 9, pp. 4766–4781, Jul. 2014. doi: 10.1109/TWC.2014.2337308.
[18] Q. Li and D. Han, "Sum secrecy rate maximization for full-duplex two-way relay networks," in *Proc. IEEE International Conference on Acoustics, Speech and Signal Processing*, Shanghai, China, pp. 3641–3645, Mar. 2016. doi: 10.1109/ICASSP.2016.7472356.
[19] D. W. K. Ng, E. S. Lo, and R. Schober, "Robust beamforming for secure communication in systems with wireless information and power transfer," *IEEE Transactions on Wireless Communications*, vol. 13, no. 8, pp. 4599–4615, Aug. 2014. doi: 10.1109/TWC.2014.2314654.
[20] Q. Shi, W. Xu, J. Song, and E. Song, "Secure beamforming for MIMO broadcasting with wireless information and power transfer," *IEEE Transactions on Wireless Communications*, vol. 14, no. 5, pp. 2841–2853, May 2015. doi: 10.1109/TWC.2015.2395414.

[21] W. Wu and B. Wang, "Efficient transmission solutions for MIMO wiretap channels with SWIPT," *IEEE Communications Letters*, vol. 19, no. 9, pp. 1548–1551, Jun. 2015. doi: 10.1109/LCOMM.2015.2451179.
[22] H. Zhang, Y. Huang, C. Li, and L. Yang, "Secure beamforming design for SWIPT in MISO broadcast channel with confidential messages and external eavesdroppers," *IEEE Transactions on Wireless Communications*, vol. 15, no. 11, pp. 7807–7819, Nov. 2016. doi: 10.1109/TWC.2016.2607705.
[23] A. Sethi, V. Tapio, and M. Junti, "Self-interference channel for full duplex Transceiver" in *Proc. IEEE Wireless Communications and Networking Conference*, Istanbul, Turkey, 2014. doi: 10.1109/WCNC.2014.6952167.
[24] A. A. Okandeji, M. R. A. Khandaker, K-K. Wong, et al., "SWIPT in MISO full-duplex systems," *Journal of Communications and Networks*, to be published.
[25] J. Lie, Z. Han, M. A. V. Castro, and A. Hjorungnes, "Secure satellite communication systems design with individual secrecy rate constraints," *IEEE Transactions on Information Forensics and Security*, vol. 6, no. 3, pp. 661–671, Sept. 2011. doi: 10.1109/TIFS.2011.2148716.
[26] A. S. Mansour, R. F. Schaefer, and H. Boche, "The individual secrecy capacity of degraded multi-receiver wiretap broadcast channels," in *Proc. IEEE International Conference on Communications*, London, UK, 2015, pp. 4181–4186. doi: 10.1109/ICC.2015.7248979.
[27] S. Boyd and L. Vandenberghe, *Convex Optimization*. Cambridge, UK: Cambridge University Press, 2004.
[28] D. H. N. Nguyen, L. B. Lem, and Z. Han, "Optimal uplink and downlink channel assignment in a full-duplex multiuser system," in *Proc. IEEE International Conference on Communications*, Kuala Lumpur, Malaysia, May 2016. doi: 10.1109/ICC.2016.7510742.
[29] M. Grant and S. Boyd. (2010, Apr.). *CVX: Matlab software for disciplined convex programming* [Online]. Available: http://cvxr.com/cvx

Manuscript received: 2017-11-01

Biographies

Alexander A. Okandeji (alexander.okandeji@iuokada.edu.ng) received the B.Sc. degree (First class honours) from Olabisi Onabanjo University, Ogun State, Nigeria in 2010, M.Sc. degree from Loughborough University, UK in 2013, and Ph.D. degree from the Department of Electronic and Electrical Engineering, University College London, UK in 2017. His Ph.D. was funded by the Federal Government of Nigeria under the presidential special scholarship scheme for innovation and development (PRESSID) scheme. Dr. Okandeji presently lectures at the Department of Electrical and Computer Engineering, Igbinedion University, Nigeria where he teaches control systems engineering, electromagnetic field and wave theory, communication systems, telecommunication principle, and reliability and maintainability of systems. His research interests include full-duplex radio, MIMO, energy harvesting wireless communications, physical layer security, digital signal processing, and cloud computing.

Muhammad R. A. Khandaker (m.khandaker@ucl.ac.uk) received his Ph.D. degree in electrical and computer engineering from Curtin University, Australia in 2013. He has held a number of academic positions in Bangladesh. Since 2013, he has been a post-doctoral researcher with the Department of Electronic and Electrical Engineering, University College London, UK. He received the Curtin International Postgraduate Research Scholarship for his Ph.D. study in 2009. He received the Best Paper Award at the 16th IEEE Asia-Pacific Conference on Communications, Auckland, New Zealand in 2010. He regularly serves in the technical program committees of IEEE conferences, including Globecom, ICC, and VTC. He is currently serving as an associate editor as well as the lead guest editor of the *EURASIP Journal on Wireless Communications and Networking* Special Issue on Heterogeneous Cloud Radio Access Networks. He also served as the managing guest editor of the *Physical Communication* (Elsevier) Special Issue on Self-Optimizing Cognitive Radio Technologies.

WONG Kai-Kit (kai-kit.wong@ucl.ac.uk) received the B.Eng., M.Phil., and Ph.D. degrees from The Hong Kong University of Science and Technology, China in 1996, 1998, and 2001, respectively, all in electrical and electronic engineering. He is currently a professor of wireless communications with the Department of Electronic and Electrical Engineering, University College London, UK. He is a fellow of IET. He is a senior editor of the *IEEE Communications Letters* and the *IEEE Wireless Communications Letters*.

ZHANG Yangyang (yangyang.zhang@kuang-chi.org) received the B.S. and M.S. degrees in electronics and information engineering from Northeastern University, China in 2002 and 2004 respectively, and the Ph.D. degree in electrical engineering from the University of Oxford, UK in 2008. He is currently with the Shenzhen Key Laboratory of Artificial Microstructure Design, Guangdong Key Laboratory of Meta-RF Microwave Radio Frequency and Kuang-Chi Institute of Advanced Technology, China. From 2008 to 2010, he was a postdoctoral research fellow with the University College London, UK. He is currently the Executive Vice President with the Kuang-Chi Institute of Advanced Technology, China. His research interests are mainly focused on metamaterial-based future wireless communication system, such as MIMO communication system, metamaterial-based RF devices, and metamaterial-based spatial modulation technology. He received over 20 honors from various national and international competitions and published around 40 papers in various journals and conferences.

ZHENG Zhongbin (ben@ecit.org.cn) received the bachelor's and master's degrees in information and communications engineering from Beijing University of Posts and Telecommunications, China in 2002 and 2005, respectively. He is currently the Vice Director of the China Academy of Information and Communications Technology and the East China Institute of Telecommunications. He was also the former head of the Technology Department for the East China Institute of the Ministry of Industry and Information Technology, China. He is very active in research, with a number of international paper publications as well as patents and draft standards.

DOI: 10.3969/j.issn.1673-5188.2018.01.008
http://kns.cnki.net/kcms/detail/34.1294.TN.20180108.1603.002.html, published online January 8, 2017

Phase-Locked Loop Based Cancellation of ECG Power Line Interference

LI Taihao[1,2], ZHOU Jianshe[1], LIU Shupeng[3], SHI Jinsheng[1], and REN Fuji[4]

(1. Beijing Advanced Innovation Center for Imaging Technology, Capital Normal University, Beijing 100048, China;
2. Flatley Discovery Lab, Boston 02129, USA;
3. School of Communication and Information Engineering, Shanghai University, Shanghai 200072, China;
4. Department of Information Science and Intelligent Systems, University of Tokushima, Tokushima 7708506, Japan)

Abstract

Power line (PL) interference is one significant artifact in electrocardiography (ECG) that needs to be reduced to ensure accurate recording of cardiac signals. Because PL interference is non-stationary and has varying frequency, phase, and amplitude in ECG measurement, adaptive techniques are often necessary to track and cancel the interference. In this paper we present a phase-locked loop (PLL)-based adaptive filter to cancel PL interference. The PLL obtains the reference signal that is fed into the adaptive filter to remove the PL interference at the central frequency of 50 Hz. It is found that the technique can effectively cancel PL interference in real ECG signals and, when compared with some existing techniques such as least mean squares (LMS) adaptive filter, the new technique produces better results in terms of signal-to-interference ratio (SIR).

Keywords

phase-locked loop; ECG; adaptive filter; power line cancellation

1 Introduction

Electrocardiography (ECG) is extensively used for detecting heart disease by recording the electrical activity generated by cardiac muscles. In ECG measurement, the cable linking the subjects to the ECG monitor is susceptible to the 50 Hz power line (PL) interference [1], which results in inaccurate reading because the interference frequency is located very close to the high frequency component of the true ECG signal [2]. Studies showed that, to achieve high quality for ECG, the amplitude of the PL interference must be kept at less than 0.5% of the peak-to-peak amplitude of the QRS waves [3]. Therefore, removing or cancelling the PL interference is a critical challenge in ECG signal processing. In the last several decades many methods have been proposed to cancel the PL interference and they can be generally categorized into non-adaptive and adaptive filtering. Non-adaptive filters such as notch filter have the advantage of featuring a simple structure and fixed coefficients, however, they cannot target PL interference when its frequency deviates from 50 Hz [4]–[6]. From this perspective, adaptive filtering, because of its ability to track the frequency of PL interference, may yield more robust performance in practice [7]–[11]. In implementation, adaptive filtering relies on the stochastic characteristics of a reference signal to track the PL interference. In this work, we propose a method to first use phase-locked loop (PLL) to generate the reference signal that can be used to track the frequency and phase of PL interference accurately. We then use a least mean squares (LMS) filter to cancel the PL interference from ECG signal for a better result. We use the ECG data from the MIT-BIH database to test our method and found that it performed superior to the existing techniques.

2 Methodology

The model of our ECG signal and the structure of the adaptive filter is shown in **Fig. 1**, where s is the original uncontaminated ECG signal. The PL interference at 50 Hz is represented by d. However, as the PL interference will deviate from 50 Hz in frequency and phase in practice, we model this process as a noise path filter f such that $u=f(d)$. Hence, our received signal is $r=s+u$. The adaptive filter g takes d as one of its inputs to mimic the process of f to generate an output v such that the difference between u and v is minimized, and therefore the final output e is the best estimator of s in terms of mean square error (MSE).

In our work, the adaptive filter in Fig. 1 has the form of PLL. Its detailed structure is shown in **Fig. 2**, where d_1 and d_2 are the 50 Hz reference sine waves that have a phase difference of 90°. The coefficient vector is composed of w_1 and w_2, which are updated by the adaptive filter. The adaptively estimated 50 Hz reference signal is y. Given a noisy observation r, we can

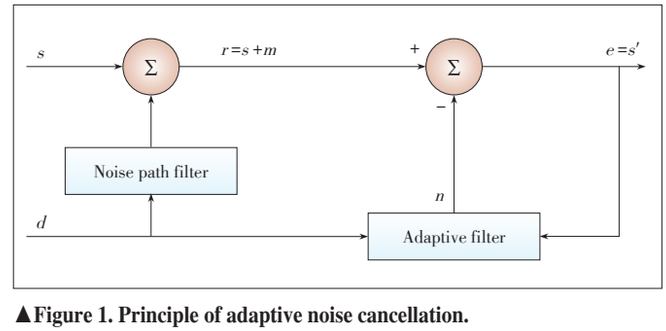

▲Figure 1. Principle of adaptive noise cancellation.

Phase-Locked Loop Based Cancellation of ECG Power Line Interference

LI Taihao, ZHOU Jianshe, LIU Shupeng, SHI Jinsheng, and REN Fuji

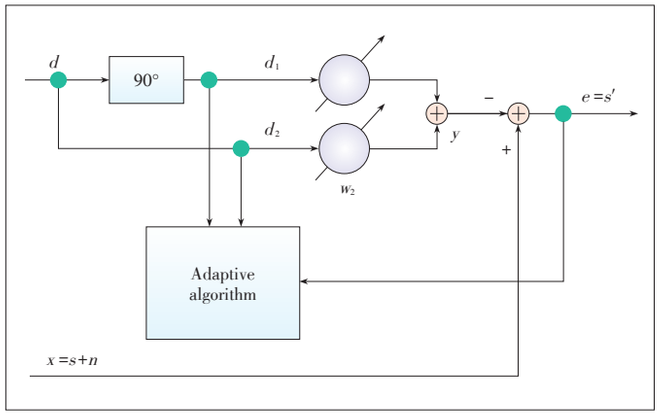

▲Figure 2. The cancellation scheme of 50 Hz power line interference.

obtain an estimation $\hat{s}$ of the true signal in the form of a LMS filter as below:

$$w_1(n+1) = w_1(n) + \mu e(n) d_1(n), \tag{1}$$

$$w_2(n+1) = w_2(n) + \mu e(n) d_2(n), \tag{2}$$

$$v(n) = w_1(n) d_1(n) + w_2(n) d_2(n), \tag{3}$$

$$\hat{s}(n) = r(n) - v(n), \tag{4}$$

where μ is the step size of LMS process.

3 Proposed Method

It has been shown by Widrow and Glover [10] that once the parameter estimates have converged and are fixed, an adaptive power line interference (PLI) canceller is approximately equivalent to a notch filter. However, in practice the PL frequency is not stable or not accurately known a priori, and a mismatch between the reference signal frequency and the PLI frequency might lead to inadequate reduction of the PLI. In this paper we propose a new method to solve the problem and take the concept of PLL in communication theory. The PLL tracks the PLI frequency and outputs a reference signal whose frequency is perfectly equivalent to that of the PLI [11].

The proposed model is shown in **Fig. 3**.

In Fig. 3, the noisy ECG signal $s+n$ is filtered by a bandpass filter centered to 50 Hz in order to suppress signals outside PLI band, the filter output contains PLI and noise. According to PLL theory, once the input signal frequency is in the PLL hold in range, the PLL can acquire the frequency of input signal and keep an output signal synchronizing with the input signal in frequency as well as in phase [12]. The natural frequency of PLL is 50 Hz, and the PLL will track the PLI in frequency and phase. When the acquisition succeeds, the misadjustment between the parameter estimates and the actual parameters is small enough and the PLL gives a perfect reference signal whose frequency is always the same as PLI within the PLL track range.

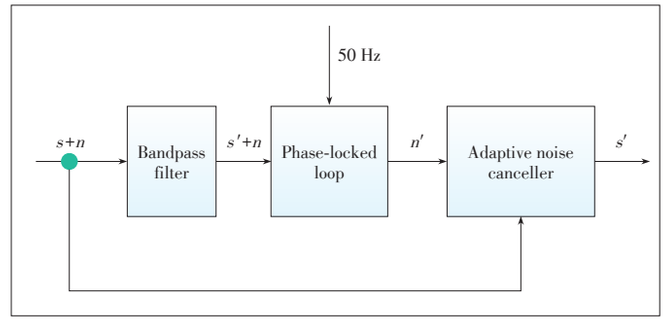

▲Figure 3. The proposed model.

The most popularly used PLL in practice is second-order, and its closed-loop transfer function may be written as follows.

$$H(s) = \frac{2\xi\omega_n s + \omega_n^2}{s^2 + 2\xi\omega_n s + \omega_n^2}, \tag{5}$$

where ω_n is the natural frequency and ξ is the loop damping ratio. The ξ usually takes the value 0.7. According the PLL theory, the lock-in range of a second-order PLL is

$$\Delta\omega = 2\xi\omega_n. \tag{6}$$

The PLL can acquire the input signal immediately as long as the input signal frequency is in the lock-in range of PLL.

4 Experimental Results and Analysis

We used the MIT-BIH ECG data to test our method and compared it with an existing technique. The database consists of 48 half-hour excerpts of two channel ambulatory ECG recordings that are digitized at 360 samples per second per channel. The data have an 11-bit resolution over a 10 mV range and they have been amplified with gain of 200 [13].

Fig. 4 shows a noisy ECG signal (the sum of record 103 and 50 Hz PL interference, Signal Noise Ratio= 0 dB) and its spectrum. The recording began at 50 second after the ECG started. The waveform of the ECG was completed submerged under the PL interference (Fig. 4a). The spectrum of the PL interference can be clearly observed in Fig. 4b. **Fig. 5** compares the performance of LMS filter and our proposed method in cancelling PL interference at different frequency deviations. Fig. 5a shows the MSE of an LMS filter to cancel PL interference at 50 Hz. Because there was no frequency deviation, the LMS filter was able to achieve satisfactory performance. When the frequency of PL interference deviated to 50.1 Hz, the performance of the LMS filter decreased as it generated more errors (Fig. 5b). When the frequency of PL interference was further deviated to 50.5 Hz, the LMS filter created much larger MSE (Fig. 5c). For the same scenario, our method was able to achieve very good performance to maintain a small MSE (Fig. 5d). The reconstructed ECG signal of our method in this case

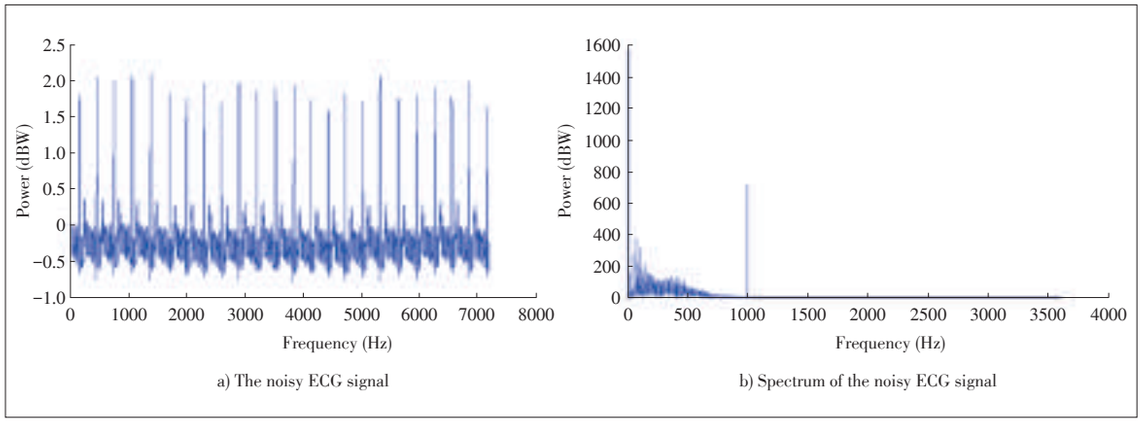

◀Figure 4.
The noisy ECG signal.

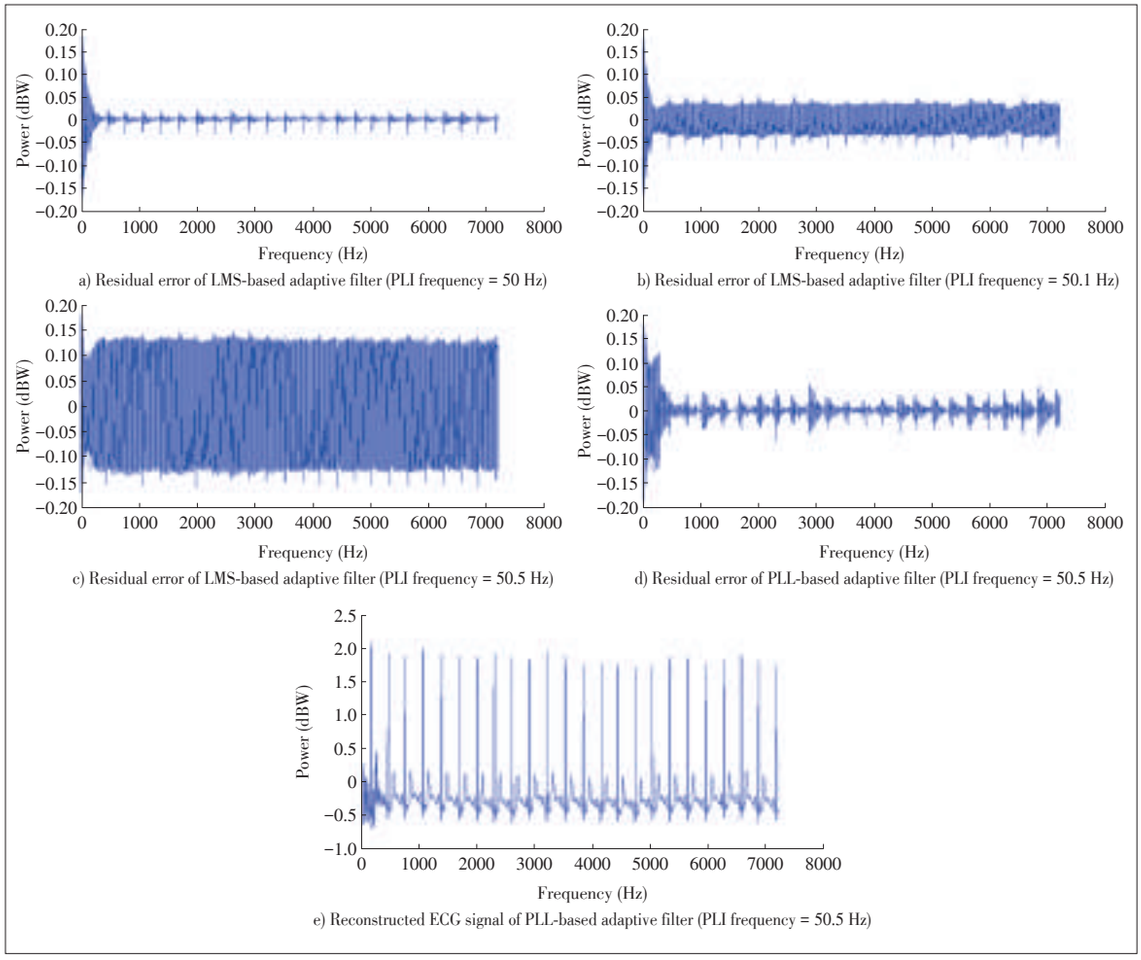

◀Figure 5.
The proposed method.

was plotted in Fig. 5e), from which we can easily observe the true ECG components. **Fig. 6** shows that the proposed PLL-based canceller can track and lock the frequency deviation in about 1 second and suppress the PL interference completely.

For quantitative comparison, we simulated different *SIRs* as the input to the noise cancellation techniques where SIR_{in} is defined as the ratio between the power of true ECG signal s and the amplitude of the PL interference. We then calculated the SIR_{out} at the output of the LMS filter and our method. For an accurate quantification of the cancellation performance, the SIR at the input and output of the canceller must be known. **Table 1** compares the performance of the two methods for a fixed PL interference frequency at different SIR_{in}.

Table 2 compares the two methods at a fixed SIR_{in} but for different degrees of frequency deviations of the PL interference. It can be seen that the PLL-based canceller is robust to

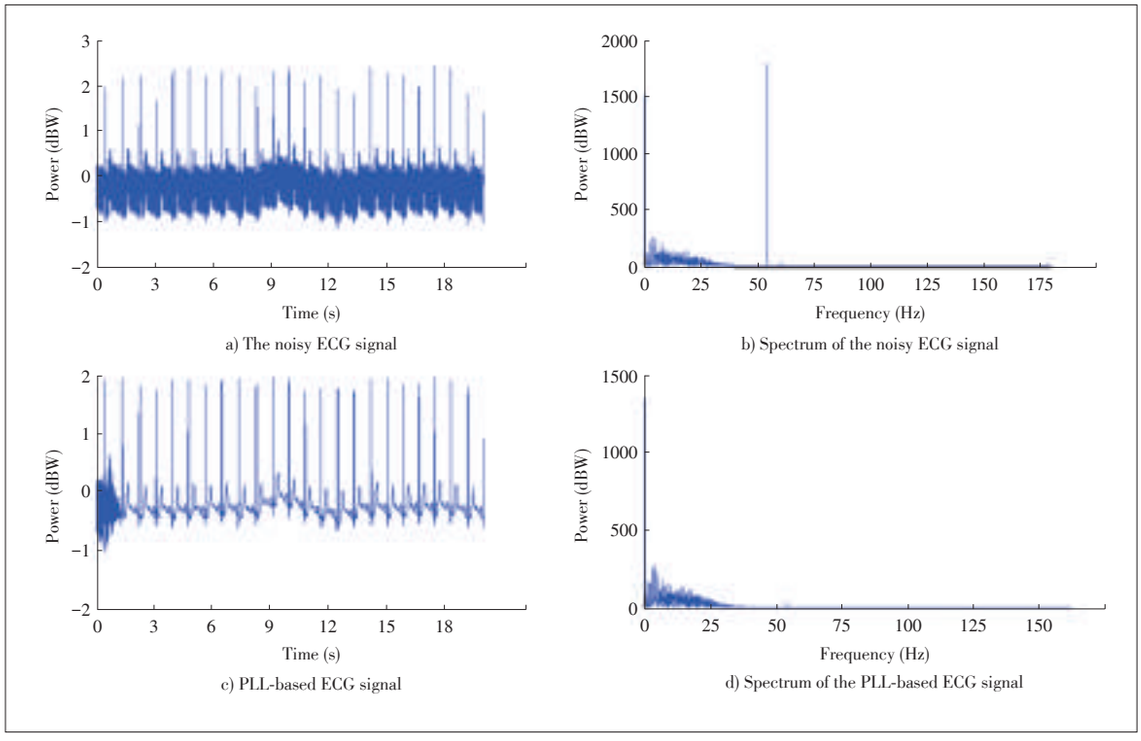

◀**Figure 6. Tracking performance (Δf/f=8%).**

▼**Table 1. Performance comparison at different SIR_{in}**

SIR_{in} (dB)	N	−20	0	20
SIR_{out} (dB)	AF	35.02	35.02	35.02
	PLL-based AF	25.87	29.47	30.07

AF: Adaptive Filter PLL: Phase-Locked Loop SIR: Signal-Interference Ratio

▼**Table 2. Performance comparison at different frequencies (SIR_{in} = 0 dB)**

Fixed SIR_{in} (dB)	SIR_{out} (dB)		
Δf/f	0.1%	1%	10%
AF	20.11	2.7	−0.92
PLL-based AF	28.16	28.59	31.42

AF: Adaptive Filter PLL: Phase-Locked Loop SIR: Signal-Interference Ratio

frequency deviation, and the SIR_{out} is about 30 dB regardless of frequency deviation.

5 Conclusions

This paper proposes a PLL-based adaptive canceller for the suppression of the PL interference in ECG recordings. The canceller comprises a second-order PLL, so except amplitude and phase, the frequency deviation can be tracked. Our experiment results showed that the proposed canceller could track PL interference even when its frequency deviated 10% from 50 Hz and lock the tracking in one second. Therefore, our method can obtain a high performance ECG output with the SIR of about 30 dB, and it is robust to frequency deviation. As a conclusion, the proposed method is superior to the common adaptive noise canceller. As a PL interference cancellation technique, our method is also applicable to neural recording such as electroencephalography [14] and wearable biomedical instruments [15].

References

[1] Y. Sun, and X. B. Yu, "Capacitive biopotential measurement for electrophysiological signal acquisition: a review," *IEEE Sensors Journal*, vol. 16, no. 9, pp. 2832–2853, May 2016. doi: 10.1109/JSEN.2016.2519392.
[2] M. F. Chimene and R. Pallas-Areny, "A comprehensive model for power line interference in biopotential measurements," *IEEE Transactions on Instrumentation and Measurement*, vol. 49, no. 3, pp. 535–540, Jun. 2000. doi: 10.1109/19.850390.
[3] A. C. Metting van Rijn, A. Peper, and C. A. Grimbergen, "High-quality recording of bioelectric events. Part 1. interference reduction, theory and practice," *Medical and Biological Engineering Computing*, vol. 28, no. 5, pp. 389–397. Sept. 1990.
[4] M. Kaur and B. Singh, "Power line interference reduction in ECG using combination of MA method and IIR notch filter," *International Journal of Recent Trends in Engineering*, vol. 2, no. 6, pp. 125–129, Jun. 2009.
[5] S. C. Pei and C. C. Tseng, "Elimination of AC interference in electrocardiogram using IIR notch filter with transient suppression," *IEEE Transactions on Biomedical Engineering*, vol. 42, no. 11, pp. 1128–1132, Nov. 1995. doi: 10.1109/10.469385.
[6] J. A. Van Alste and T.S. Schilder, "Removal of base-line wander and power-line interference from the ECG by an efficient FIR filter with a reduced number of taps," *IEEE Transactions on Biomedical Engineering*, vol. 32, no. 12, pp. 1052–1060, Dec. 1985. doi: 10.1109/TBME.1985.325514.

[7] J. M. Leski and N. Henzel, "ECG baseline wander and powerline interference reduction using nonlinear filter bank," *Signal Processing*, vol. 85, no. 4, pp. 781–793, Apr. 2005. doi: 10.1016/j.sigpro.2004.12.001.
[8] C. Levkov, G. Mihov, R. Ivanov, et al., "Removal of power-line interference from the ECG: a review of the subtraction procedure," *Biomedical Engineering Online*, vol. 4, 2005. doi: 10.1186/1475-925X-4-50.
[9] A. K. Ziarani and A. Konrad, "A nonlinear adaptive method of elimination of power line interference in ECG signals," *IEEE Transactions on Biomedical Engineering*, vol. 49, no. 6, pp. 540– 547, Jun. 2002. doi: 10.1109/TBME.2002.1001968.
[10] S. M. Martens, M. Mischi, S. G. Oei, and J. W. Bergmans, "An improved adaptive power line interference canceller for electrocardiography," *IEEE Transactions on Biomedical Engineering*, vol. 53, no. 11, pp. 2220–2231, Nov. 2006. doi: 10.1109/TBME.2006.883631.
[11] M. Ferdjallah and R. E. Barr, "Adaptive digital notch filter design on the unit circle for the removal of powerline noise from biomedical signals," *IEEE Transactions on Biomedical Engineering*, vol. 41, no. 6, pp. 529–536, Jun. 1994. doi: 10.1109/10.293240.
[12] G. C. Hsieh and J. C. Hung, "Phase-locked loop techniques—a survey," *IEEE Transactions on Industrial Electronics*, vol. 43, no. 6, pp. 609–615, Dec. 1996. doi: 10.1109/41.544547.
[13] G. B. Moody and R. G. Mark, "The impact of the MIT-BIH arrhythmia database," *IEEE Engineering in Medicine and Biology Magazine*, vol. 20, no. 3, pp. 45–50, May-Jun. 2001. doi: 10.1109/51.932724.
[14] M. R. Keshtkaran and Z. Yang, "A fast, robust algorithm for power line interference cancellation in neural recording," *Journal of Neural Engineering*, vol. 11, no. 2, article. 026017, Apr. 2014. doi: 10.1088/1741-2560/11/2/026017.
[15] M. Tomasini, S. Benatti, B. Milosevic, E. Farella, and L. Benini, "Power line interference removal for high-quality continuous biosignal monitoring with low-power wearable devices," *IEEE Sensors Journal*, vol. 16, no. 10, pp. 3887–3895, May 2016. doi: 10.1109/JSEN.2016.2536363.

Manuscript received: 2017-07-30

Biographies

LI Taihao (litaihao@heartdynamic.cn) received the M.S. and Ph.D. degrees in information system engineering from University of Tokushima, Japan in 2003 and 2006, respectively. During 2006–2011, he was a postdoc researcher at Harvard University, USA. He is now a professor with Beijing Advanced Innovation Center for Imaging Technology, Capital Normal University, China. His research interests include affective computing, natural language processing, and artificial intelligence.

ZHOU Jianshe (zhoujianshe@solcnu.net) is a board member of Chinese Linguistics Association, a director member of Expert Committee of the Linguistics Committee of Beijing, and the deputy director of Beijing Linguistics Association. He is the vice president of Capital Normal University, China and a professor with Beijing Advanced Innovation Center for Imaging Technology there. His research interests include linguistics, neuroscience, and algorithms.

LIU Shupeng (liusp@i.shu.edu.cn) received his Ph.D. degree in 2007 from Shanghai Jiaotong University, China. He is an associate professor with School of Communications and Information Engineering, Shanghai University, China. His research interests include signal processing, Raman spectra, and image processing.

SHI Jinsheng (shijsh@aliyun.com) received his Ph.d. degree from Nankai University, China. He is a professor at Capital Normal University, China. His research interests include linguistics, affective computing.

REN Fuji (ren@is.tokushima-u.ac.jp) received his B.E. and M.E. degrees from Beijing University of Posts and Telecommunications, China in 1982 and 1985, respectively. He received his Ph.D. degree in 1991 from Hokkaido University, Japan. He is a professor at the Faculty of Engineering, the University of Tokushima, Japan. His research interests include natural language processing, affective computing, artificial intelligence, and language understanding.

Research Paper

DOI: 10.3969/j.issn.1673-5188.2018.01.009
http://kns.cnki.net/kcms/detail/34.1294.TN.20180214.1416.002.html, published online February 14, 2018

Behavior Targeting Based on Hierarchical Taxonomy Aggregation for Heterogeneous Online Shopping Applications

ZHANG Lifeng, ZHANG Chunhong, HU Zheng, and TANG Xiaosheng
(Beijing University of Posts and Telecommunications, Beijing 100876, China)

Abstract

Behavior targeting (BT) based on individual web-browsing history has become more valuable in precision marketing for many companies through capturing users' interest and preference. It is common in practice that the behavior data collected from different online shopping applications are inconsistent since they are labelled by different item taxonomy, where the same behavior could have different representations and therefore analysis confusion arises. To address this issue, we propose a semantic similarity based strategy to transform the heterogeneous behavior extracted from deep packet inspection (DPI) data of a telecommunication operator into a unique standard one. The Word Mover's Distance algorithm is exploited to evaluate the semantic similarity of the distributed representations of two web-browsing histories. Moreover, the architecture of the behavior targeting platform on Hadoop is implemented, which is capable of processing data with size of PB level every day.

Keywords

BT; online shopping application; DPI; Word Mover's Distance; hierarchical taxonomy

1 Introduction

In the era of mobile Internet, ubiquitous network provides users with convenient service through mobile phones. This directly leads to large amounts of behavior data transmitted in the network pipeline. The behavior data is the uniform resource locator (URL) that a user views. It can be mined to learn user's interest and preference, further, to identify potential buyers from the large amounts of Internet users. With the development of deep packet inspection (DPI) technology, most operators and Internet service providers (ISPs) use it to extract users' behavior data and phone information (e.g. URLs, user agents, and phone numbers) for data mining [1], [2]. Furthermore, with the wide spread use of mobile phones, more and more people tend to choose online shopping on the phone due to its convenience, infinite choice, and lower price [3]–[5]. Compared with the offline shopping, online shopping behavior data can be collected through the DPI technology continuously, so that users' behavior can be consistently mined and then tagged with a semantic label to explain it.

In behavior targeting (BT) methodology, individual web-browsing behaviors are used to identify users' interest and preference. Further, advertising can take advantage of BT to achieve precise marketing. Therefore, it is of great significance to online advertising and it has been studied for applications. Natasha Singer has mined data tastes of music in Pandora [6]. WU Zenghong et al. have studied users' interest in map service based on browse behavior [7]. ZHU Qiushan et al. analyzed users' interest in video recommendation [8]. Although some studies have been conducted on online shopping platforms [9], [10], BT has not been studied on online shopping due to the heterogeneity of online stores and different hierarchical taxonomies between online stores.

For users' behavior on online shopping platforms, one of the key technical issues in BT is the problem of how to generate labels based on URL with accuracy, comprehensiveness, consistency and semantic, which mainly represents the behavior of a user, Therefore, we have to extract the information of items (products) that a user is browsing. Online shopping stores use stock-keeping units (SKU) as a unique ID to represent a unique item [11], and a SKU is transmitted in the URL when the user is browsing it. However, the SKU is just a code and it does not have semantic meaning. So there is no help on explaining users' behavior. However, the item represented by a particular SKU has a hierarchical taxonomy label on the website of online store. This hierarchical taxonomy label is a comprehensive and accurate description of the item. More importantly, the hierarchical taxonomy label that implies users' interest and preference can describe users' online shopping behavior, which is the target of BT.

BT on the shopping platform based on DPI has the following challenges. First, SKU transmits in the URL through URL parameters. The parameters are made of a key and value separated by an equals sign (=) and joined by an ampersand (&). We identify the SKU by the key from the URL. Due to the heterogeneity of online stores, the key is different between them, which makes it hard to extract SKU from different online stores. Secondly, heterogonous online stores have different taxonomy systems, which leads to the situation where one item has inconsistent representations but similar semantic labels, and may easily cause confusion. Therefore, these challenges must be con-

quered to construct accurate, comprehensive, consistent and semantic labels on users' behavior.

The main contribution of our work is the development of an extensive methodology for attaching a semantic label to users' online shopping behavior and implement this methodology on Hadoop platform. Our methodology addresses all the above challenges. First, we adopt the Word Mover's Distance (WMD) algorithm to handle inconsistent hierarchical taxonomy labels due to the different taxonomy of heterogonous online shopping applications. Second, our work extracts the item ID from URL according to the rules of regular expression. We analyze the key of SKU in the URL and find it delivered in several forms in every single online shopping application. A bunch of rules are then summarized for the online shopping applications we studied. Third, we collect the hierarchical taxonomy labels corresponding its SKUs through the web crawler. Finally, we design and implement a platform to achieve our purpose.

Our intention of this work is to develop an extensive methodology for BT on users' online shopping behavior, and detect interest-based targeting. By this we hope to provide operators and ISP with BT, which supports further data mining, such as user profiles and precision marketing [12]. The rest of the paper is organized as follows. In Section 2, we introduce the methodology of our data analysis from input to output. The implementation of the methodology based on Hadoop is presented in Section 3. Section 4 then gives the conclusion and future research directions.

2 Methodology

In this section, we introduce the methodology of attaching a hierarchical and semantic label to users' online shopping behavior based on DPI data. As for the data source, we introduce two kinds of data we used in our analysis. Then in the label processing part, we adopt the WMD algorithm to aggregate the labels with same semantic meaning but different representations. In the DPI processing part, the rules of regular expression are made to extract the item ID from URL and query the final label according to the item ID. **Fig. 1** shows the overview of the data analysis model.

2.1 Data Source

2.1.1 DPI Data

In our analysis, DPI data was provided by one of the largest operators in China. It contains more than tens of millions anonymized mobile phone data records in a period of two months in 2016. The data fields we used in our methodology are presented in **Table 1**, and other 33 data fields are omitted.

In the Table 1, the international mobile subscriber identity (IMSI) is the unique identifier tied with unique users. Moreover, it is encrypted by Message-Digest Algorithm (MD5) for privacy and security concerns. The URL represents the content that users are browsing, and only URL from online shopping applications is retained after being filtered by the domain name. Our intention is to extract the SKU, which is contained in the URL that users request from the massive DPI data. ST and ET are used to mark the behavior time of online shopping. To understand SKU easily, we denote ID as item ID in the following context.

2.1.2 Web Crawler

The item ID consists of a string of numbers or characters. It is an identifier of item and it does not have any semantic meaning. Hence it cannot help us target users' online shopping behavior. Therefore, we have to retrieve the hierarchical taxono-

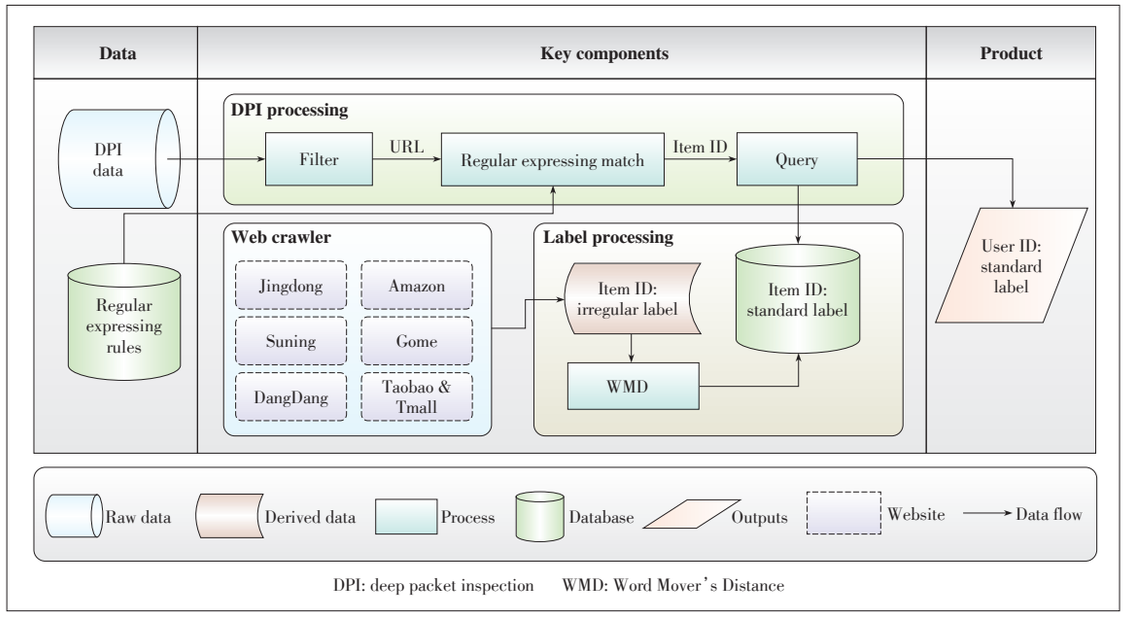

Figure 1.▶ The overview of data analysis model.

▼Table 1. The formats of DPI data

Serial number	Data field
1	IMSI
2	Start time
3	End time
4	URL
5	Domain name

IMSI: international mobile subscriber identity URL: uniform resource locator

my label through the web crawler. The hierarchical taxonomy label represents what users are browsing, and implies users' interest and preference.

According to iResearch's report, titled "Online Shopping Industry Monitoring Report in China 2016 [13]", the top six online shopping stores accounted for more than 80% of the online shopping market in China, and these top six stores are JingDong, Gome, Suning, Dangdang, Amazon, and Taobao & Tmall. We are focusing on retrieve hierarchical taxonomy labels from the above six online stores. In an online store, each product corresponds to a unique item ID while this item ID corresponds to a hierarchical taxonomy label. For example, an item from Jingdong is 133980, and its hierarchical taxonomy label is 'Men's Clothing → Bottoms → Pants'. As a result, when we extract an item ID from the URL, the hierarchical taxonomy label corresponding to this item ID can be attached to the behavior this time.

2.2 Label Processing

Because the above six online stores have different taxonomy systems, it can lead to the situation where one item has inconsistent representations but similar semantic labels and cause confusion. For example, in **Table 2** that shows the labels of iPhone 7 in four online stores, the strings before iPhone 7 represent the hierarchical taxonomy labels.

As Table 2 shows, these labels have the same meaning but different representations of hierarchical taxonomy, and the shortcoming of the original taxonomy is obvious. First, the labels in Suning and Gome are in a reversed form, i.e., Mobile Communication → Mobile Phones and Mobile Phones → Mobile Communication. Second, the label in JingDong repeats "Mobile Phones" which shows redundancy. Third, the corresponding level of taxonomy has different category grain. Last but not least, all these labels are used to describe iPhone 7, but the labels are different, which leads to confusion easily. Considering these drawbacks of original taxonomy, we normalize these labels to a unified meaning for easy understanding and this is useful for further data analysis.

▼Table 2. Different labels of iPhone 7 from four online stores

Online store	Hierarchical taxonomy
Jingdong	手机→手机通讯→手机（Mobile Phones → Mobile Communication → Mobile Phones → IPhone 7）
Amazon	电子→手机通讯→手机（Electronics → Mobile Communication → Mobile Phones → IPhone 7）
Suning	手机&数码→手机通讯→手机（Phones& Digital → Mobile Communication → Mobile Phones → IPhone 7）
Gome	手机→手机通讯→手机（Phones → Mobile Communication → Phones → IPhone 7）

We adopt one consistent taxonomy label to represent those similar semantic labels. In this paper, we call the raw hierarchical taxonomy labels crawled from the website as irregular labels. Our intention is to construct a consistent hierarchical taxonomy system based on semantic meaning. The system aggregates those similar semantic irregular labels to a unified one, and maps all these irregular labels to a standard label by standard label system. The basis of mapping irregular labels is the method of semantic similarity, which means we map irregular labels to a standard label with semantic similarity. We will also introduce how to achieve our intention through calculating the similarity between irregular and standard labels.

2.2.1 WMD Based on Word2vec

In our analysis, the irregular label and standard label are both hierarchical and contain several words, because we cannot calculate label semantic similarity directly. However, we creatively consider the label (irregular and standard) as a document, and calculate the label similarity through WMD algorithm, which measures the similarity of two documents based on word2vec embedding. The algorithm was introduced by Matt J. Kusner et al. in 2015 [14]. Before elaborating WMD in detail, we introduce its basis—word embedding.

Word embedding is a language model and a kind of feature learning technique in natural language processing (NLP), where words or phrases from the vocabulary are mapped to vectors. Although one-hot representation and distributed representation can both handle word embedding [14], [15], all the methods essentially use distributed representation in some way. Distributed representation states that words appearing in the same contexts share the semantic meaning. Then semantic similarity between words can be represented by the distance of corresponding vectors

In 2013, T. Mikolov et al. introduced word2vec. It is a particular group of models for learning word embedding from corpus and based on distributed representation [16], [17]. Their model learned a vector representation for each word, using a (shallow) neural network language model. Specifically, they proposed a neural network architecture (Continuous Bag-of-Words model and the Skip-Gram model) which consists of an input layer, a projection layer, and an output layer to predict the nearby words. After training on a large data set, the semantic similarity between words can be represented by the spatial distance of the vectors. This model has the ability to learn rela-

tionships of complex words (**Fig. 2**), which can be explained by the following equations:

$$v(phone) \approx v(cellphone), \tag{1}$$

$$(electronics) - v(phone) \approx v(sports) - v(basketball). \tag{2}$$

The learning process of word embedding is unsupervised and it can be computed on the text corpus of interest or be precomputed in advance. Although we prefer word2vec to learn word embedding, other methods of word embedding are also feasible [18]–[20]. In the following introduction of WMD, we assume that a finite vocabulary size of n words is trained by word2vec according to the specific corpus and each word in the vocabulary is represented by a vector.

In **Fig. 3**, Label 1 is Mobile Phones → Mobile Communication → Mobile Phones, and Label 2 is Electronics → Mobile Communication → Mobile Phones. Because we calculate label distance through word distance, word segmentation must be used to split the label. Fig. 3 shows Labels 1 and 2 after word segmentation. The number beside the word is the weight occupied in the corresponding label. We denote the word in Label 1 as the word i and that in Label 2 as the word j. The weight of the word is denoted by $w_{word\,i}$. It represents the frequency of the word divided by the number of total words in this label after word segmentation, because we assume that labels are represented as a normalized bag of word (nBOW) vectors. The distance between the words i and j is denoted as $d(word\,i, word\,j) = \left|\left| word\,i - word\,j \right|\right|_2$. Then we will show how to calculate the label distance by word distance.

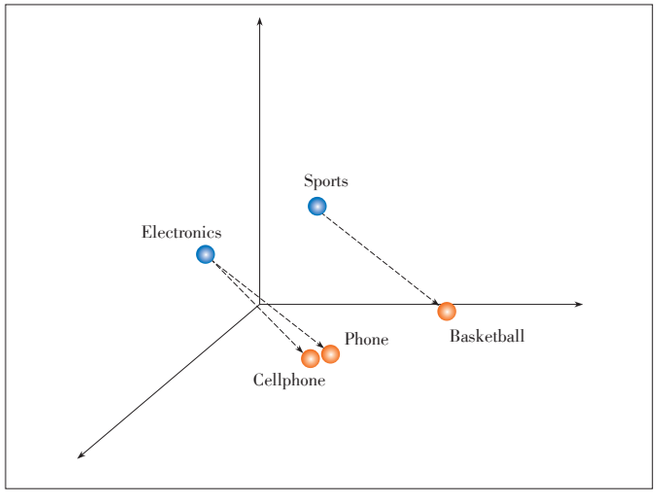

▲Figure 2. Words relationship after training by word2vec.

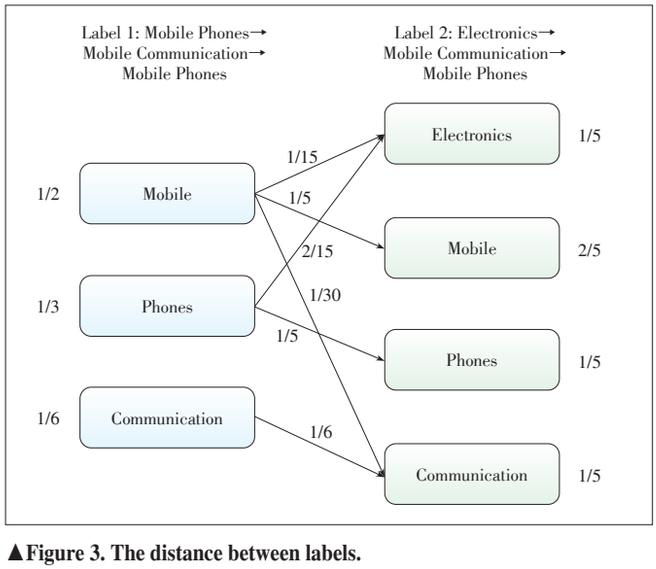

▲Figure 3. The distance between labels.

First, each word i in Label 1 is calculated with any word in label 2 in total or in parts, and we use T_{ij} to denote how many word i are involved in distance calculation with the word j. Second, to make total weights of the word involved in the distance calculation, T_{ij} should satisfy the equation $\sum_j T_{ij} = w_{word\,i}$ and $\sum_j T_{ij} = w_{word\,j}$. At last, the distance between two labels can be defined as the minimal cumulative distance of words distance. Naturally, the following linear program provides the minimal cumulative distance of Labels 1 and 2. More details can be found in [14].

$$D = \min \sum_{i,j} T_{ij} d(word\,i, word\,j), T_{ij} \geqslant 0, \tag{3}$$

and (3) is subject to (4) and (5):

$$\sum_j T_{ij} = w_{word\,i} \ \forall i \in \{1,2,\cdots,n\}, \tag{4}$$

$$\sum_i T_{ij} = w_{word\,j} \ \forall j \in \{1,2,\cdots,m\}. \tag{5}$$

According to the WMD algorithm, the distance between two documents can be calculated, but how to construct a standard label system and map the irregular label to a standard one is not mentioned. Then we will introduce the construction of a standard label system and label mapping based on the WMD algorithm.

2.2.2 Standard Label System

Because of the different taxonomy systems, labels crawled from different online stores have different representations for a particular product. Consequently, we put forward a standard label system considering the diversity of online stores. Then we map all irregular labels to standard labels. We find out that the hierarchical taxonomy of Gome is more reasonable and more complete than the other online stores. Therefore, we take the label system of Gome as the base standard label system, and complete it according to labels from other online stores. **Table 3** shows the samples of the standard label system.

▼Table 3. The samples of standard label system

Label ID	Standard label
001001001	手机数码→手机通讯→手机(Phone & Digital → Mobile Communication → Mobile Phone)
001001002	手机数码→手机通讯→对讲机(Phone & Digital → Mobile Communication → Interphone)
001002001	手机数码→手机配件→移动电源(Phone & Digital → Phone Accessories → Mobile Power)
001002002	手机数码→手机配件→蓝牙耳机(Phone & Digital → Phone Accessories → Bluetooth Earphone)
002001001	电脑→电脑整机→笔记本(Computer → Computer machine → Laptop)
002001002	电脑→电脑整机→台式主机(Computer → Computer machine → Desktop)
002002001	电脑 办公设备→打印机(Computer → Office Equipment → Printer)

In the standard label system, each label has a unique ID, which is also hierarchical. The label and its label ID both have three levels, and each three numbers (001-999) in a label ID correspond to a phrase in the label. In the data processing of DPI data, we use the label ID instead of the label to save storage and perform data analysis. We then construct the standard label system based on WMD.

First of all, we deduplicate the raw taxonomy label of Gome and take it as the initial standard label. Second, other labels are merged to this tree according to the WMD algorithm. If the distance between two labels is smaller than the threshold ε, we think these two phrases have the same semantic meaning. That is to say, these two labels can be replaced with each other semantically. The pseudo code of constructing the standard label system algorithm is elaborated in **Algorithm 1**.

Algorithm 1: Construct Standard Label System

```
Input: labels from six online stores.
Output: the standard label system.
Initial parameters:
    deduplicate label taxonomy of Gome as the standard label system, denoted as Standard_System
    deduplicate label taxonomy of other online stores, denoted as Irregular_System
for ire_label in Irregular_System {
    minDistance = INTEGER.MAX_VALUE
    for sta_label in Standard_System {
        tempDistance = WMD(ire_label, sta_label)
        If (tempDistance < minDistance) {
            minDistance = tempDistance
        }
        If(minDistance > ε){
            Standaard_System.add(ire_label)
        }else{
            continue
        }
    }
}
traversing the Standard_System, output the label and encode with its label ID
```

2.2.3 Label Mapping

After constructing the standard label system, we map all irregular labels to standard labels for consistency. The purpose of label mapping is to find the label which has the greatest semantic similarity in the standard label system for every irregular label. In other words, we should find a label in the standard label system to satisfy a given irregular label.

$$\min WMD(irregular\ lable, sl)\ sl \in standard\ label\ system. \quad (6)$$

We can easily understand the label mapping from **Fig. 4**. Given an irregular label in the left, we need to find a label from the standard label system in the right to satisfy (6). For an irregular label in a nutshell, we need to find a label in the standard label system to achieve the minimal label distance. At last, every irregular label is mapped to a standard label.

2.3 DPI Processing

In this part, our intention is to extract the item ID from URL following a bunch of rules of regular expression (Regex), a string matching algorithm. The algorithm is designed for "find" or "find and replace" operations on strings and it is perfectly suitable for our needs. But it still has two problems. First, URL contains multiple information in the form of parameters and we have to recognize which part involves item ID. Sec-

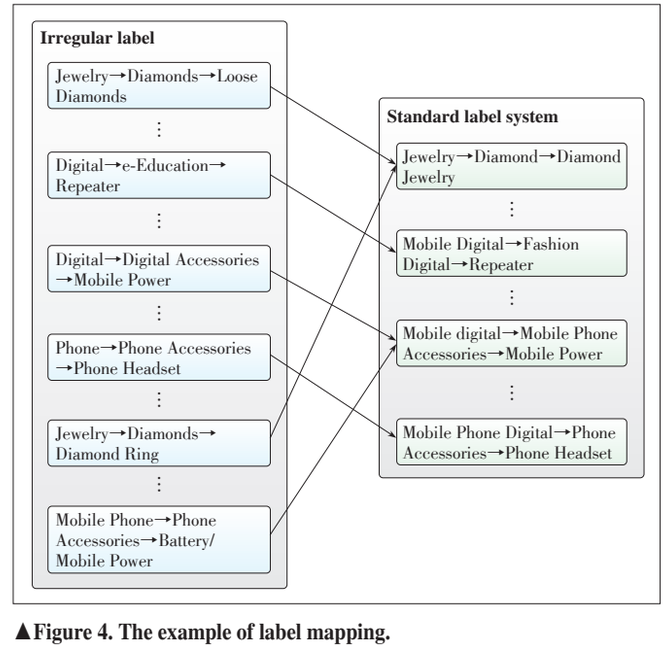

▲Figure 4. The example of label mapping.

ond, we have to consider six online shopping stores, which increases the difficulty because the keys of item ids are different between heterogonous online stores. Next we will introduce our procedure of processing DPI data and solutions to the above problems.

First of all, we filter out the data of the six online shopping applications from DPI data through the domain name. Second, we extract the item ID from the URL through Regex match. At last, we query the corresponding label according to the item ID from the database. But how to get the Regex? We summarize it manually from the large raw DPI data for particular online store, and then we introduce our methodology to summarize the Regex in an example of Jingdong.

In the beginning, we filter out a large number of URLs from Jingdong. Then we identify the key of item ID from tens of parameters of URL. In this process, we find out there are several forms of the key even in one online shopping application. Finally, the item ID with the form of key-value is transformed to Regex manually. **Table 4** shows the Regex matching item IDs in Jingdong. All these Regex has been tested by real URL that users have browsed.

Through the way above, the Regex of other five online shopping applications can also be summarized. **Table 5** shows the number of Regex of these applications.

▼**Table 4. The Regex of item IDs in Jingdong**

Serial number	Regex
1	ware[iI]d|sku(=|%3D)(\d+)
2	order.*ware[iI]d(=|%3D)(\d+)
3	jd\.com/(product/)?(\d+)\.html
4	productIds=(\d+)
5	orderComment/(\d+)
6	item\.jd\.com/(\d+)

▼**Table 5. The number of Regex of the six applications**

Application	Number
Jingdong	6
Suning	5
Amazon	4
Gome	4
Dangdang	2
Taobao & Tmall	4

3 Implementation Based on Hadoop

The data scale of telecom network has reached to PB level for each day, so a big data platform with high reliability and high effectiveness is extremely important for operators. We design a big data platform based on Hadoop to achieve our goal through the above methodology. In a nutshell, users' behavior can be consistently mined and attached to a label on this platform.

The architecture of the platform consists of four modules (**Fig. 5**). They are data storage, data collecting, label processing and data processing.

3.1 Data Storage

In the era of big data, it is impossible to store extremely massive amounts of data in a single machine with varieties of demands. Therefore, alternative technologies have been investigated in order to solve this issue. Hadoop Distributed File System (HDFS) works as a part of a Hadoop cluster or as a stand-alone universal distributed file system. It is widely used as a storage system in industry area because of its high stability and scalability. In our data storage module, we also adopt HDFS as our storage system for DPI data. Haddop's database (HBase) is a non-relational database and HDFS is served as its physical storage. However, their functions are different in our system.

1) HDFS. In our system, HDFS mainly stores two kinds of files. One is the raw DPI data from telecom operators, which generates every day in a directory named by date and province. The other is temporary result, it contains the raw item labels crawled from the web, the standard labels after label processing and the final results of data processing module, that is, the user ID, timestamps and standard label connected by comma.
2) HBase. We adopt HBase to store the item ID and its standard label. HBase can support storage and query in the form of key-value pairs compared with HDFS, which just meets our demands for the storage of item ID and standard label and the query by item ID. Second, HBase is a member of Hadoop, which can be well integrated with MapReduce in data processing.

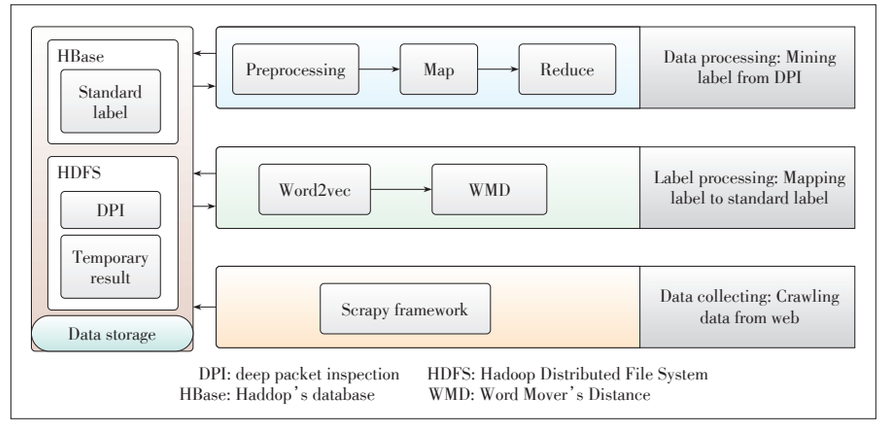

▲**Figure 5. Data analysis architecture.**

Before we adopt HBase as our key-value database, we compared the performance of HBase and Redis [21], which is a key-value database based on in-memory storage. The results show that Redis supports higher concurrent requests, while HBase can also satisfy our concurrent requests. Finally, considering the stability and price, we adopt HBase as our database to store item information.

In our implementation, the format of item information and samples are shown in **Table 6**. The column family: qualifier and timestamp can be set by a default value, while Rowkey and cell value must store the corresponding item ID and its standard label. Furthermore, six tables need to be created to store the information of six different online stores.

3.2 Data Collection

This module is used to collect data from websites, in other way, crawl the item ID and irregular labels from the online store. We implement this function to extract the data from websites based on an open source and collaborative framework named Scrapy [22]. **Fig. 6** shows the framework of Scrapy.

This framework is responsible for crawling item information from the website without considering the scheduler and downloader because they are implemented by the framework. All we need to do is to implement the spider module in the Fig. 6, and focus on the design of our spider. The design of our spider takes hierarchical labels into consideration, because three-level hierarchical label corresponds to three-level hierarchical websites. Therefore, we start our web crawler from the starting page, which corresponds to the first level of the hierarchical label. Then we find all secondary page and save it. Furthermore, all the secondary pages are crawled and the last level page of the website is saved. At last, we crawl all last pages and save all hierarchical labels.

We need to pay attention to one problem, that is, the item information is always changing slowly. Therefore, spiders should be launched periodically to re-crawl the item information. The new items browsed by users cannot be attached to a label because we have not crawled this item information. Therefore, we calculate the percentage of the URL from which we can match the item ID but cannot get the label. Once this percentage is greater than 5, we launch our spiders and re-crawl the website. As for new item information, if item ID exists in the last version, we just update the hierarchical label when it changes, and if the item ID does not exist, we add this item information to HBase.

▼Table 6. The store format of item information and samples

Rowkey	Column family: qualifier	Timestamp	Cell value
Item ID	"label:standard"	default	Standard label
4005363	"label:standard"	default	(Computer → Computer → Laptop)
3726830	"label:standard"	default	(Phone & Digital → Mobile Communication → Mobile Phone)

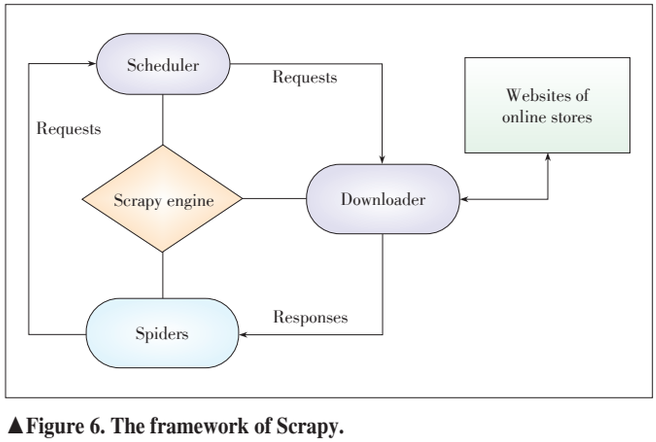

▲Figure 6. The framework of Scrapy.

3.3 Label Processing

This section focuses on transferring the item ID → the irregular label to the item ID → standard label. The main algorithm is introduced in Section 2.2, and the realization of the label processing is as follows.

1) Construct a vocabulary of word embedding, which is trained by word2vec according to the specific corpus from the web. The word2vec is trained with the corpus from Sogou Labs [23]. It contains various types of content of 130 million original web pages and the amount reaches 5 TB. More importantly, the corpus may directly influence the accuracy of WMD, so a large corpus should be adopted.
2) Construct the standard label system based on the label taxonomy of Gome. In this step, threshold ε should be studied to make the standard label reasonable. We made experiments with different values of ε and found that $\varepsilon = 1.1$ makes the standard label system more reasonable. In this condition, the standard label system has 2153 hierarchical labels, which contains 25 first-level phrases, 296 second-level phrases and 1620 third-level phrases.
3) Map the item ID → the irregular label to the item ID → standard label according to the Algorithm 1. After mapping the irregular label, every item ID corresponds to a unique standard label.
4) Store the item ID → the standard label to HBase in corresponding tables. In this step, we create six tables with the same names of the corresponding online store. The item ID → standard label is written into the corresponding table in the format mentioned in Section 3.1.

3.4 Data Processing

In this part, we will focus on the processing of massive amounts of DPI data based on Hadoop MapReduce, which is the most popular open source implementation of the MapReduce framework proposed by Google [24]. The feature of Hadoop MapReduce is high fault tolerance and scalability. It is easy to program and perfectly suitable for our demands [25],

[26]. There are two stages named map and reduce in a Hadoop MapReduce job, we only have to define the map and reduce to finish our job. The input and output formats of map and reduce are shown in **Fig. 7**. The formats are denoted as a set of key-value pairs (key, value). The procedure of DPI data processing is as follows.

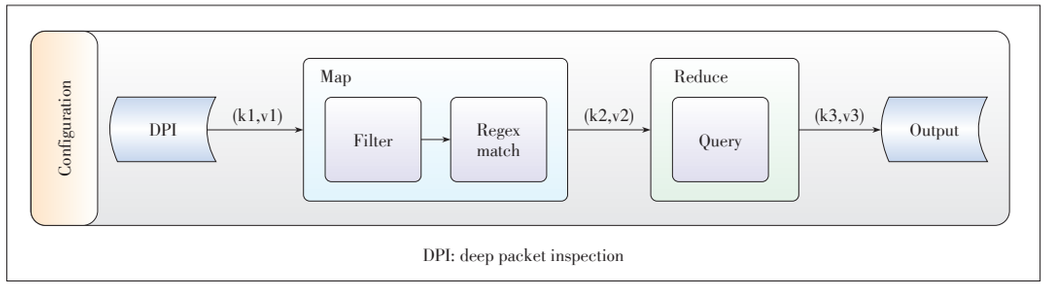

▲**Figure 7. Implementation of Hadoop MapReduce.**

1) Map

The Map process is to transfer the URL to item ID based on regular expression matching, as shown in Fig. 1. We take two modules to achieve this function in this phase, they are Filter and Regex Match.

Filter: The input format is key-value pairs of raw DPI data, which contains a lot of information. The key is offset of current line in the file and the value is raw DPI data. Filter extracts the information we need, including the use ID, URL, timestamp and domain name shown in Table 1, abandoning other information such as user agent, data size, protocol, and IP. At the same time, Filter also extracts the data from the top six online stores according to their domain names and abandon other DPI data. Moreover, we take IMSI encrypted by MD5 for privacy and security concerns as unique ID of users. In a nutshell, the output of Filter is in the form of key-value pairs (encrypted IMSI, URL from top six online stores| timestamp| domain name).

Regex Match: This module handles all URLs after Filter through Regex matching to extract the item ID. It is difficult to follow tens of rules of Regex from the top six online stores to match the item ID. We adopt two strategies to handle this problem. One is matching all rules for one URL and ignoring which application the URL is from. We call this strategy Global Match. The other one is identifying which application the URL is from first, and then matching the URL based on rules from the corresponding application. We call it Partial Match.

We found that Partial Match costs less time than Global Match based on our experiment in the **Table 7**. In the experiment, the number of nodes in our Hadoop cluster is 104, and the time refers to the duration of the Map phase. The final output of the Map phase is key-value pairs (encrypted IMSI, item ID | timestamp | domain name).

2) Reduce

Reduce finishes the last step of our data processing, that is, querying the standard label from the corresponding tables in HBase. In this process, we need to construct six table connections to HBase and then get the standard label by item ID. The item ID from the Map process is queried and then output to the (encrypted IMSI, standard label and timestamp) to a directory.

3) Configuration

Some necessary configuration parameters need to be set first in the job of launching a MapReduce. For example, the input and output format of Map and Reduce, the directory of original input and final output, and the number of Reduce.

3.5 Results

After all the work is done, we achieve the BT on the DPI data, which can attach a Hierarchical label on user behavior. **Table 8** shows the results of our methodology and implementation.

The IMSI is the unique ID tied with unique users, and encrypted by MD5 for privacy and security concerns. The URLs represent users' browsing behavior and the labels are the BT on their behavior. These labels imply users' interest and preference, which will help identify potential buyers from the large amounts of Internet users.

4 Conclusions

We developed an extensive methodology for BT on users' online shopping behavior. The methodology is based on hierar-

▼**Table 7. Experiment results**

DPI data size	Time cost in map	
	Global match	Partial match
2.7 Tb	1 h 13 min	46 min
470 Gb	17 min	10 min

▼**Table 8. The final results of the proposed scheme**

IMSI	URL	Label
898A93AA58976A4945 6222D58420B6B1	http://item.m.jd.com/ product/3368118.html	Online shopping → Appliances → Health appliance
4B0DA828BDF06C1C2 1BC8926456402CA	http://cd.jd.com/img/ channel?callback= jQuery6841693	skuId=10483088139&_= 1503617852363& Online shopping → Home building → Home textile cloth → Sheets
45DCF28D2D947447F3 C9B87E24491131	http://product.dangdang. com/23215376.html	Online shopping → Books → Political/Military
DF6D96FC9B386DABF 2E5C0AADB508BC1	http://item.m.gome.com.cn/ product-A0004771496-pop8003858741.html? cmpid=seo_baidu_kapian	Online shopping → Home appliance → Personal care → Shaver

IMSI: international mobile subscriber identity URL: uniform resource locator

chical and semantic taxonomy aggregation. As a result, we can attach a hierarchical and semantic label to online shopping behavior, which will help identify potential buyers from the large amounts of Internet users and achieve precision marketing. We adopted the WMD algorithm to aggregate similar semantic labels to a unified label, and implemented our methodology on a big data platform. It performed efficiently to mine users' behavior on online shopping applications.

Acknowledgement

The authors would like to thank Beijing University of Posts and Telecommunications, China and China Telecom for cooperation and support for this paper.

References

[1] H. Asghari, M. van Eeten, J. M. Bauer, and M. Mueller, "Deep packet inspection: effects of regulation on its deployment by internet providers," in *41st Research Conference on Communication, Information and Internet Policy*, Arlington, USA, 2013. doi: 10.2139/ssrn.2242463.
[2] R. Antonello, S. Fernandes, C. Kamienski, et al., "Deep packet inspection tools and techniques in commodity platforms: challenges and trends," *Journal of Network and Computer Applications*, vol. 35, no. 6, pp. 1863–1878, Nov. 2012. doi: 10.1016/j.jnca.2012.07.010.
[3] K. Sha, "Trends and issues related to online shopping market in China," in *IEEE 6th International Conference on Information Management, Innovation Management and Industrial Engineering*, Xi'an, China, 2013, pp. 183–187. doi: 10.1109/iciii.2013.6703114.
[4] M. Limayem, M. Khalifa, and A. Frini, "What makes consumers buy from Internet? A longitudinal study of online shopping," *IEEE Transactions on Systems, Man, and Cybernetics—Part A: Systems and Humans*, vol. 30, no. 4, pp. 421–432, 2000. doi: 10.1109/3468.852436.
[5] J. H. Wu, L. Peng, Q. Li, et al., "Falling in love with online shopping carnival on singles´ day in China: an uses and gratifications perspective," in *IEEE/ACIS 15th International Conference on Computer and Information Science (ICIS)*, Okayama, Japan, 2016, pp. 1–6. doi: 10.1109/icis.2016.7550801.
[6] J. Chen and J. Stallaert , "An economic analysis of online advertising using behavioral targeting," *MIS Quarterly*, vol. 38, no. 2, pp. 429–449, 2014. doi: 10.2139/ssrn.1787608.
[7] W. Zenghong, C. Yufen, and Z. Jun, "Personalized map service user interest acquisition based on browse behavior," in *IEEE International Conference on Control Engineering and Communication Technology (ICCECT)*, Liaoning, China, 2012, pp. 916–919. doi: 10.1109/iccect.2012.225.
[8] Q. Zhu, M. L. Shyu, and H. Wang, "Video topic: modeling user interests for content-based video recommendation," *International Journal of Multimedia Data Engineering and Management (IJMDEM)*, vol. 5, no. 4, pp. 1–21, 2014. doi: 10.4018/ijmdem.2014100101.
[9] D. I. Maditinos and K. Theodoridis, "Satisfaction determinants in the Greek online shopping context," *Information Technology & People*, vol. 23, no. 4, pp. 312–329, 2010. doi: 10.1108/09593841011087789.
[10] R. Olbrich and C. Holsing, "Modeling consumer purchasing behavior in social shopping communities with clickstream data," *International Journal of Electronic Commerce*, vol. 16, no. 2, pp. 15–40, 2011. doi: 10.2753/jec1086-4415160202.
[11] M. Pazzani and D. Billsus, "Learning and revising user profiles: the identification of interesting web sites," *Machine Learning*, vol. 27, no. 3, pp. 313–331, 1997. doi: 10.1023/A:100736990.
[12] G. E. Hinton, J. L. McClelland, and D. E. Rumelhart, "Distributed representations," in *Parallel Distributed Processing: Explorations in the Microstructure of Cognition, Vol. 1*. Cambridge, USA: MIT Press, 1984, pp. 77–109.
[13] IResearch. (2017, May). *Online shopping industry monitoring report in China 2016* [Online]. Available: http://wreport.iresearch.cn/uploadfiles/reports/636228578101640793.pdf
[14] M. J. Kusner, Y. Sun, N. I. Kolkin, and K. Q. Weinberger, "From word embeddings to document distances," in *32nd International Conference on Machine Learning*, Lille, France, 2015, pp. 957–966.
[15] W. Y. Zou, R. Socher, D. Cer, and C. D. Manning, "Bilingual word embeddings for phrase-based machine translation," in *Conference on Empirical Methods in Natural Language Processing*, Seattle, USA, 2013, pp. 1393–1398.
[16] T. Mikolov, I. Sutskever, K. Chen, G. Corrado, and J. Dean, "Distributed representations of words and phrases and their compositionality," in *26th International Conference on Neural Information Processing Systems*, Lake Tahoe, USA, 2013: 3111–3119.
[17] T. Mikolov, K. Chen, G. Corrado, and J. Dean. (2013, Sept. 7). *Efficient estimation of word representations in vector space* [Online]. Available: arxiv.org/abs/1301.3781
[18] R. Collobert and J. Weston, "A unified architecture for natural language processing: deep neural networks with multitask learning," in ACM 25th International Conference on Machine Learning, Helsinki, Finland, 2008, pp. 160–167. doi: 10.1145/1390156.1390177.
[19] A. Mnih and G. E. Hinton, "A scalable hierarchical distributed language model," in *Neural Information Processing Systems (NIPS 2008)*, Vancouver and Whistler, Canada, 2008, pp. 1081–1088.
[20] J. Turian, L. Ratinov, and Y. Bengio, "Word representations: a simple and general method for semi-supervised learning," in *48th Annual Meeting of the Association for Computational Linguistics*, Uppsala, Sweden, 2010, pp. 384–394.
[21] Redis. (2017, May). *Redis* [Online]. Available: https://redis.io
[22] Scrapy. (2017, May). *Scrapy* [Online]. Available: https://scrapy.org
[23] Sogou. (2017, May). *SogouT* [Online]. Available: http://www.sogou.com/labs/resource/t.php
[24] J. Dean and S. Ghemawat, "MapReduce: simplified data processing on large clusters," *Communications of the ACM*, vol. 51, no. 1, pp. 107–113, 2008. doi: 10.1145/1327452.1327492.
[25] A. B. Patel, M. Birla, and U. Nair, "Addressing big data problem using Hadoop and Map Reduce," in *IEEE Nirma University International Conference on Engineering (NUiCONE)*, Ahmedabad, India, 2012. doi: 10.1109/nuicone.2012.6493198.
[26] J. Dittrich and J. A. Quiané-Ruiz, "Efficient big data processing in Hadoop MapReduce," *Proceedings of the VLDB Endowment*, vol. 5, no. 12, pp. 2014–2015, Aug. 2012. doi: 10.14778/2367502.2367562.

Manuscript received: 2017-08-05

Biographies

ZHANG Lifeng (zhanglifeng@bupt.edu.cn) is a postgraduate student at Beijing University of Posts and Telecommunications, China. His research interests include data mining and massively parallel processing of data.

ZHANG Chunhong (zhangch@bupt.edu.cn) is a lecture of School of Information and Communication Engineering, Beijing University of Posts and Telecommunications, China. She received her Ph.D. degree in computer science, M.Eng. degree in information technology, B.Eng. degree in telecommunication engineering in 1993, 1996 and 2013 respectively. She was a visiting scholar at Illinois Institute of Technology, USA in 2015. Her research interests include data mining, natural language processing, and ubiquitous computing.

HU Zheng (huzheng@bupt.edu.cn) received his Ph.D. degree from Beijing University of Posts and Telecommunications, China in 2008. He is working in the State Key Laboratory of Networking and Switching Technology, Beijing University of Posts and Telecommunications. His current research interests lie in the user behavior modeling and analysis in mobile internet and social networks. He has published more than 30 papers and been granted more than 10 patents in related area.

TANG Xiaosheng (txs@bupt.edu.cn) received his Ph.D. degree from Beijing University of Posts and Telecommunications, China. He is working in the Beijing University of Posts and Telecommunications. His current research interests include user behavior modeling and analysis in mobile internet and social networks. He has published more than 20 papers and been granted more than 10 patents in related areas.

DOI: 10.3969/j.issn.1673-5188.2018.01.007
http://kns.cnki.net/kcms/detail/34.1294.TN.20180321.1038.002.html, published online March 21, 2018

Overview of Co-Design Approach to RF Filter and Antenna

ZHANG Wenmei and CHEN Xinwei
(Shanxi University, Taiyuan 030006, China)

Abstract

The filter and antenna are two key components of the radio frequency (RF) front-end. When the antenna is directly connected with the filter, additional mismatch losses will be caused. Therefore, the antenna and filter are integrated into a single device to provide both filtering and radiating functions. In this way, many advantages, like low cost, light weight, small size and lower insertion loss can be obtained. In this paper, the co-design approaches of RF filter-antenna are reviewed. Based on the open literatures, the integrated approaches of filtering antenna can be classified into five main categories:1) Co-design by optimizing the interfacing impedance, 2) co-design according to the synthesis approach of filter, 3) co-design by embedding novel resonators within the feeding structures, 4) co-design by employing auxiliary physical structures, and 5) other methods. The RF filter-antenna system can improve the integration degree of RF front-end, reduce its size and cost, and optimize its performance.

Keywords

filtering antenna; Co-design; RF front-end

1 Introduction

Miniaturization and low cost are the two most fundamental demands for the radio frequency (RF) receiver front-end. Nowadays, dual-function or multifunction integrated modules become more and more popular in wireless communication systems for their miniaturized circuit size and satisfying overall performance. For example, the noise figure of a RF antenna-filter low-noise-amplifier (LNA) system has been significantly improved with the co-design strategy [1]. In [2], antennas were co-designed with the amplifier and transceiver to attain higher integration degree. The filter and the antenna are independent component in most of the RF front-end. The antenna is used to receive and transmit signal, and the bandpass filter is cascaded right after the antenna for filtering the spurious signals. Generally, the bandpass filter and antenna are designed separately and connected by a 50 Ω transmission line. This transmission line not only degrades the performance of the system but also occupies the additional circuit area. Recently, many scholars have begun to study the co-design method for the bandpass filter and antenna. Based on the open literatures, it is possible to categorize co-design approach in five main categories: 1) Co-design by optimizing the interfacing impedance; 2) co-design according to the synthesis approach of filter; 3) co-design by embedding novel resonators within the feeding structures; 4) co-design by employing auxiliary physical structures; 5) other methods.

2 Survey and Analysis

2.1 Co-Design by Optimizing the Interfacing Impedance

One of the simply co-design way by optimizing the interfacing impedance between the filter and antenna is displayed in **Fig. 1**. Here, the filter and antenna are layered and share the same ground plane to reduce the dimensions [3]. The advantages of this co-design approach are that the miniaturized dimensions can be obtained compared to the version before the co-design. Also, the design process of the filter and antenna is mutually independent. By optimizing the impedance at the interfaces of the filter and antenna, the performance can be improved. Various integrated filtering antennas using this method have been reported [3]–[6]. An example has been developed in [3].

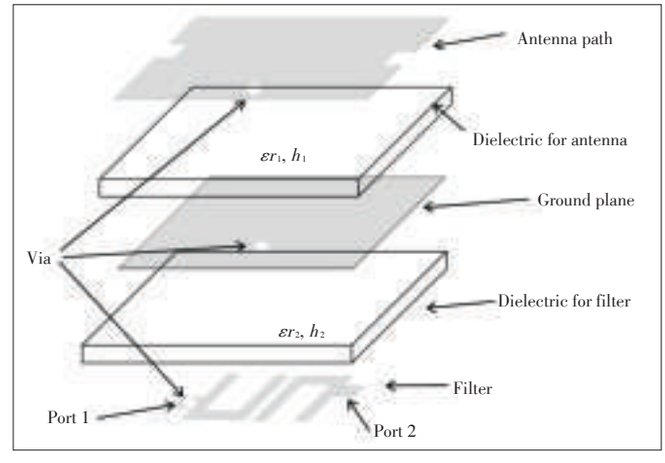

▲Figure 1. A co-designed filtering antenna.

This work was supported by the National Science Foundation of China under Grant No. 61771295 and the Natural Science Young Foundation of Shanxi Province under Grant Nos. 2014021021-1 and 2015011042.

The S_{11} and gain before and after the co-design are shown in **Fig. 2**. It can be seen that, for the co-designed version, the measured pass-band is located at 4.06–4.26 GHz. As compared to 4.03–4.14 GHz for the traditional version, a wider bandwidth is obtained. Meantime, the corresponding peak gain is 4.3 dBi, better than 2.8 dBi for the traditional version.

2.2 Co-Design According to the Synthesis Approach of Filter

In this approach, the last stage of filter network is replaced with an antenna which acts as one of the resonators. The synthesis and design process is same as the filter. The advantages of this approach are that the realized filtering antenna has a high integration degree. The disadvantages are, in some designs, extra filtering circuits are inserted to the antenna feeding networks, causing extra insertion loss and degrading antenna gains.

Many of the filtering antennas according to the synthesis approach of filter use the microstrip structure [7]–[15]. Most of them obtained compact dimensions, such as 0.41lg × 0.6lg [12] and 0.23lg × 0.29lg [13]. A typical example and corresponding results can be found in **Fig. 3** [9]. It is demonstrated that this simple filtering antenna possesses a flat realized gain response within its operational band and has good band-edge selectivity.

This co-design method can also be used for filtering antennas fed by coplanar waveguide (CPW) [16]–[18] and filtering dielectric resonator antennas. Especially in [17], a reconfigurable filtering slot antenna (FSA) is designed. Its structure and results are shown in **Fig. 4** [17]. Compared to the ordinary slot antenna, the proposed FSA has a wider bandwidth, flat antenna gain in the passband, and good frequency skirt selectivity in both states.

Recently, this co-design method is applied for designing the filtering microstrip antenna array [19], [20]. In [20], two filtering microstrip antenna arrays fed by a uniform/nonuniform power divider network have been designed, fabricated, and measured. **Fig. 5** displays its photograph fed by a uniform power divider network [20]. Both the antenna arrays have achieved good impedance matching characteristic as well as filtering response, such as a flat gain frequency response, sharp band edge characteristic, and high stopband suppression. The filtering antenna array fed by a nonuniform power divider has presented a low sidelobe performance.

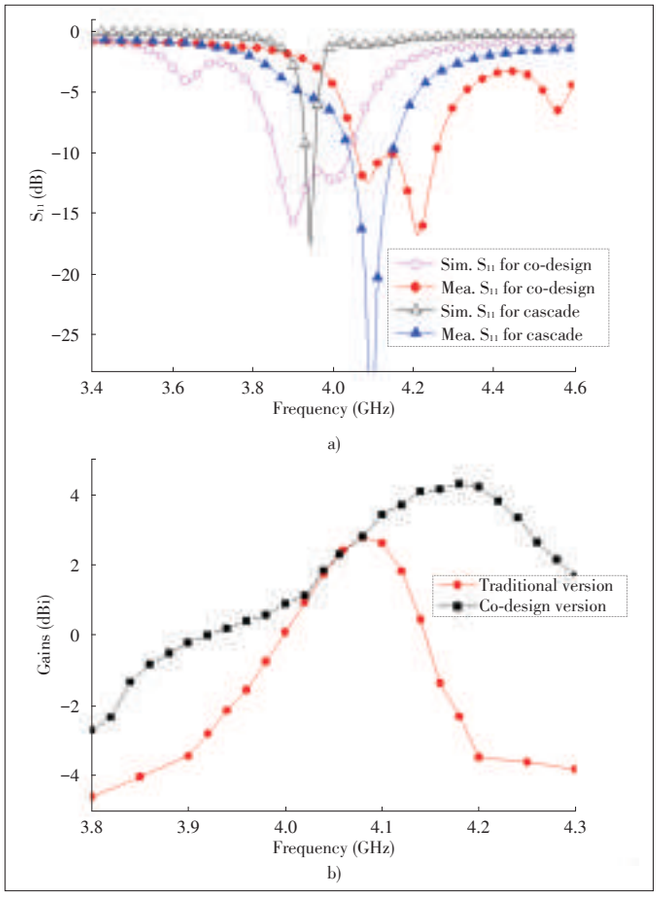

▲Figure 2. a) Measured and simulated S_{11} and b) Measured gains for the co-designed and traditional filtering antennas.

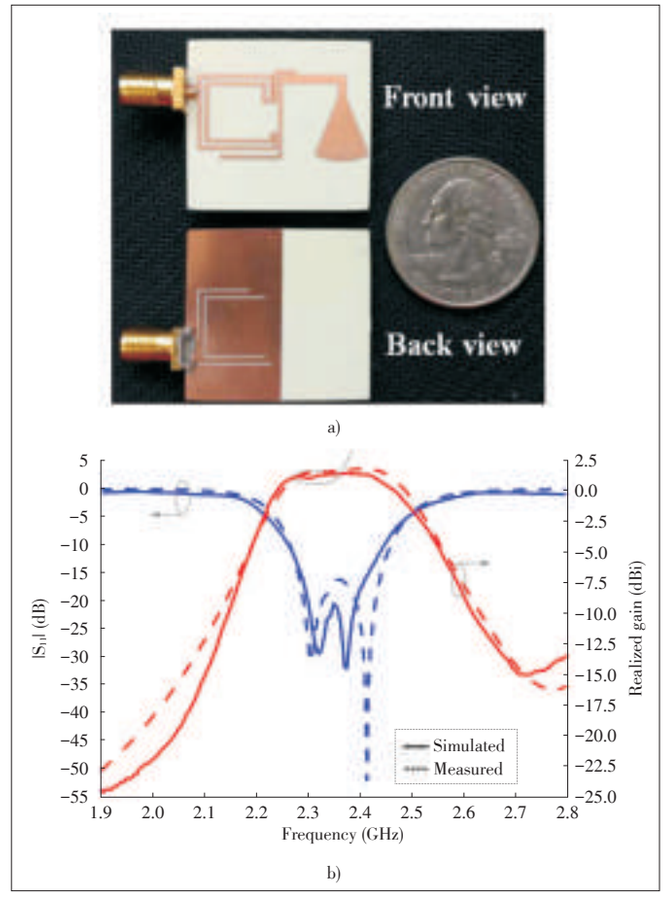

▲Figure 3. a) The first electrical small filtering antenna and b) measured and simulated $|S_{11}|$ and realized gain values of the filtering antenna.

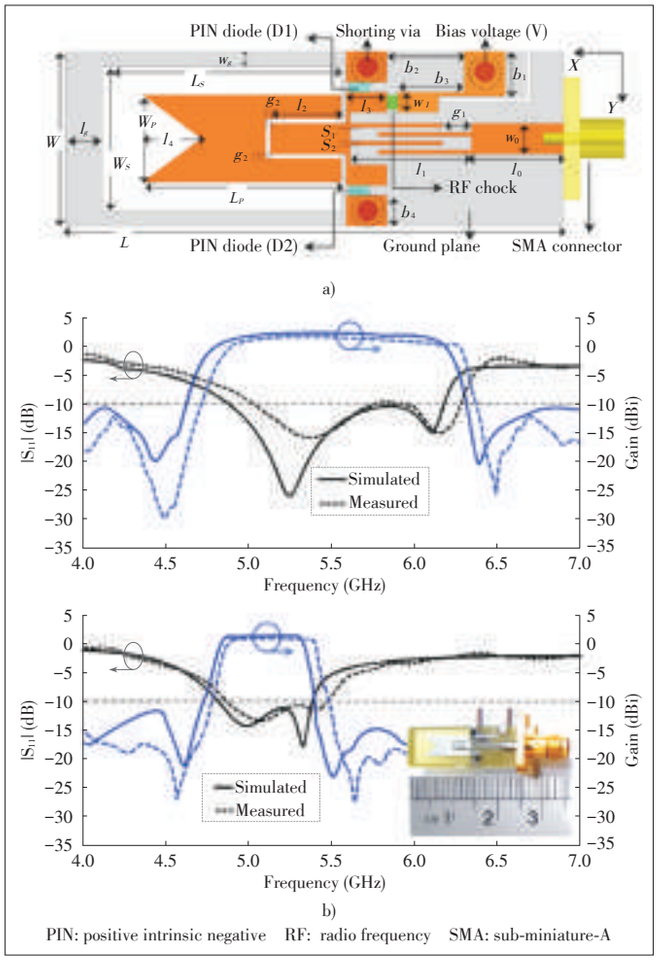

▲Figure 4. a) Layout of the proposed reconfigurable filtering slot antenna and b) simulated and measured S_{11} and gain of the FSA for OFF and ON states.

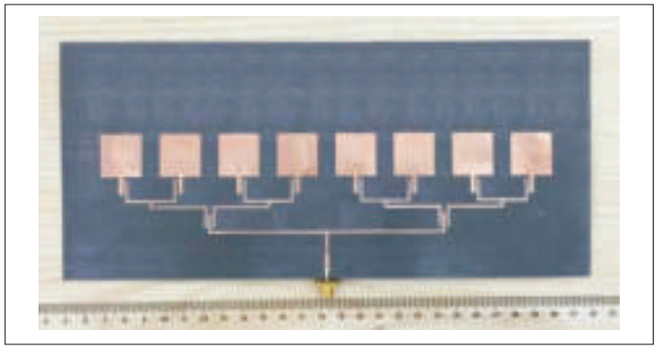

▲Figure 5. Photograph fed by a uniform power divider network.

2.3 Co-Design by Embedding Novel Resonators Within the Feeding Structures

In order to control the performance of filtering patch antennas, many designs embed the resonator within the feeding structure of antenna. The advantages of this approach are that its design can be more flexible and free. Also, since no complex filtering and matching networks are involved, the proposed dual-band filtering antenna is very compact and the insertion loss of feeding circuit is desirably low.

This approach is often used to realize multi-band and UWB filtering antennas [21]–[28]. Typical planar structure can be found in [23]. Its configuration and the corresponding S_{11}, gain are shown in **Fig. 6** [23]. It can be seen that the two operating bands locate at 1.9 GHz and 2.6 GHz for LTE applications. The out-of-band gains are less than -10 dBi, indicating more than 16 dB out-of-band radiation rejection levels, which can meet the requirement of LTE MIMO for customer premise equipment (CPE). It is also seen that radiation nulls are generated at 1.85 GHz and 2.10 GHz for the lower band, and 2.50 GHz and 2.91 GHz for the upper band, resulting in better filtering performance for two bands.

It is worth mentioning that in [28], the tunability has been achieved by centrally loading the resonator with only a single varactor diode (**Fig. 7**). Since the frequency tuning technique is achieved at the feeding line of the antenna without affecting the antenna radiation characteristics, the radiation patterns are stable over the interesting frequency range. This makes the pro-

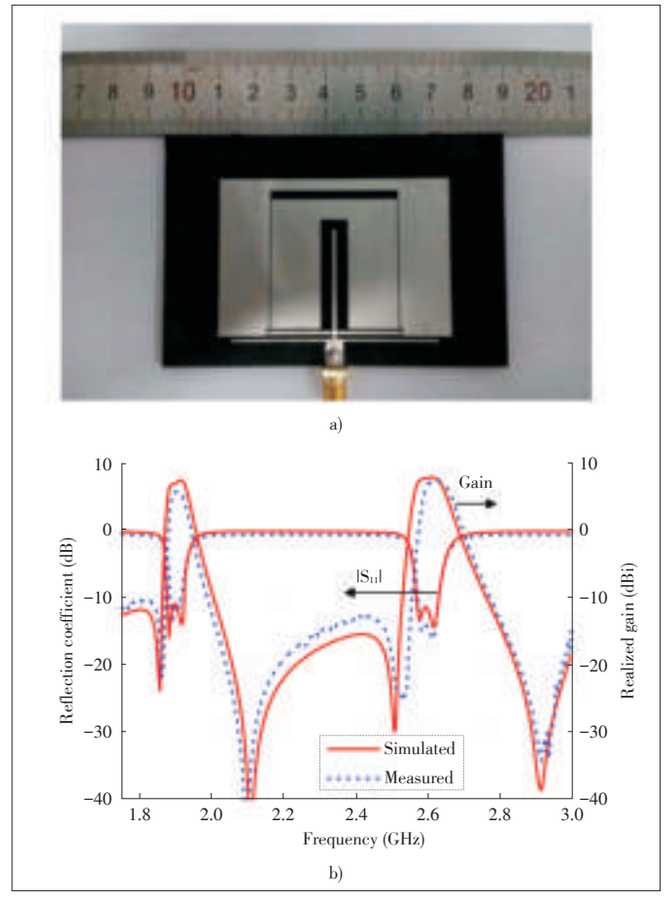

▲Figure 6. a) Fabrication prototype of the dual-band filtering antenna and b) simulated and measured results of the proposed antenna.

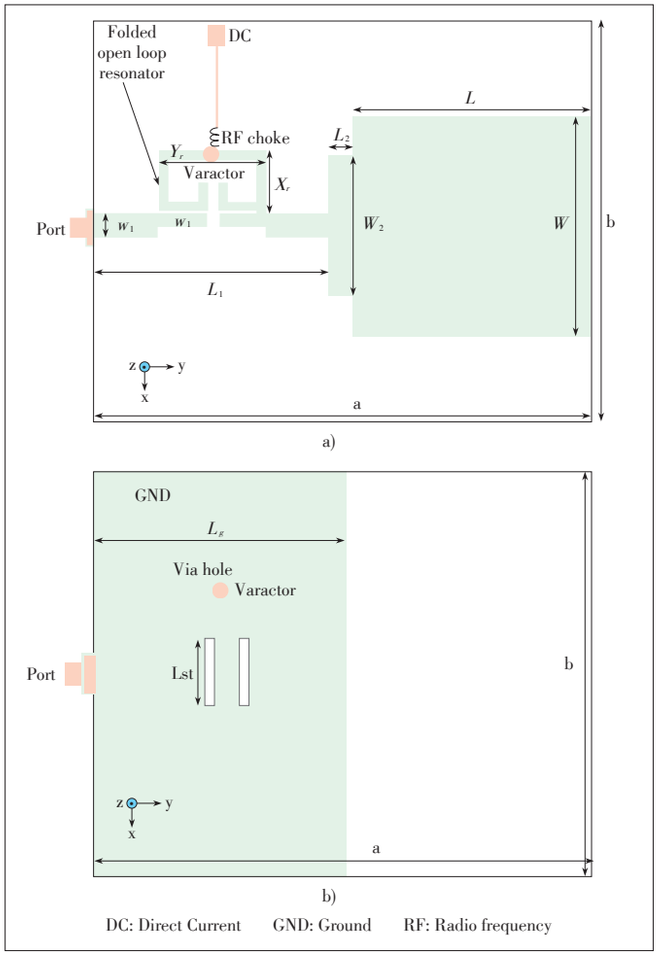

▲Figure 7. Schematic of the proposed tunable bandpass filtering antenna: a) The top layer; b) the bottom layer.

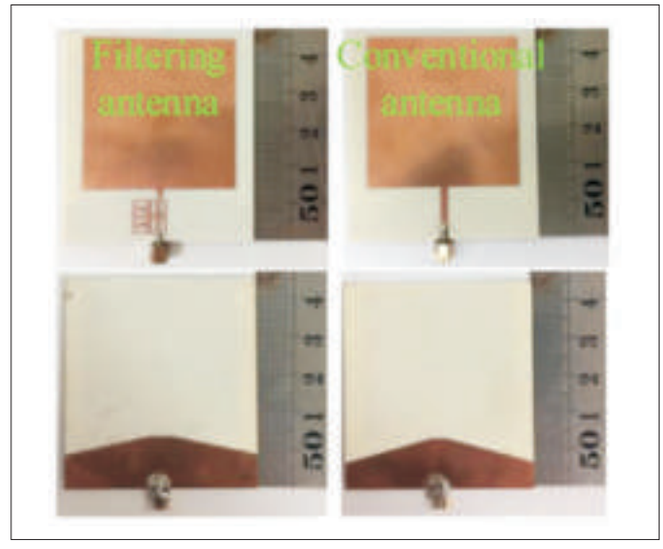

▲Figure 8. Photographs (top view and back view) of the co-designed filtering antenna and the conventional planar printed monopole antenna.

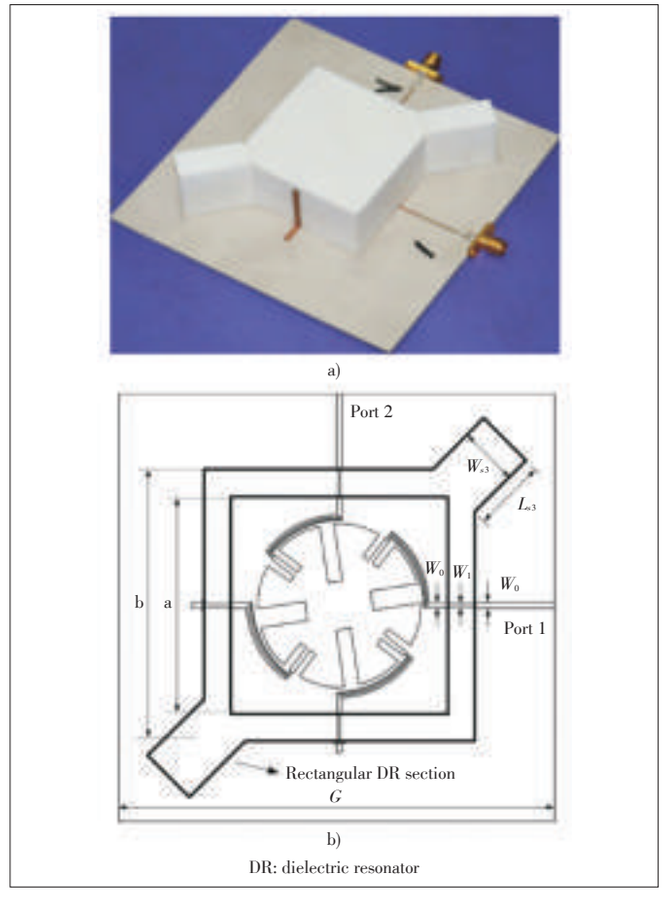

▲Figure 9. a) Photograph of the designed wideband filtering CP antenna and b) configuration of the proposed wideband filtering CP antenna.

posed filter-antenna convenient for the interweave Cognitive Radio (CR) communication applications. In addition, in [24], a filtering antenna which consists of the conventional microstrip-fed monopole antenna and the recently developed high-frequency-selective two-stage filter based on the twist-modified Split Ring Resonator (SRR), is demonstrated in **Fig. 8**. To filter out the unwanted out-of-band radiation, the used filter unit is inserted directly into the feeding line of the monopole antenna without adding extra space.

This co-design method can also be used for the filtering dielectric resonator antenna (DRA) [29]–[31]. The common performance of three designs are that they show better second harmonic suppression, with out-of-band suppression of more than 23 dB within very wide stopband. To the best of our knowledge, it is the broadest passband and stopband that can be obtained thus far from a simple co-designed broadside filtering antenna. **Fig. 9** shows the interesting filtering circular polarization (CP) antenna in [31]. Here, the coupled line sections are introduced on the flexible snowflake shaped patch element to obtain wideband, excellent bandpass filtering and harmonic suppression characteristics. A hollow DRA is integrated with this coupler for the implementation of a wideband filtering CP

antenna. The realized antenna exhibits a wide overlapping bandwidth of 27.8%. Moreover, the proposed antenna achieves a wide stopband up to the third harmonics with a suppression level larger than 19 dB.

2.4 Co-Design by Employing Auxiliary Physical Structures

In order to improve the integration and reduce the insertion loss caused by inserting extra filtering circuits, filtering antennas by employing auxiliary physical structures are proposed [32]–[35]. Since no extra filtering circuit is involved, the antenna is very simple. Moreover, due to eliminating insertion loss of filtering elements, this type of filtering antennas can provide a relatively high gain.

In this co-design approach, the auxiliary physical structures can be merged with the original antenna [32] or realized in the driven patch [33], [34]. For example, in [32], the filtering antenna is realized by adding a parasitic loop to a unidirectional loop antenna. As a result, two radiation nulls in the gain curve versus frequency are obtained at the lower and upper band-edges, showing enhanced skirt selectivity. In [33], as a high efficient radiator, the metasurface is elaborately designed to provide a sharp roll-off rate at upper band edge for the filtering function. In [34] and [35], a filtering antenna composed of a driven patch and a stacked patch is proposed. In the driven patch, three shorting pins and a U-slot are embedded to enhance out-of-band suppression and skirt selectivity near the lower band-edge, whereas the stacked patch provides a sharp roll-off rate at the upper band-edge and also an enhanced gain.

2.5 Other Methods

In addition, there are other kinds of filtering antenna, such as horn filtering antenna [36] and substrate integrate waveguide (SIW) filter-antenna [37]–[40]. In [36], the single- and dual-band split-ring resonator (SRR) etched on a Rogers Duroid RT5870 dielectric substrate are inserted within the metallic flare of the horn at a proper distance from the throat. At the resonant frequencies of the SRR, transmission is highly reduced and the notched-bands are obtained. For the SIW filter-antenna, it is demonstrated that the co-design can be used to reduce the transmission loss, enhance bandwidth and suppress signals of adjacent frequency band. This antenna array can be used as mm-wave front end which demands for compact size and low noise disturbing.

3 Conclusions

An overview of reported filtering antenna in open literatures has been presented. As the requirement for various applications grows, there are a greater number of filtering antennas that can be classified in a wide range of different types. This article reports the filtering antennas based on the co-design approaches. It is demonstrated that the co-design is an efficient method to improve the integration degree, reduce the size and cost, and optimize the performance.

References

[1] S. Alalusi and R. Brodersen, "Antenna-filter-CMOS LNA co-design strategy," in Proc. CPD2000, Zurich, Switzerland, 2001, pp. 81–87.
[2] J. J. Wang, Y. P. Zhang, K. M. Chua, and A. C. W. Lu, "Circuit model of microstrip patch antenna on ceramic land grid array package for antenna-chip co-design of highly integrated RF transceivers," *IEEE Transactions on Antennas and Propagation*, vol. 53, no. 12, pp. 3877–3883, Dec. 2005. doi: 10.1109/TAP.2005.859907.
[3] J. H. Zuo, X. W. Chen, G. R. Han, L. Li, and W. M. Zhang, "An integrated approach to RF antenna-filter co-design," *IEEE Antennas and Wireless Propagation Letters*, vol. 8, pp. 141–144, Jan. 2009. doi: 10.1109/LAWP.2009.2012732.
[4] C. X. Mao, S. Gao, Z. P. Wang, et al., "Integrated filtering-antenna with controllable frequency bandwidth," in *European Conference on Antennas and Propagation*, Lisbon, Portugal, 2015, pp. 1–4.
[5] Z. H. Jiang, M. D. Gregory, and D. H. Werner, "Design and experimental investigation of a compact circularly polarized integrated filtering antenna for wearable biotelemetric devices," *IEEE Transactions on Biomedical Circuits and Systems*, vol. 10, no. 3 pp. 328–338, Apr. 2016. doi: 10.1109/TBCAS.2015.2438551.
[6] L. Li and G. Liu, "A differential microstrip antenna with filtering response," *IEEE Antennas and Wireless Propagation Letters*, vol. 15, pp. 1983–1986, Dec. 2016. doi:10.1109/LAWP.2016.2547884.
[7] Z. H. Jiang and D. H. Werner, "A compact, wideband circularly polarized co-designed filtering antenna and its application for wearable devices with low SAR," *IEEE Transactions on Antennas and Propagation*, vol. 63, no. 9, pp. 3808–3818, Sept. 2015. doi: 10.1109/TAP.2015.2452942.
[8] Z. H. Jiang and D. H. Werner, "A co-designed wideband circularly polarized integrated filtering antenna," in *Asia-pacific Microwave Conference*, Nanjing, China, 2015, pp. 1–3. doi: 10.1109/APMC.2015.7413370.
[9] M. C. Tang, Y. Chen, and R. W. Ziolkowski, "Experimentally validated, planar, wideband, electrically small, monopole filtennas based on capacitively loaded loop resonators," *IEEE Transactions on Antennas and Propagation*, vol. 64, no. 8, pp. 3353–3360, Aug. 2016. doi: 10.1109/TAP.2016.2576499.
[10] C. K. Lin and S. J. Chung, "A compact filtering microstrip antenna with quasi-elliptic broadside antenna gain response," *IEEE Antennas and Wireless Propagation Letters*, vol. 10, pp. 381–384, Apr. 2011. doi: 10.1109/LAWP.2011.2147750.
[11] L. Chen and Y. L. Luo, "Compact filtering antenna using CRLH resonator and defected ground structure," *Electronics Letters*, vol. 50, no. 21, pp. 1496–1498, Oct. 2014. doi: 10.1049/el.2014.2703.
[12] W. J. Wu, Y. Z. Yin, S. L. Zuo, Z. Y. Zhang, and J. J. Xie, "A new compact filter-antenna for modern wireless communication systems," *IEEE Antennas and Wireless Propagation Letters*, vol. 10, pp. 1131–1134, Oct. 2011. doi: 10.1109/LAWP.2011.2171469.
[13] X. W. Chen, L. Y. Yan, and W. M. Zhang, "A compact filtering antenna with flat gain response within the passband," *IEEE Antennas and Wireless Propagation Letters*, vol. 12, pp. 857–860, Jul. 2013. doi: 10.1109/LAWP.2013.2271972.
[14] S. Chen, Y. Zhao, M. Peng, and Y. Wang, "A co-designed compact dual-band filtering antenna with PIN loaded for WLAN applications," *International Journal of Antennas & Propagation*, vol. 2014, pp. 1–6, May 2014. doi: 10.1155/2014/826171.
[15] B. Ding, X. Wei, C. Wang, M. Zhang, and Z. He, "A compact printed filtering antenna with flat gain using annular slot and UIR," *in 15th International Conference Electronic Packaging Technology (ICEPT)*, Chengdu, China, 2014, pp. 1252–1255. doi: 10.1109/ICEPT.2014.6922871.
[16] W. Tian, J. Zhang, F. Zhang, and W. Chen, "Compact dual-band CPW-fed filtering antenna for WLAN applications," in *8th International Symposium on Computational Intelligence and Design (ISCID)*, Hangzhou, China, 2016, pp. 606–609. doi: 10.1109/ISCID.2015.93.
[17] M. M. Fakharian, P. Rezaei, A. A. Orouji, and M. Soltanpur, "A wideband and reconfigurable filtering slot antenna," *IEEE Antennas and Wireless Propagation Letters*, vol. 15, pp. 1610–1613, Sept. 2016. doi: 10.1109/LAWP.2016.2518859.
[18] B. Sahu, P. Tripathi, S. Singh, M. K. Meshram, and S. P. Singh, "A simple

structured filtering dielectric resonator antenna," in *IEEE Uttar Pradesh Section International Conference on Electrical, Computer and Electronics Engineering (UPCON)*, Varanasi, India, pp. 543–545, 2016. doi: 10.1109/UPCON.2016.7894712.

[19] A. K. Sahoo, R. D. Gupta, and M. S. Parihar, "A 2x2 integrated filter antenna array," in *European Conference on Antennas and Propagation*, Paris, France 2017, pp. 2205–2208, doi: 10.23919/EuCAP.2017.7928306.

[20] F. C. Chen, H. T. Hu, R. S. Li, et al., "Design of filtering microstrip antenna array with reduced sidelobe level," *IEEE Transactions on Antennas and Propagation*, vol. 65, no. 2, pp. 903–908, Feb. 2017. doi: 10.1109/TAP.2016.2639469.

[21] C. X. Mao, S. Gao, Y. Wang, et al., "An integrated filtering antenna array with high selectivity and harmonics suppression," *IEEE Transactions on Microwave Theory and Techniques*, vol. 64, no. 6, pp. 1798–1805, May 2016. doi: 10.1109/TMTT.2016.2561925.

[22] C. Y. Hsieh, C. H. Wu, and T. G. Ma, "A compact dual-band filtering patch antenna using step impedance resonators," vol. 14, pp. 1056–1059, May 2015. doi: r 10.1109/LAWP.2015.2390033.

[23] X. Y. Zhang, Y, Zhang,Y. M. Pan, and W. Duan, "Low-profile dual-band filtering patch antenna and its application to LTE MIMO system," *IEEE Transactions on Antennas and Propagation*, vol. 65, no. 1, pp. 103–113, Jan. 2017. doi: 10.1109/TAP.2016.2631218.

[24] W. B. Cheng, "Compact 2.4-GHz filtering monopole antenna based on modified SRR-inspired high-frequency-selective filter," *Optik*, vol. 127, pp. 10653–10658, Jan. 2016. doi: 10.1016/j.ijleo.2016.08.086.

[25] S. Koley and D. Mitra, "A planar microstrip-fed tri-band filtering antenna for WLAN/WiMax applications," *Microwave and Optical Technology Letter*, vol. 57, no. 1, pp. 233–237, Jan. 2015. doi: 10.1002/mop.28813.

[26] Y. M. Pan, P. F. Hu, X. Y. Zhang, and S. Y. Zheng, "A low-profile high-gain and wideband filtering antenna with metasurface," *IEEE Transactions on Antennas and Propagation*, vol. 64, no. 5, pp. 2010–2016, May 2016. doi: 10.1109/TAP.2016.2535498.

[27] M. I. Sabran, S. K. A. Rahim, C. Y. Leow, et al., "Compact circularly polarized truncated square ring slot antenna with suppressed higher resonances," *PLoS One*, vol. 12, no. 2, pp. 1–13, Feb. 2017. doi: 10.1371/journal.pone.0172162.

[28] H. A. Atallah, A. B. Abdel-Rahman, K. Yoshitomi, and R. K. Pokharel, "Compact frequency tunable filtenna with wide continuous tuning range using capacitively loaded folded arms open loop resonator for interweave cognitive radio application," in *33rd National Radio Science Conference (NRSC)*, Aswan, Egypt, Feb. 2016, pp. 87–93. doi: 10.1109/NRSC.2016.7450815.

[29] P. F. Hu, Y. M. Pan, X. Y. Zhang, and S. Y. Zheng, "Broadband filtering dielectric resonator antenna with wide stopband," *IEEE Transactions on Antennas and Propagation*, vol. 65, no. 4, pp. 2079–2084, Apr. 2017. doi: 10.1109/TAP.2017.2670438.

[30] P. F. Hu, Y. M. Pan, X. Y. Zhang, and S. Y. Zheng, "A compact filtering dielectric resonator antenna with wide bandwidth and high gain," *IEEE Transactions on Antennas and Propagation*, vol. 64, no. 8, pp. 3645–3651, Aug. 2016. doi: 10.1109/TAP.2016.2565726.

[31] B. J. Xiang, S. Y. Zheng, Y. M. Pan, and Y. X. Li, "Wideband circularly polarized dielectric resonator antenna with bandpass filtering and wide harmonics suppression response," *IEEE Transactions on Antennas and Propagation*, vol. 65, no. 4, pp. 2096–2101, Apr. 2017. doi:10.1109/TAP.2017.2671370.

[32] J. N. Wu, Z. Q. Zhao, Z. P. Nie, and Q. H. Liu, "A printed unidirectional antenna with improved upper band-edge selectivity using a parasitic," *IEEE Transactions on Antennas and Propagation*, vol. 60, no. 4, pp. 1832–1837, Jan. 2015. doi: 10.1109/TAP.2015.2392112.

[33] Y. M. Pan, P. F. Hu, X. Y. Zhang, and S. Y. Zheng, "A low-profile high gain and wideband filtering antenna with metasurface," *IEEE Transactions on Antennas Wireless Propagation*, vol. 64, no. 5, pp. 2010–2016, May 2016. doi: 10.1109/TAP.2016.2535498.

[34] X. Y. Zhang, W. Duan, and Y. M. Pan, "High-gain filtering patch antenna without extra circuit," *IEEE Transactions on Antennas Wireless Propagation*, vol. 63, no. 12, pp. 5883–5888, Dec. 2015. doi: 10.1109/TAP.2015.2481484.

[35] W. Duan, X. Y. Zhang, Y. M. Pan, J. X. Xu, and Q. Xue, "Dual-polarized filtering antenna with high selectivity and low cross polarization," vol. 64, no. 10, pp. 4188–4195, Oct. 2016. doi:10.1109/TAP.2016.2594818.

[36] M. Barbuto, F. Trotta, F. Bilotti, and A. Toscano, "Horn antennas with integrated notch filters," vol. 63, no. 2, pp. 781–785, Feb. 2015. doi: 10.1109/TAP.2014.2378269.

[37] U. Naeem, A. Iqbal, M. F. Shafique, and S. Bila, "Efficient design methodology for a complex DRA-SIW filter-antenna," *International Journal of Antennas and Propagation*, vol. 2017, pp. 1–9, Apr. 2017. doi: 10.1155/2017/6401810.

[38] Y. Chen, H. Wei, Z. Q. Kuai, and H. M. Wang, "Ku-band linearly polarized omnidirectional planar filtenna," *IEEE Antennas and Wireless Propagation Letters*, vol. 11, pp. 310–313, Apr. 2012. doi: 10.1109/LAWP.2012.2191259.

[39] Y. Chen and H. Wei, "37-38 GHz substrate integrated filtenna for wireless communication application," *Microwave and Optical Technology Letter*, vol. 54, no. 2, pp. 346–351, Feb. 2012. doi: 10.1002/mop.26589.

[40] X. Liu, H. Wang, S. Quan, et al., "Design of a W band filter antenna array with low sidelobe level using gap waveguide," *in 11th International Symposium on Antennas, Propagation and EM Theory (ISAPE)*, Guilin, China, 2016, pp. 132–134. doi: 10.1109/ISAPE.2016.7833900.

Manuscript received: 2018-10-13

Biographies

ZHANG Wenmei (zhangwm@sxu.edu.cn) received the B.S. and M.S. degrees from Nanjing University of Science and Technology, China in 1992 and 1995, respectively, and the Ph.D. degree in electronic engineering from Shanghai Jiao Tong University, China in 2004. Now she is a professor of the College of Physics and Electronics, Shanxi University, China. Her research interests include microwave and millimeter-wave integrated circuits, EMC, and microstrip antennas.

CHEN Xinwei (chenxw@sxu.edu.cn) received the B.S. and Ph.D. degrees from Shanxi University, China in 2002 and 2013. Now he is an associate professor of the College of Physics and Electronics, Shanxi University. His research interest is microwave filters.

ZTE Communications Guidelines for Authors

Remit of Journal

ZTE Communications publishes original theoretical papers, research findings, and surveys on a broad range of communications topics, including communications and information system design, optical fiber and electro–optical engineering, microwave technology, radio wave propagation, antenna engineering, electromagnetics, signal and image processing, and power engineering. The journal is designed to be an integrated forum for university academics and industry researchers from around the world.

Manuscript Preparation

Manuscripts must be typed in English and submitted electronically in MS Word (or compatible) format. The word length is approximately 3000 to 8000, and no more than 8 figures or tables should be included. Authors are requested to submit mathematical material and graphics in an editable format.

Abstract and Keywords

Each manuscript must include an abstract of approximately 150 words written as a single paragraph. The abstract should not include mathematics or references and should not be repeated verbatim in the introduction. The abstract should be a self–contained overview of the aims, methods, experimental results, and significance of research outlined in the paper. Five carefully chosen keywords must be provided with the abstract.

References

Manuscripts must be referenced at a level that conforms to international academic standards. All references must be numbered sequentially in–text and listed in corresponding order at the end of the paper. References that are not cited in–text should not be included in the reference list. References must be complete and formatted according to ZTE Communications Editorial Style. A minimum of 10 references should be provided. Footnotes should be avoided or kept to a minimum.

Copyright and Declaration

Authors are responsible for obtaining permission to reproduce any material for which they do not hold copyright. Permission to reproduce any part of this publication for commercial use must be obtained in advance from the editorial office of *ZTE Communications*. Authors agree that a) the manuscript is a product of research conducted by themselves and the stated co–authors, b) the manuscript has not been published elsewhere in its submitted form, c) the manuscript is not currently being considered for publication elsewhere. If the paper is an adaptation of a speech or presentation, acknowledgement of this is required within the paper. The number of co–authors should not exceed five.

Content and Structure

ZTE Communications seeks to publish original content that may build on existing literature in any field of communications. Authors should not dedicate a disproportionate amount of a paper to fundamental background, historical overviews, or chronologies that may be sufficiently dealt with by references. Authors are also requested to avoid the overuse of bullet points when structuring papers. The conclusion should include a commentary on the significance/future implications of the research as well as an overview of the material presented.

Peer Review and Editing

All manuscripts will be subject to a two–stage anonymous peer review as well as copyediting, and formatting. Authors may be asked to revise parts of a manuscript prior to publication.

Biographical Information

All authors are requested to provide a brief biography (approx. 100 words) that includes email address, educational background, career experience, research interests, awards, and publications.

Acknowledgements and Funding

A manuscript based on funded research must clearly state the program name, funding body, and grant number. Individuals who contributed to the manuscript should be acknowledged in a brief statement.

Address for Submission

http://mc03.manuscriptcentral.com/ztecom
12F Kaixuan Building, 329 Jinzhai Rd, Hefei 230061, P. R. China

ZTE COMMUNICATIONS
中兴通讯技术(英文版)

ZTE Communications has been indexed in the following databases:

- Abstract Journal
- Cambridge Scientific Abstracts (CSA)
- China Science and Technology Journal Database
- Chinese Journal Fulltext Databases
- Inspec
- Ulrich's Periodicals Directory
- Wanfang Data—Digital Periodicals

ZTE COMMUNICATIONS
Vol. 16 No. 1 (Issue 61)
Quarterly
First English Issue Published in 2003

Supervised by:
Anhui Science and Technology Department

Sponsored by:
Anhui Science and Technology Information Research Institute;
Magazine House of ZTE Communications

Published and Circulated (Home and Abroad) by:
Magazine House of ZTE Communications

Editorial Correspondence:
Add: 12F Kaixuan Building, 329 Jinzhai Road,
Hefei 230061, P. R. China
Tel: +86-551-65533356
Fax: +86-551-65850139
Email: magazine@zte.com.cn

Annual Subscription: RMB 80

Printed by:
Hefei Tiancai Color Printing Company

Publication Date: February 25, 2018

Publication Licenses:

ISSN 1673-5188
CN 34-1294/ TN